

Research manual 3

ECMWF forecast model

Physical parametrization

ECMWF Research Department

Meteorological Bulletin

Keywords: Physical parametrization,
radiation, vertical diffusion,
gravity wave drag
moist convection, stratiform
precipitation, soil processes

M1.6/2

RESEARCH MANUAL 3
ECMWF FORECAST MODEL
PHYSICAL PARAMETRIZATION

ECMWF Research Department

This Meteorological Bulletin is bound separately.

Sheets replaced by updates should be retained at the back of the manual.

2/84 Original Version
1/88 2nd Edition
7/91 3rd Edition

Shinfield Park, Reading, Berkshire RG2 9AX, England. Telephone: U.K. (0734) 499000,
International (+44 734) 499000, Telex: 847908 ECMWF G, Telefax (0734) 869450



European Centre for Medium-Range Weather Forecasts
Europäisches Zentrum für mittelfristige Wettervorhersage
Centre européen pour les prévisions météorologiques à moyen terme

Table 1 List of constants and symbols	v
---	---

CHAPTER 1

Overview

1.1 INTRODUCTION	1.1
1.2 OVERVIEW OF THE CODE	1.4

CHAPTER 2

Radiation

2.1 RADIATIVE HEATING	2.1
2.2 LONGWAVE RADIATION	2.1
2.2.1 Vertical integration	2.2
2.2.2 Spectral integration	2.3
2.2.3 The incorporation of the effects of clouds	2.5
2.3 SHORTWAVE RADIATION	2.6
2.3.1 Spectral integration	2.7
2.3.2 Vertical integration	2.9
2.3.2.1 Cloudy fraction of the layer	2.10
2.3.2.2 Clear-sky fraction of the layers	2.13
2.3.3 Multiple reflections between layers	2.14
2.3.4 Cloud shortwave optical properties	2.16
2.4 HORIZONTAL INTERPOLATION	2.16
2.5 INPUT TO THE RADIATION SCHEME	2.17
2.5.1 Model variables	2.17
2.5.2 Clouds	2.17
2.5.3 Aerosols	2.19
2.5.4 Carbon dioxide and ozone	2.19
2.5.5 Ground albedo	2.20
2.5.6 Solar zenith angle	2.21
2.6 THE RADIATION CODE	2.22
2.6.1 Definition of constants	2.22
2.6.2 Main routines	2.23
2.6.3 Specialized routines	2.25
2.6.4 Heating rate computation	2.26
REFERENCES	2.27

CHAPTER 3
Vertical diffusion and interaction with the surface

3.1	THEORY	3.1
3.1.1	Basic equations	3.1
3.1.2	Surface fluxes	3.3
3.1.3	Definition of the transfer coefficients over land	3.6
3.1.4	Transfer coefficients over sea	3.9
3.1.5	Definition of the exchange coefficients	3.10
3.1.6	Definition of the top of the boundary layer	3.11
3.1.7	Kinetic energy dissipation	3.12
3.2	CODE: Subroutine VDFMAIN	3.13
3.2.1	Preliminary computation	3.13
3.2.2	VDFSURF	3.13
3.2.3	VDFEXCS	3.13
3.2.4	VDFEVAP	3.14
3.2.5	VDFHEIGHT	3.14
3.2.6	VDFEXCU	3.14
3.2.7	VDFDIFM and VDFDIFH	3.15
3.2.8	VDFINCR	3.15
3.2.9	VDFSDRV	3.16
3.2.10	VDFT2M	3.17
	REFERENCES	3.18

CHAPTER 4
Gravity wave drag

4.1	THEORY	4.1
4.1.1	The formulation of the scheme	4.1
4.2	CODE: Subroutine GWDRAG	4.4
4.2.1	Preliminary computations (GWSETUP)	4.4
4.2.2	$\tau_w(p_s)$ [GWSTRESS]	4.5
4.2.3	The profile of stress τ_w [GWPROFIL]	4.5
4.2.4	The tendencies	4.6
4.2.5	Diagnostics	4.7
4.2.6	Implicitness	4.7
	REFERENCES	4.8

CHAPTER 5
Convection

5.1	CUMULUS CONVECTION	5.1
5.1.1	Large-scale budget equations	5.1
5.1.2	Cloud model equations	5.2
5.1.2.a	Penetrative convection	5.5
5.1.2.b	Shallow convection	5.7
5.1.2.c	Midlevel convection	5.8
5.1.3	Discretization of the model equations	5.8
5.1.4	Melting of snow	5.10
5.1.5	Evaporation of rain	5.10
5.2	STRATOCUMULUS	5.11
5.3	CODE	5.13
	REFERENCES	5.16

CHAPTER 6
Stratiform precipitation

6.1	THEORY	6.1
6.1.1	Definition of the saturation specific humidity	6.1
6.1.2	Equilibrium values T^* , q^* at saturation, starting from T and q	6.1
6.1.3	Derivative of $q_{SAT}(T,p)$ with respect to T	6.2
6.1.4	Evaporation of precipitation	6.3
6.1.5	Melting of snow	6.3
6.2	CODE: Subroutine COND	6.4
6.3	REMOVAL OF NEGATIVE MOISTURE VALUES: subroutine QNEGAT	6.6
	REFERENCES	6.7

CHAPTER 7
Soil processes

7.1	THEORY	7.1
7.1.1	Sea points	7.1
7.1.2	Land points	7.1
7.1.2(a)	Temperature	7.1
7.1.2(b)	Moisture	7.3

7.1.2(c) Snow	7.6
7.1.2(d) Snow melting	7.6
7.1.2(e) Time-stepping	7.8
7.2 CODE: Subroutine SURF	7.10
REFERENCES	7.12

APPENDIX 1

Climatological data used in the model

1. OROGRAPHY	A.1
2. LAND-SEA MASK	A.1
3. ROUGHNESS LENGTH	A.2
4. ALBEDO	A.3
5. DEEP-LAYER SOIL TEMPERATURE	A.3
6. DEEP-LAYER SOIL MOISTURE	A.3
7. VEGETATION	A.3
8. OZONE DISTRIBUTION	A.4
REFERENCES	A.5

TABLE 1 LIST OF CONSTANTS AND SYMBOLS

<u>Symbol</u>	<u>Definition</u>	<u>Value</u>	<u>Unit</u>
a	earth radius	6.371×10^6	m
a_i	ice heat diffusivity/soil heat diffusivity	0.3	-
Δ	optical coefficient matrix		-
A_{pm}	minimum planetary albedo		-
A_s	soil albedo		-
A_g	solar albedo of ground		-
$A_{s_{mrv}}$	albedo of snow covered ice dew free part		-
A_{SND}	albedo of the grid box, ice dew free		-
A_{SNO}	maximum value for the snow albedo	0.8	-
A_{SNM}	minimum value for the snow albedo	0.4	-
A_T	thermal albedo of ground		-
B	Planck's black body function		$W m^{-2}$
C_h	transfer coefficient for heat and moisture		-
C_m	transfer coefficient for momentum		-
C_{char}	Charnock constant	0.018	-
C_r	reduction of thermal diffusion under vegetation	0.5	-
C_{ST}	temperature interval for the snow albedo	5	K
C_v	vegetation ratio		-
CVS	effective snow cover for thermal properties		-
$CVSA$	effective snow cover for albedo		-
CVS_{BL}	snow cover for bare land		-
C_s	fraction of the grid box covered by skin reservoir		-
$C_{v_{sn}}$	fraction of the vegetation covered by snow		-
C_A	fractional area covered by convective precipitation	0.5	-
CP	convective precipitation		m
C	cloud cover		-

C_c	convective cloud	-
C_H	high cloud	-
C_L	low cloud	-
C_M	middle cloud	-
C_{pd}	specific heat of dry air at constant pressure	1005.46 $J kg^{-1} K^{-1}$
C_{sn}	snow cover fraction	-
C_1	wet skin fraction	-
C_{vet}	vegetation ratio (climatology)	-
C_{pv}	specific heat of water vapour at constant pressure	1869.46 $J kg^{-1} K^{-1}$
C_ψ	transfer coefficient for variable ψ	-
C_ψ	transfer coefficient for ψ	-
CIP	efficiency coefficient of interception of rain	-
D_i	thickness of soil layer i	m
DEV	evaporation from bare soil	$W m^{-2}$
e_s	saturation partial pressure of water vapour	Pa
E	evapotranspiration efficiency factor	-
E_T	thermal emissivity of ground	-
Ext_i	root uptake in soil layer i	$W m^{-2}$
F	radiative flux	$W m^{-2}$
\dot{F}	difference to the black body flux	$W m^{-2}$
\bar{F}	flux in isothermal atmosphere	$W m^{-2}$
f_m, f_h	stability functions for momentum and heat	-
F_o	"grey" flux	$W m^{-2}$
F_s	solar flux	$W m^{-2}$
F_T	thermal flux	$W m^{-2}$
F^d	diffuse downward flux	$W m^{-2}$
F^p	parallel flux	$W m^{-2}$

F^u	diffuse upward flux		$W m^{-2}$
g	acceleration of gravity	9.80665	$m s^{-2}$
h	relative humidity at the surface		-
h_{cnv}	height of the dry convective boundary layer		m
h_{dyn}	height of the dynamical (frictional) boundary layer		m
h_{pbl}	height of the planetary boundary layer		m
I_f	infiltration rate		$kg m^{-2} s^{-1}$
I_{fmax}	maximum infiltration rate		$kg m^{-2} s^{-1}$
I_o	solar constant	1376	$W m^{-2}$
J_{gw}	moisture flux effective to wet the soil		$Kgm^{-2} s^{-1}$
J_ψ	vertical eddy flux of variable ψ		$[\psi]kgm^{-2}s^{-1}$
k	absorption coefficient		Pa^{-1}
k	von Karman constant	0.4	-
K_ψ	diffusion coefficient for ψ		$m^2 s^{-1}$
l_m, l_h	mixing lengths for momentum and heat		m
L	Monin-Obukhov length		m
L_s	latent heat of sublimation	2.8345×10^6	$J kg^{-1}$
L_t	leaf area index	4	-
L_v	latent heat of vapourisation	2.5008×10^6	$J kg^{-1}$
M_m	snow melting		$kg m^{-2} s^{-1}$
p	pressure		Pa
p_s	surface pressure		Pa
P_R	precipitation flux		$kg m^{-2} s^{-1}$
P_S	snow fall flux		$kg m^{-2} s^{-1}$
p_t	pressure at the top of the planetary boundary layer		Pa
PAR	Photosynthetic Active Radiation		$W m^{-2}$
q	specific humidity		$kg kg^{-1}$

q_{SAT}	saturation specific humidity		$kg\ kg^{-1}$
Q_{AC}	moisture convergence (or accession)		Pa
R	precipitation rate		$kg\ m^{-2}\ s^{-1}$
R_{co}	minimum stomatal resistance		$s\ m^{-1}$
R_{crit}	critical Richardson number		-
R_d	gas constant for dry air	287.05	$J\ kg^{-1}\ K^{-1}$
R_i	root density in soil layer i		-
R_R	rain precipitation rate		$kg\ m^{-2}\ s^{-1}$
R_s	snow precipitation rate		$kg\ m^{-2}\ s^{-1}$
R_{SR}	surface runoff efficiency		-
R_v	gas constant for water vapour	461.51	$J\ kg^{-1}\ K^{-1}$
RH	relative humidity		-
Ri	Richardson number		-
RO_1, RO_2	different contributions to surface runoff		$kg\ m^{-2}\ s^{-1}$
s	dry static energy		$m^2\ s^{-2}$
s_s	scaling dry static energy		$m^2\ s^{-2}$
\underline{S}	source function vector		$W\ m^{-2}$
S_o	solar flux at the top of the atmosphere		$W\ m^{-2}$
Sn	snow depth (liquid water equivalent)		m
Sn_{cr}	Critical depth for snow cover fraction	0.015	m
T	temperature		K
t	time		s
Δt	time step		s
T_o	ice melting temperature	273.16	K
T_s	surface temperature		K
T_v	virtual temperature		K
$\underline{u} = (u, v)$	horizontal wind vector		$m\ s^{-1}$
u_s	scaling velocity		$m\ s^{-1}$

u_{eff}	effective absorber amount		Pa
Δu_j	absorber amount in a layer		Pa
Vor	non directional variance of sub-grid scale orography		m^2
Vor_{max}	characteristic variance	750^2	m^2
Vor_{min}	threshold variance	50^2	m^2
W_{cl}	soil moisture (climatology)		m
W	soil moisture (root zone)		m
W_{cr}	critical soil moisture ($0.6 \cdot W_{scap}$)		m
W_d	soil moisture (deep layer)		m
W_1	skin reservoir		m
W_{1max}	maximum skin reservoir content	2.10^{-4}	m
W_{1max}	local maximum skin reservoir content over bare soil or per layer of vegetation		-
W_{pwp}	permanent wilting point ($0.3 \cdot W_{scap}$)		m
W_s	soil moisture (superficial layer)		m
W_{sat}	soil wetness at the soil porosity		-
W_{scap}	field capacity	0.02	m
z	height		m
Δz	layer thickness		m
z_o	roughness length		m
α	implicitness parameter	1.5	-
β	upscattered fraction for parallel solar beam		-
β	ratio of moistening to moisture convergence		-
$\tilde{\beta}$	backscattered fraction for diffuse beams		-
γ	hydraulic conductivity	10^{-10}	$m \ s^{-1}$
ε	R_d/R_v		-
ε_e	effective emissivity		-
η	vertical coordinate		-
ϕ	gz, geopotential		$m^2 \ s^{-2}$

ϕ_m, ϕ_h	universal flux profile functions for momentum and heat		-
κ	thermal diffusivity in soil	$7.5 \cdot 10^{-7}$	$m^2 s^{-1}$
λ	hydraulic diffusivity in soil	1.10^{-7}	$m^2 s^{-1}$
λ_m, λ_h	asymptotic mixing length for momentum and heat		-
μ_o	cosine of solar zenith angle		-
ρ	air density		$kg m^{-3}$
$\rho_s C_s$	soil heat capacity (per unit volume)	2.4×10^6	$Jm^{-3} K^{-1}$
$\rho_i C_i$	ice heat capacity (per unit volume)	2.09×10^6	$Jm^{-3} K^{-1}$
$\rho_s C_s$	combination of the previous two		$Jm^{-3} K^{-1}$
ρ_{H_2O}	liquid water density	1000	$kg m^{-3}$
ΣF	sum of surface heat fluxes		-
τ_i^l	transmission function for gas i and wavenumber interval l .		-
τ	optical depth		-
τ_e	effective transmissivity		-
$\tau^j, j=p, u, d$	transmission function for parallel, upward or downward flux		-
ω	single scattering albedo		-
ψ	u, v, s or q		-
ψ^-	ψ at $t+1$		-
ψ^o	ψ for implicit evaluation of diffusive flux		-
ψ_s	surface value of ψ		-

CHAPTER 1

Overview

1.1 INTRODUCTION

Processes associated with turbulent and convective transfer, condensation and radiation are important for the development of the atmospheric large-scale flow. Since these processes are related to spatially small or even molecular phenomena, they cannot be explicitly included in numerical models which only resolve scales larger than grid size in grid point models or the truncation wave number in spectral models.

Fig.1.1 shows the processes which are thought to be important for a medium-range forecast. For simplicity the diagram corresponds to flat land surfaces, excluding some parametrization aspects such as gravity wave drag. It shows how the different processes (printed within ellipses) depend on the variables given by the model (printed in rectangles). The thickness of the arrows represents qualitatively the importance of the interactions. For example, the effect of radiation on the ground temperature is very fast: it only takes a few hours for the sun to heat the ground; but the relationship between radiation and the temperature of the air is much weaker: condensation, diffusion and the flux of sensible heat from the ground change the air temperature more effectively. Any closed loop in the diagram (e.g. Temperature→Evaporation→Ground temperature→Sensible heat flux→Temperature) indicates a feed-back phenomenon. The reader can amuse himself by counting the number of closed loops in order to get a feeling for the complexity of the atmospheric system.

The effect of the sub-grid scale processes on the large-scale flow which we want to predict can only be considered by means of parametrization, i.e. formulating the ensemble effect in terms of the resolved grid-scale variables.

Large efforts have been made in the recent past to design reliable parametrization schemes for different processes. Based on a large amount of observational data the parametrization of the turbulent fluxes in the planetary boundary layer has been considerably improved. A significant effort has been directed towards accounting for vegetation effects on the surface fluxes. Progress has also been made in calculating the radiative fluxes, and a hierarchy of schemes differing with respect to the degree of approximation of the equations of radiative transfer were developed.

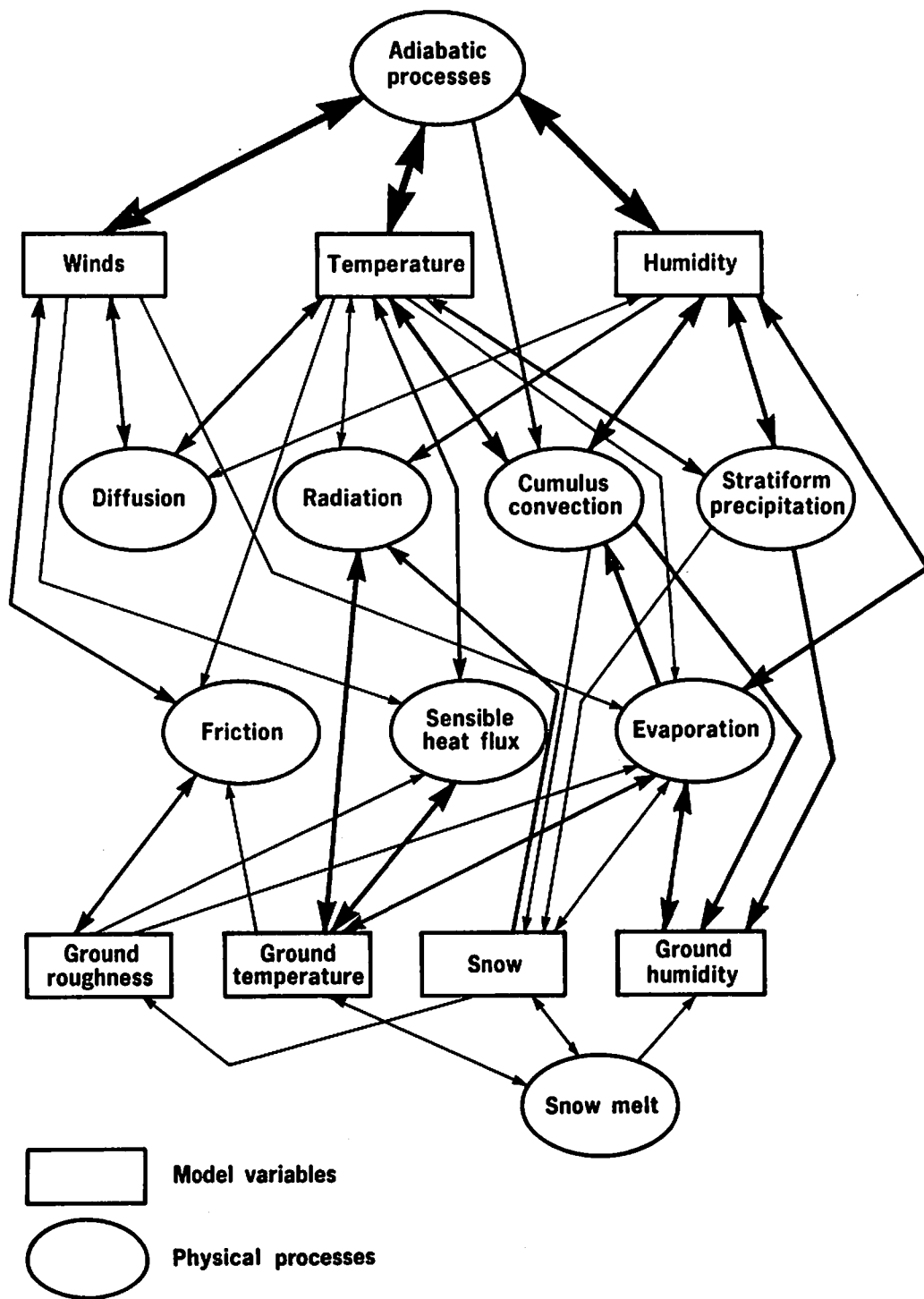


Fig. 1.1 Schematic representation of the processes included in the ECMWF model.

Finally, there are also processes which have only occasionally been the subject of parametrization studies as, for instance, mesoscale circulations, topographically induced circulations, thin layer clouds and coastal effects.

This volume describes the physical parametrization schemes used in the ECMWF operational forecast model. Since these schemes are also used in other experimental models of the Centre, such as the limited area model or the single-column model, it was decided to publish this manual on its own, separately from the rest of the model documentation. Information on the dynamics, diagnostics, initialization and file handling of the forecast model can be found in the manual entitled: *ECMWF Forecast Model: Adiabatic Part* (Research Manual 2; ECMWF Publication M1.6/3).

The radiation scheme (chapter 2) is designed to take the cloud-radiation interactions into account, in considerable detail. It allows partial cloud cover in any layer of the model, and considers multiple scattering. The effect of gases is subsequently taken into account, using an exponential sum fitting of the transmission functions.

The dissipation processes are described in chapter 3. The vertical eddy fluxes are simulated as a diffusive process. The dependence of the surface fluxes and diffusion coefficients on the stability of the atmosphere is based on the Monin-Obukhov similarity theory.

An additional process by which momentum may be removed from the atmosphere is through the excitation of gravity waves when stably stratified flow interacts with the orography. This so-called 'gravity-wave' drag (chapter 4) is parametrized using directionally dependent subgridscale orographic variances.

The moist processes are separated into convective and stratiform (chapters 5 and 6). The convective processes are simulated by a mass flux scheme, in which the convection is driven by the large-scale convergence of moisture. Stratiform precipitation simply removes moisture from supersaturated layers. Precipitation can re-evaporate in the dry layers below the clouds.

The effect of vegetation on surface evapotranspiration as well as the dependence of sensible heat fluxes on snow coverage is described in chapter 7. The ground processes include a prediction of the soil temperature and moisture, using a 3-level, finite-difference approximation of the diffusion equation, and imposing climate values in the bottom layer. A prediction of the snow cover is also included.

The horizontal diffusion, which is used in the operational model to keep the forecast from developing small scale noise, is included in the documentation of the adiabatic part.

1.2 OVERVIEW OF THE CODE

In order for the reader to understand the relationship between the physics and the rest of the ECMWF forecast model, we present here a quick overview of the structure of the code.

Fig.1.2 is a flow diagram of the main routines of the model. After setting up constants, including some constants for the physics, routine CONTROL calls INITIAL, for a new run, or RESTART. Their function is mainly to read the initial data and set up the work files, but INITIAL can also, if required, call routines to perform a normal mode initialisation of the data. This involves running some time steps of the model. Control of the run is then transferred to routine STEPON which advances the calculation.

The initial data exists as Fourier coefficients on individual latitude lines, but parts of the computation are done in grid-point space and in spectral space (using spherical harmonics). The computation is divided into two scans through the latitude lines. During the first scan, all the calculations in Fourier and grid-point space are done, then direct Legendre transforms produce spherical harmonics coefficients. After performing the end of the semi-implicit adjustment and the horizontal diffusion in spectral space, a second scan is used to go back to Fourier space by inverse Legendre transform.

All the physical parametrization is done in grid point space. It is controlled by routine PHYSC, called by GPC. The routine which computes the radiative heating rates uses a forward time step, from $t-1$ to $t+1$, using some input computed at less frequent interval, as described in Chapter 2. The vertical diffusion also uses a forward time step, but it is performed implicitly in order to keep it numerically stable despite the fine vertical resolution near the ground. The moist convection modifies the tendencies previously computed, and the stratiform precipitation routine adjusts the $t+1$ moisture and temperature fields by removing supersaturation.

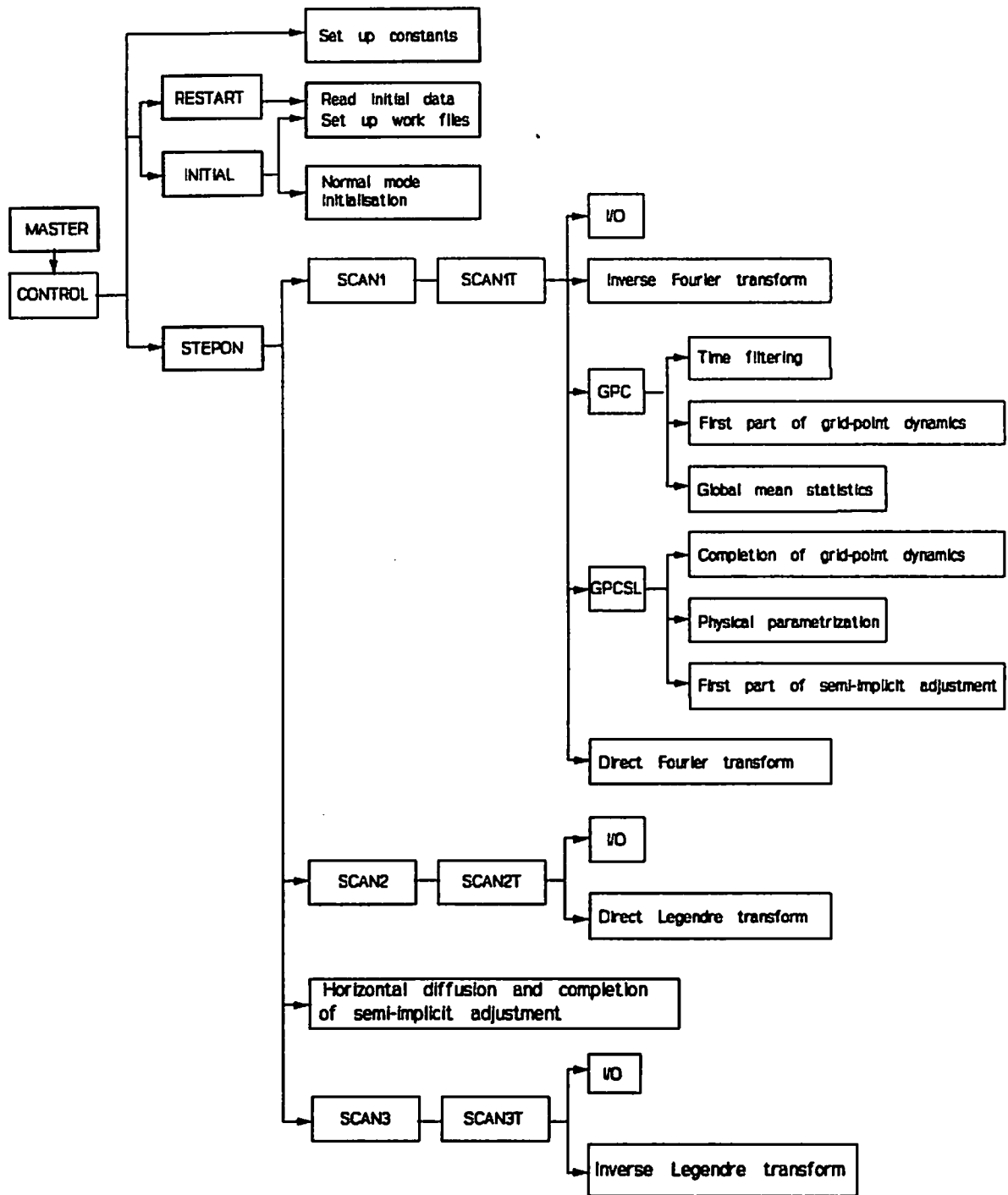


Fig. 1.2 Simplified flow diagram of the ECMWF forecast model

Fig.1.3 shows all the routines of the model directly associated with the physical parametrization. The computations of the geopotential height and the pressure of the model levels are self-explanatory and not described here. The routines associated with diagnostics can be found in ECMWF document RM-02 (Adiabatic part).

The various parts of the physical parametrization scheme will be described in the following Chapters in the order in which they are called in the model.

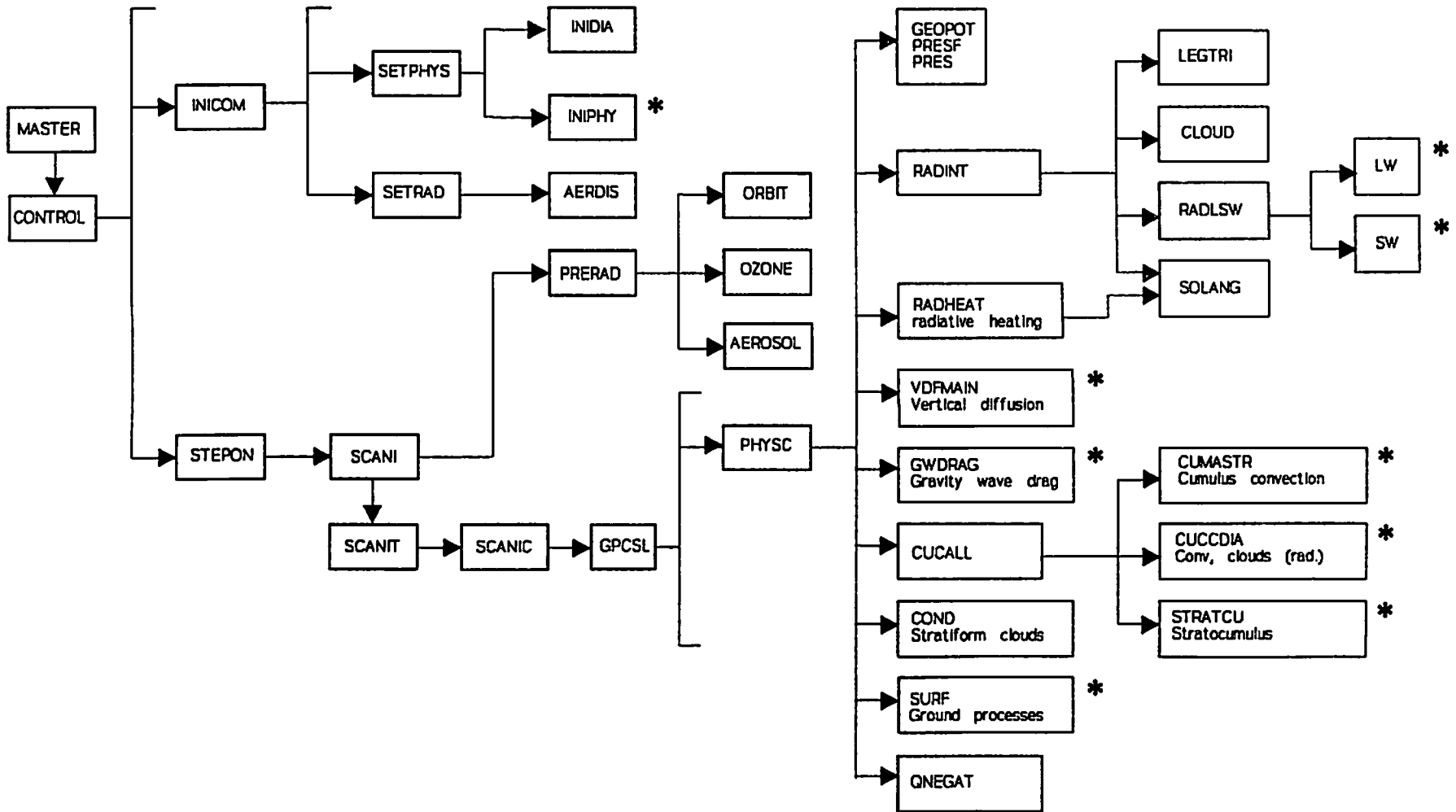


Fig. 1.3 Diagram of the subroutines involved in the physical parametrization. * See text in relevant sections.

CHAPTER 2

Radiation

2.1 RADIATIVE HEATING

The radiative heating rate is computed as the divergence of net radiation fluxes F :

$$\left(\frac{\partial T}{\partial t}\right)_{rad} = - \frac{g}{C_{pd}(1 + (\delta-1)q)} \frac{\partial F}{\partial p} \quad (2.1)$$

Sect.2.2 and 2.3 describe the computation of the longwave and shortwave radiative fluxes respectively. The solution of the radiative transfer equation to obtain the fluxes is unfortunately very expensive, and we cannot afford to do it more than every 3 hours at every fourth grid point. We want however, to take into account the change in temperature and solar zenith angle between the times when the full radiation computation is performed. To do so we define an effective emissivity ϵ_e and transmissivity τ_e of the model level such that:

$$F_T = \epsilon_e \pi B(T)$$

and

$$F_S = \tau_e S_0 \quad (2.2)$$

where F_T and F_S are the net thermal (long wave) and solar (short wave) fluxes respectively. $B(T)$ is the Planck function for the temperature T and S_0 is the solar flux at the top of the atmosphere. The values of ϵ_e and τ_e are kept constant between full radiation time steps and the net fluxes are recomputed at every time step, using (2.2) and (2.3) with the correct temperature and solar angle, for every grid point.

2.2 LONGWAVE RADIATION

The rate of atmospheric cooling by emission-absorption of longwave radiation is

$$\frac{\partial T}{\partial t} = - \frac{g}{C_p} \frac{\partial F}{\partial p} \quad (2.3)$$

where F is the net total longwave flux.

Assuming a non-scattering atmosphere in local thermodynamic equilibrium, F is given by

$$F = \int_{-}^{+} \frac{1}{\mu} d\mu \int_0^{\infty} dv \left[L_v(p_s, \mu) t_v(p_s, p, \mu) + \int_{p_s}^0 L_v(p', \mu) dt_v \right] \quad (2.4)$$

where $L_\nu(p, \mu)$ is the monochromatic radiance of wavenumber ν at level p propagating in a direction such as μ is the cosine of the angle that this direction makes with the vertical, and $t_\nu(p, p', \mu)$ is the monochromatic transmission through a layer whose limits are at p and p' seen under the same angle θ .

After separating the upward and downward components, and integrating by parts, we obtain the radiation transfer equation as it is actually estimated in the radiation code

$$F_\nu^+(p) = [B_\nu(T_p) - B_\nu(T_{0+})] t_\nu(p, p; r) + B_\nu(T_p) - \int_{p'}^p t_\nu(p, p'; r) dB_\nu \quad (2.5)$$

$$F_\nu^-(p) = [B_\nu(T_p) - B_\nu(T_\infty)] t_\nu(p, 0; r) + B_\nu(T_p) + \int_p^0 t_\nu(p', p; r) dB_\nu$$

where, taking benefit of the isotropic nature of the longwave radiation, the radiance L_ν of (2.4) is replaced by Planck function $B_\nu(T)$ in unit of flux, Wm^{-2} (hereafter B_ν always includes the π factor). T_s is the surface temperature, T_{0+} that of the air just above the surface, T_p is the temperature at level of pressure p , T_∞ that at the top of the atmospheric model. The transmission t_ν is evaluated as the radiance transmission in a direction θ to the vertical such that $r = \sec \theta$ is the diffusivity factor (Elsasser, 1942). Such an approximation for the integration over the angle is usual in radiative transfer calculations, and tests on the validity of this approximation have been presented by Rodgers and Walshaw (1966) among others. The use of the diffusivity factor gives cooling rates within 2% of those obtained with a 4-point Gaussian quadrature.

2.2.1 Vertical integration

The integrals in (2.5) are evaluated numerically, after discretization over the vertical grid, considering the atmosphere as a pile of homogeneous layers. As the cooling rate is strongly dependent on local conditions of temperature and pressure, and energy is mainly exchanged with the layers adjacent to the level where fluxes are calculated, the contribution of the distant layers is simply computed using a trapezoidal rule integration, but the contribution of the adjacent layers is evaluated with a 2-point Gaussian quadrature, thus

$$\int_{p_i}^{p_j} t_\nu(p, p'; r) dB_\nu = \sum_{l=1}^2 dB_\nu(l) w_l t_\nu(p, p_l; r) + \frac{1}{2} \int_{j-1}^{l-2} dB_\nu(j) [t_\nu(p, p_j; r) + t_\nu(p, p_{j-1}; r)] \quad (2.6)$$

where p_1 and w_1 are the pressure corresponding to the Gaussian root and the Gaussian weight, respectively. $dB_\nu(f)$ and $dB_\nu(l)$ are the Planck function gradients calculated between two interfaces, and between mid-layer and interface, respectively.

2.2.2 Spectral integration

The integration over wavenumber ν is performed using a band emissivity method, as first discussed by *Rodgers (1967)*. The longwave spectrum is divided into six spectral regions

1.	0	-	350 cm ⁻¹	+	1450 - 1880 cm ⁻¹
2.	500	-	800 cm ⁻¹		
3.	800	-	970 cm ⁻¹	+	1110 - 1250 cm ⁻¹
4.	970	-	1110 cm ⁻¹		
5.	350	-	500 cm ⁻¹		
6.	1250	-	1450 cm ⁻¹	+	1880 - 2820 cm ⁻¹

corresponding to the centers of the rotation and vibration-rotation bands of H₂O, the 15 micron band of CO₂, the atmospheric window, the 9.6 micron band of O₃, the 25 micron "window" region, and the wings of the vibration-rotation band of H₂O, respectively. Over these spectral regions, band fluxes are evaluated with the help of band transmissivities precalculated from the narrow-band model of *Morcrette and Fouquart (1985)* -- See Appendix of *Morcrette et al. (1986)* for details --.

Integration of (2.5) over wavenumber ν within the k -th spectral region gives the upward and downward fluxes as

$$F_k^+(\rho) = [B_k(T_p) - B_k(T_{0,\downarrow})] t_{B_k}(ru(\rho, \rho), T_u(\rho, \rho)) + B_k(T_p) + \int_{p'}^{\rho} t_{dB_k}(ru(\rho, p'), T_u(\rho, p')) dB_k \quad (2.7a)$$

$$F_k^-(\rho) = [B_k(T_{0,\uparrow}) - B_k(T_{\downarrow})] t_{B_k}(ru(\rho, 0), T_u(\rho, 0)) - B_k(T_p) - \int_p^0 t_{dB_k}(ru(p', \rho), T_u(p', \rho)) dB_k \quad (2.7b)$$

The formulation accounts for the different temperature dependences involved in atmospheric flux calculations, namely that on T_p , the temperature at the level where fluxes are calculated, and that on T_u , the temperature that governs the transmission through the temperature dependence of the intensities and half-widths of the lines absorbing in the concerned spectral region. The band transmissivities are non-

isothermal accounting for the temperature dependence that arises from the wavenumber integration of the product of the monochromatic absorption and the Planck function. Two normalized band transmissivities are used for each absorber in a given spectral region: the first one for calculating the first r.h.s. term in (2.5), involving the boundaries; it corresponds to the weighted average of the transmission function by the Planck function

$$t_B(\overline{u_p}, T_p, T_u) = \frac{\int_{\nu_1}^{\nu_2} B_\nu(T_p) t_\nu(\overline{u_p}, T_u) d\nu}{\int_{\nu_1}^{\nu_2} B_\nu(T_p) d\nu} \quad (2.8a)$$

the second one for calculating the integral terms in (2.5) is the weighted average of the transmission function by the derivative of the Planck function

$$t_{dB}(\overline{u_p}, T_p, T_u) = \frac{\int_{\nu_1}^{\nu_2} B_\nu(T_p) t_\nu(\overline{u_p}, T_u) d\nu}{\int_{\nu_1}^{\nu_2} B_\nu(T_p/dT) d\nu} \quad (2.8b)$$

where $\overline{u_p}$ is the pressure weighted amount of absorber.

In the scheme, the actual dependence on T_p is carried out explicitly in the Planck functions integrated over the spectral regions. Although normalized relative to $B(T_p)$ or $dB(T_p/dT)$, the transmissivities still depend on T_u , both through Wien's displacement of the maximum of the Planck function with temperature and through the temperature dependence of the absorption coefficients. For computational efficiency, the transmissivities have been developed into Padé approximants

$$t(\overline{u_p}, T_u) = \frac{\sum_{l=0}^2 C_l u_{eff}^{l/2}}{\sum_{l=0}^2 D_l u_{eff}^{l/2}} \quad (2.9)$$

where $u_{eff} = r \overline{u_p} f(T_u, \overline{u_p})$ is an effective amount of absorber which incorporates the diffusivity factor r , the weighting of the absorber amount by pressure $\overline{u_p}$ the temperature dependence of the absorption coefficients, with

$$f(T_u, \overline{u_p}) = \exp[a(\overline{u_p})(T_u - 250) + b(\overline{u_p})(T_u - 250)^2] \quad (2.10)$$

The temperature dependence due to Wien's law is incorporated although there is no explicit variation of

the coefficients C_i and D_j with temperature. These coefficients have been computed for temperatures between 187.5 and 312.5 K with a 12.5 K step, and transmissivities corresponding to the reference temperature the closest to the pressure weighted temperature T_g are actually used in the scheme.

2.2.3 The incorporation of the effects of clouds

The incorporation of the effects of clouds on the longwave fluxes follows the treatment discussed by *Washington and Williamson (1977)*. Whatever the state of cloudiness of the atmosphere, the scheme starts by calculating the fluxes corresponding to a clear-sky atmosphere and stores the terms of the energy exchange between the different levels (the integrals in (2.5)). Let $F_0^+(i)$ and $F_0^-(i)$ be the upward and downward clear-sky fluxes. For any cloud layer actually present in the atmosphere, the scheme then evaluates the fluxes assuming a unique overcast cloud of unity emissivity. Let $F_n^+(i)$ and $F_n^-(i)$ the upward and downward fluxes when such a cloud is present in the n -th layer of the atmosphere. Downward fluxes above the cloud and upward fluxes below it have kept their clear-sky values

$$\begin{aligned} F_n^+(i) &= F_0^+(i) \quad \text{for } i \leq n \\ F_n^-(i) &= F_0^-(i) \quad \text{for } i > n \end{aligned} \quad (2.11)$$

Upward fluxes above the cloud ($F_n^+(k)$ for $k \geq n+1$) and downward fluxes below it ($F_n^-(k)$ for $k > n$) can be expressed with expressions similar to (2.5) provided the boundary terms are now replaced by terms correspond to possible temperature discontinuities between the cloud and the surrounding air.

$$\begin{aligned} F_n^+(k) &= [F_{cloud}^+ - B(n-1)] t(p_k, p_{n+1}; r) + B(k) + \int_{p_{n-1}}^{p_k} t(p_k, p'; r) dB \\ F_n^-(k) &= [F_{cloud}^- - B(n)] t(p_k, p_n; r) + B(k) + \int_{p_k}^{p_n} t(p', p_k; r) dB \end{aligned} \quad (2.12)$$

where $B(i)$ is now the total Planck function (integrated over the whole longwave spectrum) at level i , and F_{cloud}^+ and F_{cloud}^- are the fluxes at the upper and lower boundaries of the cloud. Terms under the integrals correspond to exchange of energy between layers in clear-sky atmosphere and have already been computed in the first step of the calculations. This step is repeated for all cloudy layers. The fluxes for the actual atmosphere (with semi-transparent, fractional and/or multi-layered clouds) are derived from a linear combination of the fluxes calculated at the previous steps with some cloud overlap assumption in the case of clouds present in several layers. Let C be the index of the layer containing the highest cloud. C_i the fractional cloud cover in layer i , with $C_0 = 1$ for the upward flux at the surface, and with C_{N+1}

= 1 and $F_{N+1}^- = F_0^-$ to have the right boundary condition for downward fluxes above the highest cloud.

For example, for a cloud random overlap assumption, the cloudy upward (F^+) and downward (F^-) fluxes are obtained as

$$\begin{aligned}
 F^+(i) &= F_0^+(i) && \text{for } i = 1 \\
 F^+(i) &= C_{i-1}(i) + \int_{n=0}^{i-2} C_n F_n^+(i) \prod_{l=n+1}^{i-1} (1 - C_l) && \text{for } 2 \leq i \leq N+1 \\
 F^+(i) &= C_N(i) + \int_{n=0}^{N-1} C_n F_n^+(i) \prod_{l=n+1}^N (1 - C_l) && \text{for } i \geq N+2
 \end{aligned} \tag{2.13}$$

In case of semi-transparent clouds, the fractional cloudiness entering the calculations is an effective cloud cover equal to the product of the emissivity by the horizontal coverage of the cloud layer, with the emissivity related to the cloud liquid water amount by

$$\varepsilon_{cloud} = 1 - \exp(-K_{obs} \mu_{LWP}) \tag{2.14}$$

where K_{obs} is the liquid water mass absorption coefficient set to $158 \text{ m}^2 \text{ kg}^{-1}$ according to *Stephens* (1978, 1979).

2.3 SHORTWAVE RADIATION

The rate of atmospheric heating by absorption and scattering of shortwave radiation is

$$\frac{\partial T}{\partial t} = - \frac{g}{C_p} \frac{\partial F}{\partial p} \tag{2.15}$$

where F is the net total shortwave flux.

$$F(\delta) = \int_0^\infty d\nu \int_0^{2\pi} d\phi \int_{-1}^{+1} \mu L_\nu(\delta, \mu, \phi) d\mu d\phi \tag{2.16}$$

is the diffuse radiance at wavenumber ν , in a direction given by ϕ the azimuth angle and $\mu = \cos \theta$ with θ the zenith angle. In (2.16), we assume a plane parallel atmosphere, and the vertical coordinate is the optical depth δ a convenient variable when the energy source is outside the medium

$$\delta(p) = \int_p^0 \beta_\nu(p) dp \tag{2.17}$$

$\beta_\nu^{ext}(p)$ is the extinction coefficient equal to the sum of the scattering coefficient β_ν^{scat} of the aerosol or

cloud particle absorption coefficient β_v^{abs} , and of the purely molecular absorption coefficient k_v . The diffuse radiance L_v is governed by the radiation transfer equation

$$\begin{aligned} \mu \frac{dL_v(\delta, \mu, \phi)}{d\delta} - L_v(\delta, \mu, \phi) - \frac{\bar{\omega}_v(\delta)}{4} P_v(\delta, \mu, \phi, \mu_0, \phi_0) E_v^0 e^{-\frac{\delta}{\mu_0}} \\ - \frac{\bar{\omega}_v(\delta)}{4} \int_0^{2\pi} \int_{-1}^{+1} P_v(\delta, \mu, \phi, \mu', \phi') L_v(\delta, \mu', \phi') d\mu' d\phi' \end{aligned} \quad (2.18)$$

E_v^0 is the incident solar irradiance in the direction $\mu_0 = \cos \theta_0$, $\bar{\omega}_v$ is the single scattering albedo ($= \beta_v^{scat}/K_v$) and $P(\delta, \mu, \phi, \mu', \phi')$ is the scattering phase function which defines the probability that radiation coming from direction (μ', ϕ') is scattered in direction (μ, ϕ) . The shortwave part of the scheme, originally developed by *Fouquart and Bonnel* (1980) solves the radiation transfer equation and integrates the fluxes over the whole shortwave spectrum between 0.2 and 4 microns. Upward and downward fluxes are obtained from the reflectances and transmittances of the layers, and the photon path distribution method allows to separated the parametrization of the scattering processes from that of the molecular absorption.

2.3.1 Spectral integration

Solar radiation is attenuated by absorbing gases, mainly water vapour, carbon dioxide, oxygen and ozone, and scattered by molecules (Rayleigh scattering), aerosols and cloud particles. Since scattering and molecular absorption occur simultaneously, the exact amount of absorber along the photon path length is unknown, and band models of the transmission function cannot be used directly as in longwave radiation transfer (see 2.2). The approach of the photon path distribution method is to calculate the probability $p(U) dU$ that a photon contributing to the flux F_c in the conservative case (i.e., no absorption, $\bar{\omega}_v = 1$, $k_v = 0$) has encountered an absorber amount between U and $U + dU$. With this distribution, the radiative flux at wavenumber ν is related to F_c by

$$F_\nu = F_c \int_0^\infty p(U) \exp(-k_\nu U) dU \quad (2.19)$$

and the flux averaged over the spectral interval $\Delta\nu$ can then be calculated with the help of any band model of the transmission function $t_{\Delta\nu}$

$$F = \frac{1}{\Delta\nu} \int_{\Delta\nu} F_\nu d\nu = F_c \int_0^\infty p(U) t_{\Delta\nu}(U) dU \quad (2.20)$$

To find the distribution function $p(U)$, the scattering problem is solved first, by any method, for a set of arbitrarily fixed absorption coefficients k_1 , thus giving a set of simulated fluxes F_{k_1} . An inverse Laplace transform is then performed on (2.19) to get $p(U)$ (Fouquart, 1974). The main advantage of the method is that the actual distribution $p(U)$ is smooth enough that (2.19) gives accurate results even if $p(U)$ itself is not known accurately. In fact, $p(U)$ needs not be calculated explicitly as the spectrally integrated fluxes are

$$F = F_c t_{\Delta\nu}(\langle U \rangle) \quad \text{in the limiting case of weak absorption}$$

$$F = F_c t_{\Delta\nu}(\langle U^{\mu} \rangle) \quad \text{in the limiting case of strong absorption}$$

where $\langle U \rangle = \int_0^{\infty} p(U) U dU$ and $\langle U^{\mu} \rangle = \int_0^{\infty} p(U) U^{\mu} dU$.

The atmospheric absorption in the vapour bands is generally strong, and the scheme determines an effective absorber amount U_e between $\langle U \rangle$ and $\langle U^{\mu} \rangle$ derived from

$$U_e = \ln(F_{k_e}/F_c)/k_e \quad (2.21)$$

where k_e is an absorption coefficient chosen to approximate the spectrally averaged transmission of the clear-sky atmosphere

$$k_e = \frac{1}{U_{tot}/\mu_0} \ln(t_{\Delta\nu}(U_{tot}/\mu_0)) \quad (2.22)$$

where U_{tot} is the total amount of absorber in a vertical column and $\mu_0 = \cos \phi_0$. Once the effective absorber amounts of H_2O and uniformly mixed gases are found, the transmission functions are computed using Padé approximants

$$t_{\Delta\nu}(U) = \frac{\sum_{i=0}^N a_i U^{i-1}}{\sum_{j=0}^N b_j U^{j-1}} \quad (2.23)$$

Absorption by ozone is also taken into account, but since ozone is located at low pressure levels for which molecular scattering is small and Mie scattering is negligible, interactions between scattering processes and ozone absorption are neglected. Transmission through ozone is computed using 3.100 where U_{O_3} the amount of ozone is

$$U_{O_3}^d = M \int_p^0 dU_{O_3} \quad \text{for the downward transmission of the direct solar beam,}$$

$$U_{O_3}^d = M \int_{p_s}^0 dU_{O_3}(p_s) \quad \text{for the upward transmission of the diffuse radiation;}$$

$r = 1.66$ is the diffusivity factor (see 3.), and M is magnification factor (Rodgers, 1967) used instead of μ_0 to account for the sphericity of the atmosphere at very small solar elevations

$$M = 35 / \sqrt{1224 \mu_0^2 + 1} \quad (2.24)$$

To perform the spectral integration, it is convenient to discretize the solar spectral interval into subintervals in which the surface reflectance can be considered as constant. Since the main cause of the important spectral variation of the surface albedo is the sharp increase in the reflectivity of the vegetation in the near infrared, and since water vapour does not absorb below $0.68 \mu\text{m}$, the shortwave scheme considers two spectral intervals, one for the visible ($0.2 - 0.68 \mu\text{m}$), one for the near infrared ($0.68 - 4.0 \mu\text{m}$) parts of the solar spectrum. This cut-off at $0.68 \mu\text{m}$ also makes the scheme more computationally efficient, inasmuch as the interactions between gaseous absorption (by water vapour and uniformly mixed gases) and scattering processes are accounted for only in the near-infrared interval.

2.3.2 Vertical integration

Contrarily to the scheme of Geleyn and Hollingsworth (1979), the fluxes are not obtained through the solution of a system of linear equations in a matrix form. Rather, assuming an atmosphere divided into N homogeneous layers, the upward and downward fluxes at a given layer interface j are given by

$$F^-(j) = F_0 \prod_{k=j}^N T_b(k)$$

$$F^+(j) = F^-(j) j R_t(j-1) \quad (2.25)$$

where $R_t(j)$ and $T_b(j)$ are the reflectance at the top and the transmittance at the bottom of the j -th layer. Computations of R_t 's start at the surface and work upward, whereas those of T_b 's start at the top of the atmosphere and work downward. R_t and T_b account for the presence of cloud in the layer

$$R_t = C R_{cdy} + (1 - C) R_{clr}$$

$$T_b = C T_{cdy} + (1 - C) T_{clr} \quad (2.26)$$

clr and cdy respectively refer to the clear-sky and cloudy fractions of the layer, and C is the cloud fractional coverage.

2.3.2.1 Cloudy fraction of the layer

$R_{t,cb}$ and $T_{b,cb}$ are the reflectance at the top and transmittance at the bottom of the cloudy fraction of the layer calculated with the Delta-Eddington Approximation. Given δ_c , δ_a , and δ_g , the optical thickness for the cloud, the aerosol and the molecular absorption ($= k_a U$), and g_c and g_a the cloud and aerosol asymmetry factors, $R_{t,cb}$ and $T_{b,cb}$ are calculated as functions of the total optical thickness of the layer

$$\delta = \delta_c + \delta_a + \delta_g$$

of the total single scattering albedo

$$\omega^* = \frac{\delta_c + \delta_a}{\delta_c + \delta_a + \delta_g} \quad (2.27)$$

of the total asymmetry factor

$$g^* = \frac{\delta_c}{\delta_c + \delta_a} g_c + \frac{\delta_a}{\delta_c + \delta_a} g_a$$

of the reflectance R_- of the underlying medium (surface or layers below the j -th interface), and of an effective solar zenith angle $\mu_e(j)$ which accounts for the decrease of the direct solar beam and the corresponding increase of the diffuse part of the downward radiation by the upper scattering layers.

$$\mu_e(j) = [(1 - C^{al}(j)) / \mu + rC^{al}(j)]^{-1} \quad (2.28)$$

with

$$C^{al}(j) = 1 - \prod_{i=j+1}^N (1 - C(i) E(i))$$

and

$$E(i) = 1 - \exp \left[- \frac{(1 - \omega_c(i) g_c(i)^2) \delta_c(i)}{\mu} \right] \quad (2.29)$$

$\delta_c(i)$, $\omega_c(i)$ and $g_c(i)$ are the optical thickness, single scattering albedo and asymmetry factor of the cloud in the i -th layer, and r is the diffusivity factor. The scheme follows the Eddington Approximation first proposed by *Shettle and Weinman* (1970), then modified by *Joseph et al.* (1976) to account more accurately for the large fraction of radiation directly transmitted in the forward scattering peak in case of highly asymmetric phase functions. Eddington's approximation assumes that, in a scattering medium of optical thickness τ^* , of single scattering albedo ω , and of asymmetry factor g , the radiance L entering (2.18) can be written as

$$L(\delta, \mu) = L_0(\delta) + \mu L_1(\delta) \quad (2.30)$$

In that case, when the phase function is expanded as a series of associated Legendre functions, all terms of order greater than one vanish when (2.18) is integrated over μ and ϕ . The phase function is therefore given by

$$P(\theta) = 1 + \beta_1(\theta) \cos \theta$$

where θ is the angle between incident and scattered radiances. The integral in (2.18) thus becomes

$$\int_0^{2\pi} \int_{-1}^{+1} P(\mu, \phi, \mu', \phi') L(\mu', \phi) d\mu' d\phi' = 4\pi(L_0 + \pi L_1) \quad (2.31)$$

where

$$g = \frac{\beta_1}{3} = \frac{1}{2} \int_{-1}^{+1} P(\theta) \cos \theta d(\cos \theta)$$

is the asymmetry factor.

Using (2.31) in (2.18) after integrating over μ and dividing by 2π , we get

$$\begin{aligned} \mu \frac{d(L_0 + \mu L_1)}{d\delta} = & - (L_0 + \mu L_1) + \omega (L_0 + g \mu L_1) \\ & + \frac{1}{4} \omega F_0 \exp(-\delta/\mu_0) (1 + 3g \mu_0 \mu) \end{aligned} \quad (2.32)$$

We obtain a pair of equations for L_0 and L_1 by integrating (2.32) over μ

$$\frac{dL_0}{d\delta} = -3(1 - \omega)L_0 + \frac{3}{4} \omega F_0 \exp(-\delta/\mu_0) \quad (2.33)$$

$$\frac{dL_1}{d\delta} = -(1 - \omega g)L_1 + \frac{3}{4} \omega g \mu_0 F_0 \exp(-\delta/\mu_0) \quad (2.34)$$

For the cloudy layer assumed non-conservative ($w < 1$), the solutions to (2.33) and (2.34), for $0 \leq \delta \leq \delta^*$, are

$$\begin{aligned} L_0(\delta) &= C_1 \exp(-k\delta) + C_2 \exp(+k\delta) - \alpha \exp(-\delta/\mu_0) \\ L_1(\delta) &= p (C_1 \exp(-k\delta) - C_2 \exp(+k\delta)) - \beta \exp(-\delta/\mu_0) \end{aligned} \quad (2.35)$$

where

$$\begin{aligned}
k &= [3(1-\omega)(1-\omega g)]^{1/4} \\
p &= [3(1-\omega)/(1-\omega g)]^{1/4} \\
\alpha &= 3\omega F_0 \mu_0^2 [1 + g(1-\omega)] / 4(1 - k^2 \mu_0^2) \\
\beta &= 2\omega F_0 \mu_0 [1 + 3g(1-\omega) \mu_0^2] / 4(1 - k^2 \mu_0^2)
\end{aligned}$$

The two boundary conditions allow to solve the system for C_1 and C_2 ; the downward directed diffuse flux at the top of the layer is zero, i.e.,

$$F^-(0) = \left[L_0(0) + \frac{2}{3} L_1(0) \right] = 0$$

which translates into

$$(1 + 2p/3) C_1 + (1 - 2p/3) C_2 = \alpha + 2\beta/3 \quad (2.36)$$

the upward direction flux at the bottom of the layer is equal to the product of the downward directed diffuse and direct fluxes and the corresponding diffuse and direct reflectances (R_d and R_- , respectively) of the underlying medium

$$\begin{aligned}
F^+(\delta^*) &= \left[L_0(\delta^*) - \frac{2}{3} L_1(\delta^*) \right] \\
&= R_- \left[L_0(\delta^*) + \frac{2}{3} L_1(\delta^*) \right] + R_d \mu_0 F_0 \exp(-\delta^*/\mu_0)
\end{aligned}$$

which translates into

$$\begin{aligned}
&(1 - R_- - 2(1 + R_-) p/3) C_1 \exp(-k\delta^*) \\
&+ (1 - R_- + 2(1 + R_-) p/3) C_2 \exp(+k\delta^*) \\
&= ((1 - R_-) \alpha - 2(1 + R_-) \beta/3 + R_d \mu_0 F_0) \exp(-\delta^*/\mu_0)
\end{aligned} \quad (2.37)$$

In the Delta-Eddington approximation, the phase function is approximated by a Dirac delta function forward scatter peak and a two-term expansion of the phase function

$$P(\theta) = 2f(1 - \cos \theta) + (1 - f)(1 + 3g' \cos \theta)$$

where f is the fractional scattering into the forward peak and the g' the asymmetry factor of the truncated phase function. As shown by *Joseph et al.* (1976), these parameters are

$$\begin{aligned}
f &= g^2 \\
g' &= g/(1 + g)
\end{aligned} \quad (2.38)$$

The solution of the Eddington's equations remains the same provided that the total optical thickness, single scattering albedo and asymmetry factor entering (2.32)-(2.37) take their transformed values

$$\begin{aligned}\delta' &= (1 - \omega f) \delta^* \\ \omega' &= \frac{(1 - f) \omega}{1 - \omega f}\end{aligned}\quad (2.39)$$

Practically, the optical thickness, single scattering albedo, asymmetry factor, and solar zenith angle entering (2.36)-(2.39) are δ^* , ω^* , g^* and u^e defined in (2.27) and (2.28).

2.3.2.2. Clear-sky fraction of the layers

In the clear-sky fraction of the layers, the shortwave scheme accounts for scattering and absorption by molecules and aerosols. As the optical thickness for both Rayleigh and aerosol scattering is small, $R_{clr}(j-1)$ and $T_{clr}(j)$, the reflectance at the top and transmittance at the bottom of the j -th layer can be calculated using respectively a first and a second-order expansion of the analytical solutions of the two-stream equations similar to that of *Coakley and Chylek (1975)*. For Rayleigh scattering, the optical thickness, single scattering albedo and asymmetry factor are respectively δ_R , $W_R = 1$, and $g_r = 0$, so that

$$\begin{aligned}R_R &= \frac{\delta_R}{(2\mu + \delta_R)} \\ T_R &= \frac{2\mu}{(2\mu + \delta_R)}\end{aligned}\quad (2.40)$$

The optical thickness τ of an atmospheric layer is simply

$$\delta_R = \delta_R^* (p(j) - p(j-1)) / P_{surf}$$

where δ_R^* is the Rayleigh optical thickness of the whole atmosphere parametrized as a function of the solar zenith angle (*Deschamps et al., 1983*)

$$\delta_R^* = \sum_{i=0}^5 a_i \mu_0^{i-1}$$

For aerosol scattering and absorption, the optical thickness, single scattering albedo and asymmetry factor are respectively δ_a , w_a (with $1 - w_a \ll 1$) and g_a , so that

$$\begin{aligned}den &= 1 + (1 - w_a + back(\mu_a)w_a) \delta_a / \mu_a \\ &+ (1 - w_a) (1 - w_a + 2 back(\mu_a)w_a) \delta_a^2 / \mu_a^2\end{aligned}$$

$$R(\mu_e) = \frac{\text{back}(\mu_e) \omega_a \delta_a / \mu_e}{\text{den}} \quad (2.41)$$

$$T(\mu_e) = \frac{1}{\text{den}}$$

where $\text{back}(\mu_e) = (2 - 3 \mu_e g_a) / 4$ is the backscattering factor.

Practically, R_{clr} and T_{clr} are computed using (2.41) and the combined effect of aerosol and Rayleigh scattering comes from using modified parameters corresponding to the addition of the two scatterers with provision for the highly asymmetric aerosol phase function through Delta-approximation of the forward scattering peak (as in (2.38)-(2.39))

$$\delta^* = \delta_R + \delta_a (1 - \omega_a g_a^2)$$

$$g_* = \frac{g_a}{1 + g_a} \frac{\delta_a}{(\delta_R + \delta_a)} \quad (2.42)$$

$$\omega^* = \frac{\delta_R}{\delta_R + \delta_a} \omega_R + \frac{\delta_a}{\delta_R + \delta_a} \frac{\omega_a (1 - g_a^2)}{1 - \omega_a g_a^2}$$

As for their cloudy counterparts, R_{clr} and T_{clr} must account for the multiple reflections due to the layers underneath

$$R_{clr} = R(\mu_e) + (R_- T(\mu_e)) / (1 - R^* R_-)$$

$$T_{clr} = T(\mu_e) / (1 - R^* R_-) \quad (2.43)$$

with $R^* = R(1/r)$ and $T^* = T(1/r)$

and R_- is the reflectance of the underlying medium $R_- = R_j(j-1)$ and r is the diffusivity factor.

Since interactions between molecular absorption and Rayleigh and aerosol scattering are negligible, the radiative fluxes in a clear-sky atmosphere are simply those calculated from (2.25) and (2.43) attenuated by the gaseous transmissions (2.23).

2.3.3 Multiple reflections between layers

To deal properly with the multiple reflections between the surface and the cloud layers, it should be necessary to separate the contribution of each individual reflecting surface to the layer reflectances and

transmittances inasmuch as each such surface gives rise to a particular distribution of absorber amount. In case of an atmosphere including N cloud layers, the reflected light above the highest cloud consists of photons directly reflected by the highest cloud without interaction with the underlying atmosphere, and of photons that have passed through this cloud layer and undergone at least one reflection on the underlying atmosphere. In fact, (2.20) should be written

$$F = \sum_{i=0}^N F_{cl} \int_0^{\infty} p_i(U) t_{\Delta v}(U) dv \quad (2.44)$$

where F_{cl} and $p_i(U)$ are the conservative fluxes and the distributions of absorber amount corresponding to the different reflecting surfaces.

Fouquart and Bonnel (1980) have shown that a very good approximation to this problem is obtained by evaluating the reflectance and transmittance of each layer (using (2.37) and (2.43)) assuming successively a non-reflecting underlying medium ($R_- = 0$), then a reflecting underlying medium ($R_- \neq 0$). First calculations provide the contribution to reflectance and transmittance of those photons interacting only with the layer into consideration, whereas the second ones give the contribution of the photons with interactions also outside the layer itself.

From those two sets of layer reflections and transmittances (T_{to} , T_{bo}) and (R_{ts} , T_{bs}) respectively, effective absorber amounts to be applied to computing the transmission functions for upward and downward fluxes are then derived using (3.8) and starting from the surface and working the formulas upward

$$\begin{aligned} U_{e0}^- &= \ln (T_{bo}/T_{bc})/k_e \\ U_s^- &= \ln (T_{bs}/T_{bc})/k_e \\ U_{e0}^+ &= \ln (R_{to}/R_{tc})/k_e \\ U_{es}^+ &= \ln (R_{ts}/R_{tc})/k_e \end{aligned} \quad (2.45)$$

where R_{tc} and T_{bc} are the layer reflectance and transmittance corresponding to a conservative scattering medium.

Finally the upward and downward fluxes are obtained as

$$F^+(j) = F_0 [R_{to} t_{\Delta v}(U_{e0}^+) + (R_{ts} - R_{to}) t_{\Delta v}(U_{es}^+)] \quad (2.46a)$$

$$F^-(j) = F_0 [T_{bo} t_{\Delta v}(U_{e0}^-) + (T_{bs} - T_{bo}) t_{\Delta v}(U_{es}^-)] \quad (2.46b)$$

2.3.4 Cloud shortwave optical properties

As seen in section 3.2.1, the cloud radiative properties depend on three different parameters: the optical thickness δ_c , the asymmetry factor g_c , and the single scattering albedo ω_c .

δ_c is related to the cloud liquid water amount u_{LWP} by

$$\delta_c = \frac{3 u_{LWP}}{2 r_e} \quad (2.47)$$

where r_e is the mean effective radius of the size distribution of the cloud droplets. Presently r_e is fixed to 15 μm , but this radius may vary with height from 5 μm in the planetary boundary layer to 40 μm at 100 hPa, in an empirical attempt at dealing with the variation of cloud type with height. Smaller water droplets are observed with the variation of cloud type with height. Smaller water droplets are observed in low-level stratiform clouds whereas larger particles are found in cumuliform and cirriform clouds.

In the two spectral intervals of the shortwave radiation scheme, g_c is fixed to 0.865 and 0.910, respectively, and ω_c is given as a function of μ_c following *Fouquart (1987)*

$$\begin{aligned} \omega_{c1} &= 0.9999 - 5 \times 10^{-4} \exp(-0.5 \delta_c) \\ \omega_{c2} &= 0.9988 - 2.5 \times 10^{-3} \exp(-0.05 \delta_c) \end{aligned} \quad (2.48)$$

These cloud shortwave radiative parameters have been fitted to *in situ* measurements of stratocumulus clouds (*Bonnel et al., 1983*).

2.4 HORIZONTAL INTERPOLATION

In order to cut down the computing costs of the 'full radiation time steps' for frequent calculations (e.g. with diurnal cycle) the option of a spatial interpolation has been introduced in the code and will be described briefly.

The interpolation is done only in the zonal direction because of the strong meridional variation of radiative processes and the internal organisation of the model code. For each row, variables relevant to the input of the radiation calculation are transformed to a coarser subgrid via Fourier transformation, truncation in Fourier space and a subsequent inverse Fourier transform. On this coarser grid, fluxes are then evaluated as described in the previous sections. Finally, effective transmissivities and emissivities are computed and transformed back to the full resolution of the model via direct and indirect FFTs.

2.5 INPUT TO THE RADIATION SCHEME

2.5.1 Model variables

Temperature values are needed at the boundaries of the layers, where the fluxes are computed. They are derived from the full level temperatures with a pressure weighted interpolation:

$$T_{k+\frac{1}{2}} = T_k \frac{P_k (P_{k+1} - P_{k+\frac{1}{2}})}{P_{k+\frac{1}{2}} (P_{k+1} - P_k)} + T_{k+1} \frac{P_{k+1} (P_{k+\frac{1}{2}} - P_k)}{P_{k+\frac{1}{2}} (P_{k+1} - P_k)} \quad (2.49)$$

At the bottom of the atmosphere, the ground temperature T_g is used, while at the top the model's first full level temperature is used.

2.5.2 Clouds

The cloud prediction scheme allows for four cloud types - convective and three layer clouds (high, middle and low level). The convective cloud can fill any number of model layers, its depth being determined by the convection scheme. The layer clouds can exceed one layer in thickness. The atmosphere is divided into three parts to compute the various components of the cloudiness. No cloud is allowed in the lowest model layer.

Convective cloud

Convective cloud (C_c) is determined from the scaled time-averaged precipitation rate (\bar{P}) from the model's convection scheme using:

$$C'_c = \min (0.8, 0.125 \text{ Log}_e (\bar{P}) - 1.5)$$

$$C_c = 0.4 C'_c \quad (2.50)$$

Base and top heights are also derived from the convection scheme.

High cloud

For high clouds (C_H) the scheme distinguishes between two types of cirrus, that associated with outflow from deep convection, and that associated with frontal disturbances. Anvil cirrus is parameterised using:

$$C_H = 2.0 (C'_c - 0.3) \quad (2.51)$$

provided that convection extends above $\eta = 0.4$ and C'_c exceeds 40%. Extratropical and frontal cirrus is determined from a function of the layer relative humidity (RH_e) after adjustment for the presence of convective clouds:

$$RH_e = RH - C_c \quad (2.52)$$

assuming that the cloudy part, C_c , is saturated

$$C_H = \left\{ \max \left[\frac{RH_e - 0.8}{0.2}, 0 \right] \right\}^2 \quad (2.53)$$

Middle level clouds

Middle level clouds (C_M) are generally characterised by generally moist air and large scale ascent. They are parameterised using relative humidity and vertical velocity (ω).

$$C'_M = \left\{ \max \left[\frac{RH_e - 0.8}{0.2}, 0 \right] \right\}^2 \quad (2.54)$$

$C_M = 0$, if there is subsidence, i.e. $\omega \geq 0$.

There is a linear transition up to a weak ascent

$$C_M = C'_M \omega / \omega_c \quad \text{for } \omega_c \leq \omega \leq 0$$

where ω_c is a critical vertical velocity varying between -0.1 at $\eta = 0.8$ and 0 at $\eta = 0.45$. Otherwise

$$C_L = C'_L.$$

Low level cloud

Low clouds seem to fall predominantly into two classes; those associated with extratropical fronts and tropical disturbances and those that occur in relatively quiescent conditions and are directly associated with the boundary layer. The first class of clouds are diagnosed as the middle level clouds from relative humidity and vertical velocity:

$$C'_L = \left\{ \max \left[\frac{RH_e - 0.7}{0.3}, 0 \right] \right\}^2 \quad 2.55$$

$C_L = 0$ if there is subsidence, i.e. $\omega \geq 0$

There is a linear transition up to a weak ascent

$$C_L = C'_L \omega / \omega_c \quad \text{for } \omega_c \leq \omega \leq 0.$$

where the critical velocity ω_c is $-0.1 \text{ Pa s}^{-1} \equiv 3.6 \text{ hPa hr}^{-1}$.

Otherwise $C_L = C'_L$. Again RH_e is the relative humidity of the environmental air after allowing for convective clouds.

The second class of low level clouds are strongly linked to the boundary layer and are invariably associated with low level inversions in temperature and humidity. They are parameterised using:

$$C'_L = -10 \left(\frac{\Delta v}{\Delta p} \right)_{\min} - 0.9 \quad (2.56)$$

where $(\Delta v/\Delta p)_{\min}$ is the lapse rate (K hPa⁻¹) in the most stable layer below $\eta = 0.8$. An additional dependence on the relative humidity at the base of the inversion has been introduced to prevent cloud forming under dry inversions such as those over deserts and the winter pole.

$$C_L = 0 \quad \text{if} \quad RH_{e,base} < 0.5$$

$$C_L = C'_L \left(1 - \frac{0.7 - RH_{e,base}}{0.2} \right) \quad \text{for} \quad 0.5 < RH_{e,base} < 0.7$$

$$C_L = C'_L \quad \text{otherwise.}$$

The optical properties of the clouds are defined assuming a supersaturation of 5% within the stratiform clouds and a fixed mass mixing ratio of liquid water of 1×10^{-4} kg/kg for the convective clouds.

2.5.3 Aerosols

Although provision is made to have various types of aerosols (oceanic, desert, urban, stratospheric and background), the present operational model uses only one type of aerosol whose concentration depends on height only.

2.5.4 Carbon dioxide and ozone

The carbon dioxide has a constant mass mixing ratio over the whole globe corresponding to a volume concentration of 345 ppmv.

The ozone mixing ratio R_{O_3} depends on height, latitude, longitude and season. Its vertical distribution is assumed to be such that its integral from 0 to the pressure p is:

$$\int_0^p R_{O_3} dp = \frac{a}{1 + (b/p)^{3/2}} \quad 2.57$$

The constants a and b are related to the total amount of ozone and the height of its maximum mixing ratio. They are imposed in terms of a limited series of spherical harmonics for the geographical distribution and a Fourier series for the seasonal variation. The total amount of ozone was taken from *London et al.* (1976) and the altitude of the maximum concentration was derived from *Wilcox and Belmont* (1977). Plots of these values can be found in the Appendix.

2.5.5 Ground albedo

The background land albedo is interpolated to the model grid from the mean annual values of the climatology by *Dorman and Sellers* (1988). A plot of this albedo value is shown in the Appendix.

The sea points all have an albedo of 0.07, while sea ice assigned an albedo of 0.55.

In snow covered areas this background albedo, A_{BL} , is modified taking into account the snow depth and temperature, masking by the vegetation and the presence of ice dew. First, an effective snow cover for the grid box is defined as

$$CVSA = C_v * c_r * C_{v_{sn}} + [1 - C_v + C_v * (1 - c_r)] * CVS_{BL}$$

where c_r specifies the reduction of thermal diffusion under the vegetation ($c_r = 0.5$), $C_{v_{sn}}$ is the fraction of vegetation covered by snow and CVS_{BL} is the snow cover for bare land.

$$CVS_{BL} = \text{Min} \left\{ 1, \frac{Sn}{Sn_{cr}} \right\}$$

$$C_{v_{sn}} = \text{Min} \left\{ 1, \frac{Sn}{z_o} \right\}$$

$$(Sn_{cr} = 0.015m)$$

The albedo of the snow covered part is set to vary between a minimum A_{SNM} ($A_{SNM} = 0.4$) at melting point, and a maximum A_{SND} ($A_{SND} = 0.8$) at temperature $T_o - C_{ST}$ ($C_{ST} = 5C$).

$$A_{s_{snow}} = \text{Min} \left\{ A_{SND}, A_{SNM} + (A_{SND} - A_{SNM}) * \text{Max} \left[0, \left(\frac{T_o - T_s}{C_{ST}} \right) \right] \right\} \quad (2.58)$$

A land albedo, in the absence of ice dew, is defined as

$$A_{SND} = CVSA * A_{s_{snow}} + (1 - CVSA) * A_{s_L}$$

The final albedo is further enhanced by the presence of ice dew,

$$A_s = \text{Min} \left\{ A_{SNO} A_{SND} + (A_{SNO} - A_{SND}) * \text{Max} \left[0, \left(\frac{T_o - T_s}{C_{ST}} \right) \right] * C_I \right\} \quad (2.59)$$

where C_I is the fraction of the grid box covered by the skin reservoir (see equation (3.9)).

Finally this short wave albedo is modified for the parallel solar radiation depending on the cosine of the solar zenith μ :

$$A_s^p = \frac{1 + 0.5\mu_o \left(\frac{1}{A_s} - 1 \right)}{\left[1 + \mu_o \left(\frac{1}{A_s} - 1 \right) \right]^2} \quad (2.60)$$

The thermal emissivity E_T of the surface is assumed to be 0.996 everywhere, giving a thermal albedo A_T of 0.004.

2.5.6 Solar zenith angle

Equations to compute the annual variation of the solar constant I_u , the solar declination δ_s , and the difference between solar time and official time can be found in *Paltridge and Platt* (1976). These equations are used to give the cosine of the solar zenith angle at the ground. Because of the curvature of the earth, the zenith angle is not quite constant along the path of a sun ray. Hence a correction is applied to μ_o^a to give an average μ_o for the atmosphere:

$$\mu_o = \frac{H/a}{\mu_o^a + \frac{H}{a} \left(2 + \frac{H}{a} \right) - \mu_o^a} \quad (2.61)$$

where a is the earth radius and H is the atmospheric equivalent height. H/a is fixed at 0.001277.

When we do not want to have the diurnal cycle, the cosine of the solar zenith angle is computed on 128 points around each latitude circle, and then averaged.

2.6 THE RADIATION CODE

Routine RADHEAT is called at every time step to compute the radiative heating, using the solar zenith angle computed in SOLANG and emissivities and transmissivities (EMTER and TRSOL) computed at full radiation time steps in RADINT. The other routines are called either once at the beginning of the run (SETRAD, AERDIS) or once per full radiation step at the first row (PRERAD, ORBIT, OZONE, AEROSOL), or at every full radiation time step for all rows. In this section, we shall briefly describe the function of each routine.

2.6.1 Definition of constants

SETRAD

This routine provides the interface with the user, via the namelist RADCTL. It defines the constants of Table 2.1.

The partition factor NRPART is necessary because the radiation scheme uses too much workspace to do the computation on a whole latitude line at a time. Therefore the latitude lines are divided into NRPART parts of NRLST points and the computation done on each part separately. The user should insure that the number of points on a latitude line is a multiple of NRPART.

NAME	TYPE	PURPOSE	DEFAULT
LRAD	LOGICAL	Switch for radiation computation	TRUE
LDIUR	LOGICAL	Switch for diurnal cycle	TRUE
NRADFR	INTEGER	Frequency of full radiation computations if (NRADFR.GT.O): RAD every NRADFR time step if (NRADFR.LT.O): RAD every -NRADFR hours	(3 hrs)
NRPART	INTEGER	Partition factor for radiation computations	8
NRINT	INTEGER	Interpolation distance (in points)	4
NRPARTI	INTEGER	Partition factor for radiation interpolation	2
NRADPFR	INTEGER	Print frequency for radiation statistics	(108 hrs)
NRADPLA	INTEGER	Print statistics every NRADPLA latitude lines	15

Table 2.1 Constants controlling the radiation, contained in namelist RADCTL

AERDIS

Routine AERDIS defines the vertical distribution and the optical properties for the globally averaged aerosol model.

PRERAD

This routine sets up some time dependent parameters needed for the radiation calculations. It also calls the subroutine OZONE and if the full aerosol model is used subroutine AEROSOL supplies information about the climatology of the constituents.

ORBIT

Routine ORBIT provides the constants necessary to compute the solar zenith angle, according to the time of day and year and the characteristics of the earth's orbit.

OZONE

This routine computes the Legendre coefficients for the ozone distribution according to the time of year, using the Fourier coefficients defined in DATA statements.

AEROSOL

The geographical distribution of aerosols is defined in this routine, in terms of spectral coefficients.

The routines ORBIT, OZONE and AEROSOL are called only once per full radiation step, at the first row.

2.6.2 Main routines

RADINT

RADINT is called by PHYSC to control the radiation computation. A call to routine SOLANG provides the zenith angle for all points on the considered latitude row. Calls to LEGTRI to compute the Legendre coefficients used to calculate the horizontal distribution of ozone (and optionally aerosols) follow. Next temperature is vertically interpolated and cloud amounts are calculated in a call to CLOUD. Depending on the value of the variable NRINT an interpolation of all input variables to a coarser grid via FFT's may be carried out. It may be necessary to subdivide the latitude belt in a few parts for the actual calculation of radiative fluxes because of storage space limitations. For this reason a loop over these parts follows. Inside this loop the input is transferred to the actual black box workspace and a call to routine RADLSW provides solar and thermal fluxes for a subset of points of that latitude row. These fluxes are converted into transmissivities and emissivities and after completion of the whole latitude circle they are transferred

to the full grid when the calculations are carried out with the coarse resolution.

CLOUD

Routine CLOUD is called by RADINT to compute the cloudiness at each level.

RADSLW

Routine RADSLW is the driver routine of the radiation computation. It computes the solar and thermal fluxes by calling specialised routines LW and SW respectively.

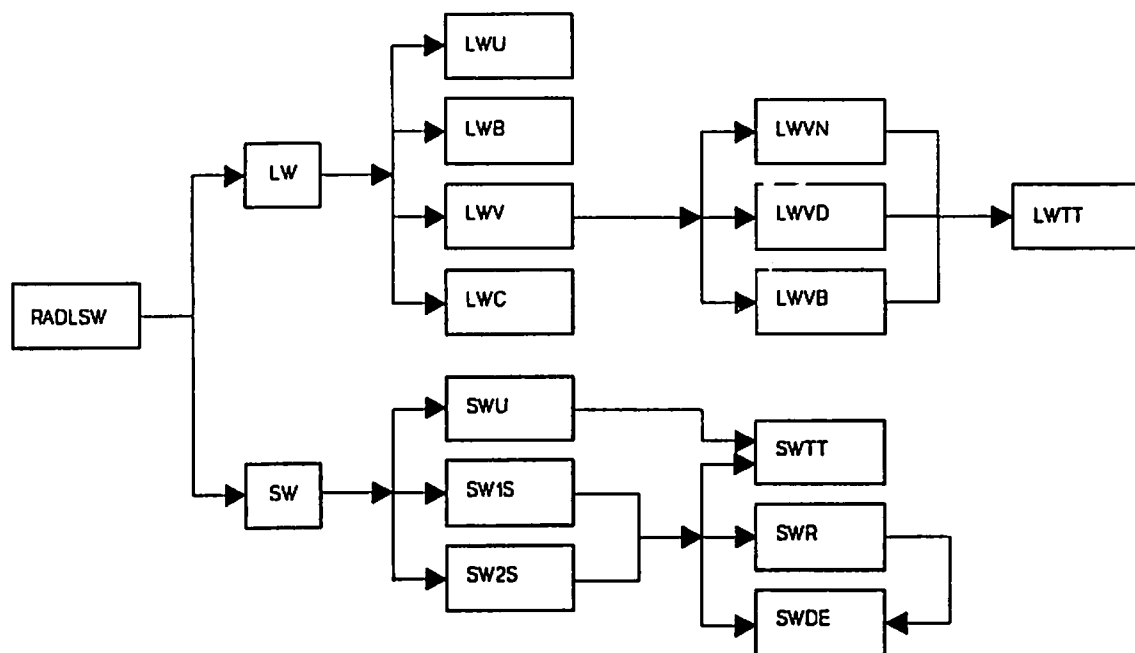


Fig. 2.2 Flowdiagram of main radiation routines

2.6.3 Specialized routines

LEGTRI

This routine computes the Legendre polynomials using recurrence formulae.

SOLANG

This routine computes the solar zenith angle along a latitude circle from the results of routine ORBIT. When the diurnal cycle is switched off, the computation is done on a standard 128 points and averaged. The fraction of the latitude circle which is in daylight is also computed.

LW

LW organizes the longwave computation by calling in turn LWU, LWB and LWV.

LWU

LWU computes the effective absorber amounts including the pressure and temperature dependencies in the spectral intervals of the longwave radiation scheme.

LWB

LWB computes the Planck function and its derivative with relation to temperature for all levels and spectral intervals.

LWV

LWV organizes the vertical integration by calling LWVN which deals with the effect of the layers adjacent to the level of computation of flux, LWVD which deals with the contribution from the more distant layers, and LWVB which computes the boundary terms.

LWTT

LWTT computes the relevant transmission functions.

SW

SW organizes the shortwave computation by calling in turn SWU, SW1S and SW2S.

SWU

SWU computes the effective absorber amounts including the pressure and temperature dependencies of the absorption.

SW1S and SW2S

SW1S and SW2S deal with the shortwave radiation transfer in the two spectral intervals used to describe the solar spectrum. They both call SWR which deals with the conservative scattering processes (Rayleigh) and the scattering/absorption by aerosols, and SWDE which computes the reflectivity and transmissivity of a layer including non-conservative scatterers (cloud particles) with the Delta-Eddington approximation.

SWTT

SWTT computes the relevant transmission functions.

POSTRAD

This routine, called after the last row calculations are performed, completes the optional printout of radiation diagnostics and releases the remaining storage space.

2.6.4 Heating rate computation

RADHEAT

Routine RADHEAT is called at each time step to recompute the net radiative fluxes from the layers' effective emissivity and transmissivity, using the actual temperature and solar angle (given by SOLANG). The vertical derivative of the net fluxes gives then the radiative heating.

REFERENCES

- Bonnell, B., Y. Fouquart, J.-C. Vanhouette, C. Fravallo, and R. Rosset, 1983: Radiative properties of some African and mid-latitude stratocumulus clouds. *Beitr.Phys.Atmos.*, 56, 409-428.
- Coakley, J.A., Jr., and P. Chylek, 1975: The two-stream approximation in radiation transfer: Including the angle of the incident radiation. *J.Atmos.Sci.*, 32, 409-418.
- Deschamps, P.-Y., M. Herman, and D. Tanre, 1983: Modelisation du rayonnement solaire réfléchi par l'atmosphère et la terre, entre 0.35 et 4 microns. Rapport ESA 4393/80/F/DC(SC), 156 pp.
- Elsasser, W.M., 1942: Heat transfer by infrared radiation in the atmosphere. *Harvard Meteorological Studies No.6*, 107 pp.
- Fouquart, Y., 1974: Utilisation des approximants de Padé pour l'étude des largeurs équivalentes de raies formées en atmosphère diffusante. *J. Quant.Spectros. Radiat. Transfer.*, 14, 497-508.
- Fouquart, Y., and B. Bonnell, 1980: Computations of solar heating of the earth's atmosphere: a new parameterization. *Beitr.Phys.Atmos.*, 53, 35-62.
- Fouquart, Y., 1987: Radiative transfer in climate modeling. NATO Advanced Study Institute on Physically-Based Modeling and Simulation of Climate and Climatic Changes, Erice, Sicily, 11-23 May 1986. M.E. Schlesinger, Ed., 223-283.
- Geleyn, J.-F., and A. Hollingsworth, 1979: An economical analytical method for the computation of the interaction between scattering and line absorption of radiation. *Beitr.Phys.Atmos.*, 52, 1-16.
- Joseph, J.H., W.J. Wiscombe, and J.A. Weinman, 1976: The Delta-Eddington approximation for radiative flux transfer. *J.Atmos.Sci.*, 33, 2452-2459.
- London, J., Bojkov, R.D., Oltmans, S. Kelley, J.I. 1976: Atlas of the global distribution of total ozone, July 1957 - June 1967. NCAR Technical Note 113+STR.
- Morcrette, J.-J., and Y. Fouquart, 1985: On systematic errors in parametrized calculations of longwave radiation transfer. *Quart.J.Roy.Meteor.Soc.*, 111, 691-708.
- Morcrette, J.-J., L. Smith, and Y. Fouquart, 1986: Pressure and temperature dependence of the absorption in longwave radiation parameterizations. *Beitr.Phys.Atmos.*, 59, 455-469.
- Rodgers, C.D., and C.D. Walshaw, 1966: The computation of the infrared cooling rate in planetary atmospheres. *Quart.J.Roy.Meteor.Soc.*, 92, 67-92.
- Rodgers, C.D., 1967: The radiative heat budget of the troposphere and lower stratosphere. Report A2, Planetary Circulation Project, Dept. of Meteorology, M.I.T., Cambridge, Mass., 99 pp.
- Shettle, E.P., and J.A. Weinman, 1970: The transfer of solar irradiance through inhomogeneous turbid atmospheres evaluated by Eddington's approximation. *J.Atmos.Sci.*, 27, 1048-1055.
- Stephens, G.L., 1978: Radiative properties of extended water clouds. Parts I and II. *J.Atmos.Sci.*, 35, 2111-2122, 2123-2132.

Stephens, G.L., 1979: Optical properties of eight water cloud types. C.S.I.R.O., Div.Atmos.Phys., Tech. Paper No. 36, 1-36.

Washington, W.M., and D.L. Williamson, 1977: A description of the NCAR GCMs. "GCMs of the atmosphere". Methods in computational physics, Vol. 17, J. Chang, Ed. Academic Press, 111-172.

Wilcox, R.W. and A.D. Belmont, 1977: Ozone concentration by latitude, altitude and month, near 80°W. Report, Control Data Corporation, Contract No.DOT- FA77WA-3999.

CHAPTER 3

Vertical diffusion and interaction with the surface

3.1 THEORY

3.1.1 Basic equations

The parametrization scheme represents the turbulent exchanges with the surface of heat, momentum and moisture and the turbulent transports of the same quantities in the lowest levels of the model. The top of the turbulent layer is computed from a combination of convective and dynamic criteria. Above this boundary layer the scheme only operates when static instability is generated. The equation for the vertical diffusion of any conservative quantity ψ is:

$$\frac{\partial \psi}{\partial t} - \frac{1}{\rho} \frac{\partial}{\partial z} \left(\rho K_{\downarrow} \frac{\partial \psi}{\partial z} \right) - \frac{1}{\rho} \frac{\partial J_{\downarrow}}{\partial z} \quad (3.1)$$

(J_{\downarrow} is positive downwards). K_{\downarrow} is the exchange coefficient and J_{\downarrow} is the vertical turbulent flux of ψ . We have the boundary conditions:

$$K_{\downarrow} \frac{\partial \psi}{\partial z} = 0 \text{ for } p = p_T \quad (3.2a)$$

and

$$K_{\downarrow} \frac{\partial \psi}{\partial z} = C_{\downarrow} |u(z)| (\psi(z) - \psi_s) \text{ for } z = 0 \quad (3.2b)$$

where p_T is the pressure at the top of the boundary layer.

The definition of the drag coefficient C_{\downarrow} is dependent on the height z above the ground at which u and ψ are taken (the natural choice is the model's lowest level) and on the stability of the layer. ψ_s represents a value of ψ at the surface.

ψ may be identified with each of the four variables u, v, q, s which are three of the prognostic variables and the dry static energy defined by

$$s = C_{pd}(1 + (\delta - 1)q) T + g z - C_p T + \phi \quad (3.3)$$

For the latter we simplify the problem by assuming that ϕ remains constant with respect to time during the evolution process (even if in reality T variations would modify $z(p)$). We also avoid a coupling with the vertical diffusion of q by assuming a constant value in time of $C_p(q)$.

Since the thickness of the model layers Δz is small near the ground, in order to avoid numerical instability when $K \frac{2 \Delta t}{(\Delta z)^2} > 1$ the time-stepping procedure must be implicit. The whole interaction with the adiabatic

and other processes, however, cannot be treated implicitly. We elected the following procedures:

Starting from ψ values at $(t-1)$ an implicit treatment of equations (3.1) and (3.3) gives new values $\psi^*(t+1)$.

Dividing the difference $\psi^*(t+1) - \psi(t-1)$ by the time-step ($2\Delta t$ or Δt at the first timestep) the result is added to the adiabatic and radiative tendencies. Thus:

$$\frac{\psi^* - \psi(t-1)}{2\Delta t} = \frac{1}{\rho} \frac{\partial}{\partial z} \left(\rho K_{\psi}^{(t-1)} \frac{\partial \psi^*}{\partial z} \right) \quad (3.4)$$

and

$$K_{\psi}^{(t-1)} \frac{\partial \psi^*}{\partial z} = C_{\psi}^{(t-1)} |u(t-1, z)| (\psi^*(z) - \psi_s(t-1)) \text{ for } z=0 \quad (3.5)$$

replace equations (3.1) and (3.2), where

$$\psi^* = \alpha \psi^* + (1-\alpha) \psi(t-\Delta t)$$

In the model, we have $\alpha=1.5$.

One can see that we do not let ψ_s vary in time for the solution of one system. If nothing else was done, this would mean that the surface sensible and latent heat flux and the surface evaporation (or dew) flux might be inconsistent (on land) with the values for the soil parameters T_s and W_s that we shall forecast for $(t+1)$. This would lead to a numerical instability in T_s and/or W_s for a too long timestep Δt . We can prevent this instability by storing not only the fluxes but also their derivatives with respect to T_s and W_s . The surface routines can then treat the fluxes as linear functions of the soil parameters and a stable (semi-implicit) algorithm can be implemented (see Chapter 6).

The K_{ψ} and C_{ψ} coefficients are assumed to be the same for u and v and also the same for q and s . We shall use m and h as subscript for momentum and heat. Our problem is now reduced to the determination of K_m and K_h (at all boundaries between two atmospheric layers) and C_m and C_h at the surface. This is done solely from atmospheric values at $t-1$ of u, v, T and q and from the surface conditions.

3.1.2 Surface fluxes

The surface fluxes for momentum and dry static energy are parametrized as

$$\begin{aligned}
 J_u &= \rho C_m |u| u^*, \\
 J_v &= \rho C_m |u| v^*, \\
 J_s &= \rho C_h |u| (s^* - s_s),
 \end{aligned}
 \tag{3.6}$$

where C_m is the drag coefficient, C_h the transfer coefficient for heat and $|u|$ the absolute value of the horizontal velocity. C_m, C_h and $|u|$ apply to the lowest model level at $t - \Delta t$. u^*, v^* and s^* are the velocity components and the dry static energy to be computed implicitly for the lowest model level. s_s is the dry static energy at the surface at $t - \Delta t$.

For the moisture flux we distinguish sea and land. Over sea

$$J_q = \rho C_h |u| \{q^* - q_{SAT}(T_s, P_s)\}
 \tag{3.7}$$

where q_{SAT} is the saturation specific humidity at surface temperature T_s and pressure P_s .

Over land, each grid square is divided into 4 fractions:

- (i) fraction C_{sn} covered with snow
- (ii) fraction $(1 - C_{sn}) C_1$ with water in skin reservoir
- (iii) fraction $(1 - C_{sn}) (1 - C_1) (1 - C_v)$ with dry bare soil
- (iv) fraction $(1 - C_{sn}) (1 - C_1) C_v$ with dry vegetation

The snow cover fraction C_{sn} depends on the snow cover Sn :

$$C_{sn} = \min \left(1, \frac{Sn}{Sn_{cr}} \right)
 \tag{3.8}$$

where Sn_{cr} is the critical snow cover (= 0.015m equivalent water depth),

The wet skin fraction C_1 is derived from the skin reservoir water content:

$$C_1 = \min \left(1, \frac{W_1}{W_{1\max}} \right) \quad (3.9)$$

where

$$W_{1\max} = W_{1\max} \{(1-C_v) + C_v L_f\} \quad (3.10)$$

W_1 is the prognostic variable for the skin reservoir content, $W_{1\max}$ is the maximum skin reservoir content, C_v is the vegetation ratio, L_f is the leaf area index (-4), and $W_{1\max}$ is the maximum amount of water that can be held on one layer of leaf or on bare soil ($= 2 \cdot 10^{-4}m$)

The grid fraction C_v occupied by vegetation is equal to the climatological field C_{vcl} (see appendix) except in dry conditions when the vegetation killer is applied:

$$C_v = \min \left(C_{vcl}, C_{vcl} \frac{W}{0.4W_{scap}} \right) \quad (3.11)$$

Quantity W is the total amount of water available in the root zone:

$$W = R_1 W_s + R_2 W_d + R_3 W_{loc} \quad (3.12)$$

where R_i represents the relative contribution of the i^{th} slab reservoir to the evapotranspiration. Operationally we have

$$R_1 = 0.5, \quad R_2 = 0.5, \quad R_3 = 0$$

Evaporation from snow and the skin reservoir is at the potential rate

$$J_q (i), (ii) = \rho C_h |u| \{ q - q_{SAT}(P_s, T_s) \} \quad (3.13)$$

For the evaporation from bare soil (no water in skin reservoirs) it is assumed that the relative humidity h at the surface is related to the water content W_s of the superficial soil layer:

$$J_q (iii) = \rho C_h |u| \{ q - h q_{SAT}(T_s, P_s) \} \quad (3.14)$$

$$h = \max \left\{ 0.5 \left(1 - \cos \frac{\pi W_s}{W_{scap}} \right), \min \left(1, \frac{q}{q_{SAT}(T_s, P_s)} \right) \right\} \quad (3.15)$$

W_{scap} is the field capacity equal to $0.02m$ for a soil layer with $0.07m$ thickness.

The evaporation from dry (no water in skin reservoir) vegetated areas is proportional to the evaporation efficiency E :

$$J \text{ (iv)} = \rho C_h |u| E \{q - q_{SAT}(T_p, P_s)\} \quad (3.16)$$

Based on *Sellers et al.* (1986), E is expressed in

$$E = \frac{1}{1 + \frac{C_H |u| R_{\infty} (PAR)}{F(W)}} \quad (3.17)$$

where $R_{\infty}(PAR)/F(W)$ is the stomatal resistance of the canopy, with a minimum value R_{∞} dependent on the Photosynthesis Active Radiation (PAR) and $F(W)$ an empirical function of the available water in the root zone.

$$1/R_{\infty} = \frac{1}{k c} \left[\frac{b}{d PAR} \ln \left(\frac{d e^{k L_t} + 1}{d+1} \right) - \ln \left(\frac{d + e^{-k L_t}}{d+1} \right) \right] \quad (3.18)$$

where,

$$d = \frac{a+b c}{c PAR}, \quad k = 0.9, \quad L_t = 4, \quad a = 5000 \text{ Jm}^{-3}, \quad b = 10 \text{ Wm}^{-2}, \quad c = 100 \text{ sm}^{-1}$$

and PAR is 55% of the net short wave radiation at the surface. In case of dew deposition ($q > q_{SAT}$) we set $E = 1$. The water stress factor $F(W)$ is

$$F(W) = \begin{cases} 1 & \text{if } W \geq W_{cr} \\ \frac{W - W_{PWP}}{W_{cr} - W_{PWP}} & \text{if } W_{PWP} < W < W_{cr} \\ 0 & \text{if } W \leq W_{PWP} \end{cases} \quad (3.19)$$

W_{cr} is a critical value taken as 60% of the field capacity W_{scwp} , and W_{PWP} is the permanent wilting point taken as 30% of W_{scwp} .

The total evaporation in a grid square combines the four fractions:

$$J_q = \rho C_h |U| \left[(C_{2s} + (1-C_{2s})C_1)\{q - q_{SAT}\} + (1 - C_{2s})(1 - C_1)(1 - C_p)\{q - hq_{SAT}\} \right. \\ \left. (1 - C_m)(1 - C_l) C_v E \{q - q_{SAT}\} \right] \quad (3.20)$$

3.1.3 Definition of the transfer coefficients over land

The method is the one described by *Louis* (1979) and updated following *Louis et al.*, (1982). Let us recall here only the main points.

We start from the Monin-Obukhov similarity theory (without humidity for simplicity). The gradients of wind and internal energy are assumed to be universal functions of a stability parameter.

$$\frac{kz}{u_*} \frac{\partial u}{\partial z} = \phi_m(z/L) \quad (3.21)$$

$$\frac{kz}{s_*} \frac{\partial s}{\partial z} = \phi_h(z/L) \quad (3.22)$$

The stability parameter L is the Obukhov length:

$$L = \frac{u_*^2 s}{k g s_*} \quad (3.23)$$

where k is von Karman's constant ($k=0.4$) and u_* and s_* are scaling parameters derived from the fluxes:

$$\rho u_*^2 = (J_u)_{z=0} = \rho C_m |u|^2 \quad (3.24)$$

$$\rho u_* s_* = (J_s)_{z=0} = \rho C_h |u| (s - s_0) \quad (3.25)$$

Equations (3.21) and (3.22) can be integrated over the lowest model layer, and L eliminated using (3.23) in order to derive C_m and C_h . However, this procedure cannot be done analytically because of the complicated form of ϕ_m and ϕ_h . We have approximated the numerical solutions by analytical expression which, formally, can be written:

$$C_m = \left(\frac{k}{\ln \frac{z}{z_0}} \right)^2 f_m \left(Rf, \frac{z}{z_0} \right) \quad (3.26)$$

and

$$C_h = \left(\frac{k}{\ln \frac{z}{z_0}} \right)^2 f_h \left(Rf, \frac{z}{z_0} \right) \quad (3.27)$$

here the Richardson number Ri is defined as:

$$Ri = \frac{g \Delta z \Delta \theta_v}{c_p \theta_v |\Delta u|^2} \quad (3.28)$$

The roughness length z_0 is a fixed climatological field as described in appendix A1. The functions f_m and f_h must have the correct behaviour near neutrality and in the asymptotic cases of high stability or instability.

a) Near neutrality we have $Ri \rightarrow 0$, $\frac{z}{L} \rightarrow 0$, $\phi_m = 1 + b_m \frac{z}{L}$ and $\phi_h = 1 + b_h \frac{z}{L}$.

We obtain then:

$$\begin{aligned} f_m &= 1 - 2b_m Ri \\ f_h &= 1 - (b_m + b_h) Ri \end{aligned} \quad (3.29)$$

Furthermore, there is some evidence, e.g. *Pandolfo* (1967), that $Ri \sim \frac{z}{L}$ which implies $b_h = 2b_m$. Thus we

have

$$f_m = 1 - 2b Ri \text{ and } f_h = 1 - 3b Ri \quad (3.30)$$

Operationally $b=5$

b) In highly unstable cases we considered only the problem of f_h in the case of vanishing u (free convection case). To have a non zero heat flux, u must vanish from $(u f_h)$ for large negative $(s-s_0)$ (that is for high negative value of Ri). So f_h must behave like $\sqrt{-Ri}$.

The analytical expression chosen for the whole unstable case ($Ri < 0$) is:

$$f_h = 1 - \frac{3b Ri}{1 + C_h \left(\frac{z}{z_0}\right) \sqrt{-Ri}} \quad (3.31)$$

For this free convection case we can write an equation for a new similarity theory, independent of J_u .

$$\frac{z}{s_*} \frac{\partial s}{\partial z} = C \quad (3.32)$$

with

$$s_* = \left[(J/\rho)^2 / \left(\frac{gz}{s} \right) \right]^{1/3}$$

Using Eq. (3.31) for the limit $Ri \rightarrow -\infty$,

$$C_h \left(\frac{z}{z_0} \right) = C \ 3b \left[\frac{k}{\ln \left(\frac{z}{z_0} \right)} \right]^2 \left[\left(\frac{z}{z_0} \right)^{1/3} - 1 \right]^{3/2} \quad (3.33)$$

One can furthermore replace $\left[\left(\frac{z}{z_0} \right)^{1/3} - 1 \right]^{3/2}$ by $\left(\frac{z}{z_0} \right)^{1/2}$ if z is much greater than z_0 , so that

$$C_h \left(\frac{z}{z_0} \right) = C \ 3b \left[\frac{k}{\ln \left(\frac{z}{z_0} \right)} \right]^2 \frac{\sqrt{z}}{z_0} \quad (3.34)$$

In order to avoid numerical problems for high z_0 values that might suppress z one replaces $\frac{z}{z_0}$ by $\frac{z}{z_0} + 1$

in (3.34) and (3.26), (3.27).

Operationally $C=5$.

In the highly unstable case, f_m is not very important since there is little wind shear on which to act. We therefore chose a similar expression to (3.31) with the same denominator to save computing time

$$f_m = 1 - \frac{2 \ b \ Ri}{1 + 3bC \left[\frac{k}{\ln \left(1 + \frac{z}{z_0} \right)} \right]^2 \sqrt{\left(1 + \frac{z}{z_0} \right)} (-Ri)} \quad (3.35)$$

c) Finally in the highly stable case we follow *Ellison* (1957) by combining two equations

$$\phi_m^4 - \frac{z}{L} \phi_m^3 - 1 = 0 \text{ KEYPS equation} \quad (3.36)$$

and

$$\frac{\phi_m}{\phi_h} = \frac{1 - \left(\frac{z}{L}\right) / \phi_m / R_{crit}}{\left(1 - \left[\frac{z}{L} / \phi_m\right]\right)^2} \quad (3.37)$$

The flux Richardson number $Ri_f = \frac{z}{L} / \phi_m$ has its critical value R_{crit} for $Ri \rightarrow \infty$.

For $\frac{z}{L} \rightarrow +\infty$ this gives us

$$f_m \sim 1/\sqrt{Ri} \text{ and } f_h \sim \frac{1}{Ri^{3/2}} \quad (3.38)$$

For lack of better information and to minimise the computing time we chose for the whole stable range ($Ri > 0$) the following expressions

$$f_m = \frac{1}{1 + 2bRi (1 + dRi)^{-1/2}} \quad (3.39)$$

$$f_h = \frac{1}{1 + 3bRi (1 + dRi)^{1/2}} \quad (3.40)$$

d is related to the critical flux Richardson number R_{crit} by

$$R_{crit} = \frac{2}{3d} \quad (3.41)$$

Operationally $d=5$.

A plot of the drag coefficients for heat and momentum, normalized by their value at neutrality, is shown on Fig. 3. 1.

3.1.4 Transfer coefficients over sea

For momentum the same parametrization is used as over land, but now the sea surface roughness length is related to the surface stress according to the Charnock relation

$$z_o = C_{char} \frac{u_*^2}{g} \quad (3.42)$$

with a minimum value of z_o of $1.5 \cdot 10^{-5} m$. The Charnock coefficient C_{char} is 0.018.

Over sea ice ($T_s < -2^\circ C$) a constant value of $z_o = 0.001 m$ is used.

For heat and moisture in unstable conditions an empirical interpolation is used between the free convection limit and the neutral approximation (see *Beljaars and Miller, 1990*).

$$C_h = C_{mn} (1 + C_h^*)^{1/\gamma} \quad (3.43)$$

$$\gamma = 1.25$$

$$C_{mn} = \left(\frac{k}{\ln \frac{z}{z_o}} \right)^2 \quad (3.44)$$

$$C_R = \frac{0.0016 (\Delta\theta_s)^{1/3}}{C_{mn} |u|} \quad (3.45)$$

In stable situations the same formulation is used as over land, with z_o according to (3.42).

3.1.5 Definition of the exchange coefficients

We use the logical extension to the atmosphere of the similarity theory for surface fluxes: the mixing length approach.

$$K_m = l_m^2 \left| \frac{\partial u}{\partial z} \right| f_m(Ri) \quad (3.46)$$

$$K_h = l_h^2 \left| \frac{\partial u}{\partial z} \right| f_h(Ri) \quad (3.47)$$

The functional dependencies of f_m and f_h on Ri are the same as for C_m and C_h except that the term

$$\left(\frac{k}{\ln \frac{z}{z_o}} \right)^2 \left[\left(\frac{z}{z_o} \right)^{1/3} - 1 \right]^{3/2}$$

in (3.33) is replaced by its equivalent

$$\frac{l^2}{(\Delta z)^{3/2} z^{1/2}} \left[\left(\frac{z+\Delta z}{z} \right)^{1/3} - 1 \right]^{3/2} \quad (3.48)$$

The intensity of the vertical diffusion in the atmosphere is dependent on the choice of l_h and l_m . We used the *Blackadar* (1962) solution that goes smoothly from the asymptotic value kz for $z \rightarrow 0$ to a constant value in the high atmosphere.

$$l_m = \frac{kz}{1 + \frac{kz}{\lambda_m}}, \quad l_h = \frac{kz}{1 + \frac{kz}{\lambda_h}} \quad (3.49)$$

We also choose to have a relationship between λ_m, λ_h and d so that the critical flux Richardson number in the atmosphere is 1 (e.g. a balance between shear generation and buoyancy destruction).

$$R_{crit}(z \rightarrow \infty) = \frac{2}{3d} \left(\frac{\lambda_h}{\lambda_m} \right) = 1 \quad (3.50)$$

gives

$$\lambda_h = \lambda_m \frac{\sqrt{3d}}{2}.$$

Operationally $\lambda_m = 160 \text{ m}$.

3.1.6 Definition of the top of the boundary layer

Two levels are computed.

a) First level above the dynamical height (Ekman layer height).

$$h_{dyn} = 0.5 u_* / f \quad (3.51)$$

Equatorwards of 20. degrees f is set to $5 \cdot 10^{-5} \text{ s}^{-1}$.

b) A dry convection level, h_{cnv} , is defined as the lowest level for which $s > s_{ndry}$.

The top of the planetary boundary layer is then given by

$$h_{pbl} = \max(h_{dyn}, h_{cnv}) \quad (3.52)$$

The above formulation takes into account early morning cases (where the dry convective boundary layer starts to develop), where considering $h_{dyn} = h_{cnv}$ would give too strong vertical constraint for the turbulence diffusion.

p_T is then calculated as the pressure of the first model level above h_{pbl} .

3.1.7 Kinetic energy dissipation

The kinetic energy lost by the mean flow through the diffusion process is assumed to go directly into the internal energy of air:

$$\delta T_{\text{dissipation}} = \frac{1}{C_p(q)} e = \frac{1}{C_p(q)} \frac{u^2 + v^2 - (\bar{u}^2 + \bar{v}^2)}{2} \quad (3.53)$$

This procedure by-passes the subgrid scale energy cascade, but it allows us to have a closed energy cycle in the model.

3.2 CODE: Subroutine VDFMAIN

Vertical diffusion, which affects temperature, velocities and humidity, is performed in subroutine VDFMAIN, which is called by PHYSC. VDFMAIN calls a sequence of auxiliary routines which are described here.

3.2.1. Preliminary computation

The first task to be performed is the computation of the dry static energy on the prognostic levels (this is done in VDFMAIN):

$$s_K = C_{pd} \{1 + (\delta - 1) q_K(t-1)\} T_K(t-1) + \phi_K(t-1), K=1, NLEV$$

3.2.2 VDFSURF

VDFSURF calculates boundary conditions including:

- the saturation specific humidity $q_{SAT} \{T_s(t-1), p_s(t-1)\}$ at the surface
- the derivative of the saturation humidity with respect to the surface temperature T_s , i.e. $\frac{\partial q_s}{\partial T_s}$ (for reference see documentation of COND)
- the relative humidity h at the surface according to equation 3.15
- the virtual surface temperature T_{vs}

$$T_{vs} = T_s \left\{ 1 + \left(\frac{1}{e} - 1 \right) h q_{SAT} (T_s, p_s) \right\}$$

- the dry static energy at the surface $s_s(\phi_s=0)$, that is

$$s_s(T_s, q_s) = T_s C_{pd} \{1 + (\delta - 1) h q_{SAT}(T_s, p_s)\}$$

- The stomatal resistance, depending on the short wave net radiation and moisture stress is computed:

$$R_c = R_{co} * [F(W)]^{-1}$$

for use in VDFEVAP.

3.2.3 VDFEXCS

VDFEXCS computes the transfer coefficients between the surface and the lowest model layers including:

- Bulk Richardson numbers
- Neutral transfer coefficients
- $(C_{m,h})^* = C_{m,h} \cdot \alpha \cdot 2\Delta t \cdot g \cdot |u|_{NLEV} \cdot \rho_s$

3.2.4 VDFEVAP

VDFEVAP computes the coefficients of q and q_{SAT} as defined by (3.20) and the dry static energy at the surface.

3.2.5 VDFHGHT

VDFHGHT determines the boundary layer height.

3.2.6 VDFEXCU

VDFEXCU computes the exchange coefficients using the following quantities.

$$|\Delta u|_{K+1/2}^2 = (u_K - u_{K+1})^2 + (v_K - v_{K+1})^2$$

- the bulk Richardson number (Eq.3.11):

$$Ri_{K+1/2} = (\phi_K - \phi_{K+1}) \frac{T_{VD} - T_{VU}}{|\Delta u|_{K+1/2}^2 \frac{1}{2} (T_{VD} + T_{VU})}$$

with

$$T_{VD} = \left[T_K + \left(\frac{\phi_K - \phi_{K+1}}{2} \right) / (C_p)_K \right] \cdot \left[1 + \left(\frac{1}{\epsilon} - 1 \right) q_K \right]$$

and

$$T_{VU} = \left[T_{K+1} - \left(\frac{\phi_{K+1} - \phi_K}{2} \right) / (C_p)_{K+1} \right] \cdot \left[1 + \left(\frac{1}{\epsilon} - 1 \right) q_{K+1} \right]$$

- the squared mixing length (discretisation analogous to Ri) for momentum and heat, accounting for the suppression of turbulence above the *PBL* top in stable conditions.
- Factors needed by the exchange calculations for f_h and f_m in stable and unstable cases respectively as well as a common factor for both cases.

Instead of the exchange coefficients $(K_{m,h})_{K+1/2}$ themselves we compute quantities $(K_{m,h})_{K+1/2}^*$ defined by:

$$(K_{m,h})_{K+1/2}^* = (K_{m,h})_{K+1/2} \propto \rho_{K+1/2} \frac{2 \Delta t g}{|\Delta z|_{K+1/2}}$$

3.2.7 VDFDIFM and VDFDIFH

VDFDIFM and VDFDIFH solve the tridiagonal matrix equation for momentum and dry static energy, moisture respectively.

The diffusion equation in finite differences is solved following *Richtmyer and Morton* (1967, Sect. 8.5):

$$-\frac{A_{K-1}}{\Delta p_K} \frac{\psi_{K-1}^*}{\alpha} + \left(1 + \frac{A_K}{\Delta p_K} + \frac{A_{K-1}}{\Delta p_K}\right) \frac{\psi_K^*}{\alpha} - \frac{A_K}{\Delta p_K} \frac{\psi_{K+1}^*}{\alpha} = \frac{\psi_K}{\alpha}$$

with:

$$A_K = (K_{m,h})_{K+1/2}^*, \quad K < NLEV$$

and, at the bottom:

$$A_{NLEV} = (C_{m,h})^*$$

Following Richtmyer and Morton the equation system (3.42) is solved by elimination back-substitution. For the momentum equations we have the boundary conditions

$$K_m \frac{\partial u^*}{\partial z} = 0 \quad \text{at } p = p_T$$

and

$$u^* = 0 \quad \text{for } z = 0$$

3.2.8 VDFINCR

VDFINCR updates tendencies and sea surface roughness lengths.

The tendencies of u_K and v_K due to vertical diffusion as difference between the result obtained implicitly and the initial values, divided by the timestep are added to the adiabatic ones. As additional result we obtain the kinetic energy dissipation according to equation (3.53) and update the roughness length over sea z_o :

$$z_o = 0.018 \frac{|u| |v|}{g} \cdot C_m$$

Tendencies for q and T are then incremented in the same way as for u and v . Since the heat diffusion worked on the dry static energy there has to be a retransformation to the temperature

$$(\Delta T)_K^* = \frac{s_K^- - s_K}{C_p}$$

where the star denotes that this is only one part of the temperature tendency due to diffusive processes. Neglecting the storage of the kinetic energy dissipation in subgrid scales we have an additional contribution:

$$(\Delta T)_K^{**} = \frac{(e_{kin})_K}{C_p}$$

And a third part is obtained from the variation of enthalpy due to diffusion of moisture:

$$(\Delta T)_K^{***} = -\Delta q_K \cdot T_k(t-1) \cdot \frac{(\delta-1)}{1+(\delta-1)q_K}$$

The total diffusive temperature increment is then the sum of these three terms.

3.2.9 VDFS DRV

VDFS DRV determines surface fluxes and derivatives with respect to surface variables for later use in SURF.

We get sensible heat flux at the surface J_s by:

$$J_s = -\rho_s |u|_{NLEV} \cdot C_h (s_s - s_{NLEV}^-)$$

and similarly, the moisture flux is obtained from:

$$J_q = J_{q_{sn}} + J_{q_i} + J_{q_v} + J_{q_o}$$

with

$$J_{q_{sn}} = -\rho_s |u|_{NLEV} \cdot C_h \cdot C_{sn} \cdot (q_{SAT} - q_{NLEV}^-)$$

$$J_{q_i} = -\rho_s |u|_{NLEV} \cdot C_h \cdot (1-C_{sn}) \cdot C_1 (q_{SAT} - q_{NLEV}^-)$$

$$J_{q_v} = -\rho_s |u|_{NLEV} \cdot C_h \cdot (1-C_{sn}) \cdot (1-C_1) \cdot C_v \cdot E \cdot (q_{SAT} - q_{NLEV}^-)$$

$$J_{q_o} = -\rho_s |u|_{NLEV} \cdot C_h \cdot (1-C_{sn}) \cdot (1-C_1) \cdot (1-C_v) \cdot (h q_{SAT} - q_{NLEV}^-)$$

The derivatives of $J_{q_{sn}}$ with respect to S_n , of J_{q_i} with respect to W_p of $(J_{q_v} + J_{q_o})$ with respect to W_s are computed for later use in subroutine SURF, along with the ratio $J_{q_v}/(J_{q_v} + J_{q_o})$.

The sensible heat flux J_s is then modified to account for the effect of having a variable C_p

$$J_s = J_s - C_{pd} (\delta-1) J_q T_s(t-1)$$

The latent heat flux at the surface has to be weighted with the snow cover, so we compute the latent heat of

vapourisation/sublimation L_{vs} for land points:

$$L_{vs} = L_s \left(\frac{Sn(t-1)}{Sn_{crit}}, 1 \right) + L_v \left(1 - \min \left(\frac{Sn(t-1)}{Sn_{crit}}, 1 \right) \right)$$

The total heat flux at the surface J_h is obtained from:

$$J_h = J_s + L_{vs} J_q$$

and its derivative with respect to T_s is calculated for further use in subroutine SURF.

3.2.10 VDFT2M

VDFT2M computes the 2m temperature (for reference see Research Manual 2, Appendix 6) providing a record of the minimum and maximum temperatures over 12 hour periods during the forecasts.

REFERENCES

- Beljaars, A., and M. Miller, 1990: The sensitivity of the ECMWF model to the parametrization of evaporation from the tropical oceans. ECMWF Tech.Memo. 170.
- Blackadar, A.K. 1962: The vertical distribution of wind and turbulent exchange in a neutral atmosphere. J.Geophys.Res., 67, 3095-3102.
- Ellison, T.H., 1957: Turbulence transfer of heat and momentum from an infinite rough plane. J.Fluid Mech., 2, 456-466.
- Louis, J.-F., 1979: A parametric model of vertical eddy fluxes in the atmosphere. Boundary-layer Meteorol., 17, 187-202.
- Louis, J.-F., M. Tiedtke, and J.-F. Geleyn, 1982: A short history of the PBL parameterization at ECMWF. Proceedings, ECMWF workshop on planetary boundary layer parameterization, Reading, 25-27 Nov. 81, 59-80.
- Pandolfo, J.P., 1967: Wind and temperature profiles for constant-flux boundary layer in lapse conditions with a variable eddy conductivity to eddy viscosity ratio. J.Atmos.Sci., 23, 495-502.
- Richtmyer, R.D. and K.W. Morton, 1967: Difference methods for initial value problems. Wiley and Sons, New York, 403 pp.
- Sellers, P.J., Y. Mintz, Y.C. Sud, A. Dalcher, 1986: A simple biosphere model (Si B) for use within General Circulation Modes. J.Atmos.Sci., 43, 505-531.

CHAPTER 4
Gravity Wave Drag

4.1 THEORY

The parametrization scheme represents the momentum transports due to subgridscale gravity waves excited by stably stratified flow over irregular terrain. The scheme is a modified form of that proposed by *Palmer et al.* (1986), in which a low-level wave stress is defined together with criteria for the reduction in stress with height as the vertically propagating waves are absorbed and/or reflected.

A revision was introduced in May 1989 which modified both the form of the low-level stress and its vertical profile. The revision parametrizes non-linear low-level wave drag processes.

The influence of these wave stresses is then in regions of wave momentum flux divergence i.e.

$$\left(\frac{\partial \vec{V}}{\partial t} \right)_{\text{gravity waves}} = -g \frac{\partial \bar{\tau}}{\partial p} \text{ gravity waves}$$

4.1.1 The formulation of the scheme

The formulation of the scheme consists of two parts

- (i) The parametric form for $\bar{\tau}(x, y, t)_{\text{surface}}$.
 - (ii) The modelling of the dynamical processes which determine the vertical distribution.
- (i) The following quantities are defined for use in the scheme, \vec{V}_L is the wind vector for a suitably defined low-level flow and ρ_L, N_L are the low-level density and Brunt-Vaisälä frequency respectively. The function $f_1(\vec{x})$ describes the orographic forcing of gravity waves and in the scheme described here $f_1(\vec{x})$ is prescribed to be a directionally dependent subgridscale orographic variance computed from the US Navy dataset containing mean orographic heights for (1/6° x 1/6°) areas. Fr is a form of Froude number for the low-level flow defined as $Fr = N_L \sqrt{f_1(\vec{x})} / U_L$ (U_L defined later). $f_2(\vec{x})$ is an orographic anisotropy function measuring the two-dimensionality of the subgridscale orography, where

$$f_2(\vec{x}) = 1 - \text{EXP}(1-\alpha), \text{ and } \alpha = \text{Max}(\alpha_1, \alpha_2) \quad (4.1)$$

and

$$\alpha_1^2 = \text{Max}(VAR_{ns}/VAR_{sw}, VAR_{sw}/VAR_{ns}), \alpha_2^2 = \text{Max}(VAR_{ne}/VAR_{nw}, VAR_{nw}/VAR_{ne}) \quad (4.2)$$

z_c is the atmospheric depth corresponding to three-quarters of a hydrostatic vertical gravity wavelength and is computed by solution of the equation

$$\int_0^{z_c} \frac{N(z')}{U(z')} dz' = \frac{3\pi}{2} \quad (4.3)$$

The scheme can then be written as $\tau_{gw}(p) = \tau_w(p) + \tau_{Fr}(p)$

The first term describes part of the low-level drag and the upper part, hence

$$\tau_w(p) = \tau_w(p_s) (1 - \beta) \frac{(p - p')}{p_s - p'} \quad \text{for } p \geq p' \quad (4.4a)$$

$$= \beta \tau_w(p_s) f(p) \quad \text{for } p < p' \quad (4.4b)$$

$f(p)$ describes the vertical stress profile, computed as described in (ii) below.

The choice of p' determines the depth for this part of the low-level drag and is currently chosen as

$p' = 0.8p_s$, and β controls the ratio of low to high level drag (currently equal to 0.3).

$$\tau_w(p) = KU_L N_L VAR^* \quad \text{where } VAR^* = \min(VAR, (Fr_c U_L / N_L)^2)$$

and Fr_c is a critical value for the low-level Froude number (currently equal to 2).

Analytical results for an isolated bell-shaped mountain give a value for $K = \pi/16a$ where a is the mountain half-width. Hence $K = 2.5 \times 10^{-5} m^{-1}$ for typical subgrid-scale orography.

The second term $\tau_{Fr}(p)$ describes the additional drag which occurs when the low-level flow is supercritical and the dynamical mechanism of resonant trapping of waves occurs leading to high-drag situations (see, for example, *Peltier and Clark, 1986*). It takes the form

$$\tau_{Fr}(p) = \tau_{Fr}(p_s) \frac{(p - p_c)}{(p_s - p_c)} \quad \text{if } Fr > Fr_c \quad (4.5a)$$

where

$$\tau_{Fr}(p_s) = K_L \rho \frac{U_L^3}{N_L} (Fr - Fr_c)^2 f_2(x) \quad \text{if } Fr > Fr_c \text{ and equals zero otherwise.} \quad (4.5b)$$

p_{z_c} is the pressure corresponding to the height z_c and K_L is currently 4K. Typical values of z_c are around 3-5km but much larger values do occur.

(ii) The vertical structure of τ_w is calculated by constructing a local wave Richardson number which attempts to describe the onset of turbulence due to the gravity waves becoming convectively unstable or encountering critical layers.

This wave Richardson number can be written in the form $\tilde{R} = \bar{R} \left\{ \frac{1 - \alpha}{(1 + \bar{R}^{1/2} \alpha)^2} \right\}$ where \bar{R} is the Richardson

number of the basic flow. The parameter $\alpha = N|\delta z|/u$ is a form of Froude number in which $|\delta z|$ represents the amplitude of the wave and u is the wind speed resolved in the direction of $\vec{\tau}_{gw}$.

By requiring that \tilde{R} never falls below a critical value \tilde{R}_{CRIT} (currently equal to 0.25), values of wave stress are defined progressively from the surface upwards.

4.2 CODE: SUBROUTINE GWDRAG

This routine computes the tendencies due to gravity wave drag. The wave drag modifies the horizontal components of the momentum equations, and the thermodynamic equation through dissipation.

GWDRAG is called from PHYSC, and calls GWSETUP, GWSTRESS and GWPROFIL.

4.2.1 Preliminary computations [GWSETUP]

A number of preliminary computations are required to run the scheme; they are as follows.

(i) Definition of low-level wind as input for wave stress.

Wind components averaged over the lowest three layers of the model are computed as:

$$U_{LOW} = \frac{1}{\sum_{k=NLEV}^{k'} \Delta p_k} \sum_{k=NLEV}^{k'} U_k \Delta p_k \quad (4.6)$$

with a similar expression for V_{LOW} , k' is chosen to be (NLEV-2)

This defines the low-level wind vector

$$\vec{V}_L = (U_{LOW}, V_{LOW})$$

These components are then used to define which quadrant the stress vector will lie for selection of the relevant subgridscale orographic variance.

(ii) Projection of winds at full levels in the direction of \vec{V}_L .

$$\text{i.e. } \hat{U}_k = \frac{U_L}{|\vec{V}_L|} U_k + \frac{V_L}{|\vec{V}_L|} V_k \quad (4.7)$$

These winds are also required at model half-levels

$$\text{i.e. } \hat{U}_{k-1/2} = (\rho_{k-1/2} - \rho_{k-1}) \hat{U}_k + (\rho_k - \rho_{k-1/2}) \hat{U}_{k-1} / (\rho_k - \rho_{k-1}) \quad (4.8)$$

and then inspected for the first critical level from the surface (if any) where $\hat{U}_{k-1/2} \rightarrow 0$.

(iii) Calculation of the Brunt-Vaisälä frequency in the form:

$$N_{k-1/2}^2 = \frac{2g^2}{C_{pd}(T_k + T_{k-1})} \left\{ 1 - C_{pd} \rho_{k-1/2} \frac{(T_k - T_{k-1})}{(\rho_k - \rho_{k-1})} \right\} \quad (4.9)$$

For the value of $N^2 (= N_L^2)$ used to compute the low-level stress this formula is modified to include the lowest three layers.

Calculation of basic flow Richardson Number

$$\bar{R}_{k-1/2} = N_{k-1/2}^2 \left\{ \frac{p_k - p_{k-1}}{g \rho_{k-1/2} (\bar{U}_k - \bar{U}_{k-1})} \right\}^2 \quad (4.10)$$

Calculation of z_c by the summation of $(N_{k+1/2} / \bar{U}_{k+1/2})$ suitably pressure-weighted.

4.2.2 $\tau_w(p_s)$ [GWSTRESS]

This is computed in the form

$$\tau_w = K \rho_{NLEV-1} N_L |\bar{V}_L| (ZVAR) \quad (4.11)$$

where $ZVAR$ is the selected orographic variance chosen in the following manner

$$ZVAR = \text{Minimum } (h_1^2, h_2^2)$$

and $h_1^2 =$ component of subgridscale orographic variance corresponding to the quadrant of \bar{V}_L and $h_2^2 = (\bar{U}_L / N_L)^2$.

Operationally, $K = 2.5 \times 10^{-5} m^{-1}$.

$$\tau_w(p_s)$$

This is computed in the form given by equation (4.5b).

4.2.3 The profile of stress τ_w [GWPROFIL]

This is computed as follows. Below a chosen η value, η_1 , the profile of $\tau_w(p)$ is defined as

$$\tau_w(p) = \tau_w(p_s) (1-\beta) \left\{ \frac{p-p_s}{p_s-p} \right\} \quad (4.12)$$

where p is the pressure of the first model level below η_1 and β controls the ratio of high to low-level drag. Operationally, $\beta = 0.3$. Immediately above this layer $\tau_w(p) = \beta \tau_w(p_s)$ and the profile computed in the following way:

First the value of $\tau_{k-\frac{1}{2}}$ is set equal to $\tau_{k+\frac{1}{2}}$ and a new wave displacement calculated

$$\tau_{k+\frac{1}{2}} - \tau_{k-\frac{1}{2}} = k \rho_{k-\frac{1}{2}} N_{k-\frac{1}{2}} |\bar{V}_{k-\frac{1}{2}}| |\delta z_{k-\frac{1}{2}}|^2$$

Solving this equation for $\delta z_{k-\frac{1}{2}}$ enables a value of the wave Richardson $\bar{R}_{k-\frac{1}{2}}$ to be computed via:

$$\bar{R}_{k-\frac{1}{2}} = \bar{R}_{k-\frac{1}{2}} (1 - \alpha_{k-\frac{1}{2}}) / (1 + \sqrt{\bar{R}_{k-\frac{1}{2}} \alpha_{k-\frac{1}{2}}})^2$$

where $\alpha_{k-\frac{1}{2}} = N_{k-\frac{1}{2}} \delta z_{k-\frac{1}{2}} / \bar{U}_{k-\frac{1}{2}}$

If $\bar{R}_{k-\frac{1}{2}} \geq R_{CRIT}$ (= 0.25 operationally) then the value of stress is retained and computation proceeds to the next higher level.

If $\bar{R}_{k-\frac{1}{2}} < R_{CRIT}$ then a new $\delta z_{k-\frac{1}{2}}$ is computed from the above equation with $\bar{R}_{k-\frac{1}{2}}$ set equal to R_{CRIT} thus defining a new value for $\tau_{k-\frac{1}{2}}$.

The profile of $\tau_{pr}(p)$ below the level \bar{p} is computed in the form

$$\tau_{pr}(p) = \tau_{pr}(\bar{p}) \left\{ \frac{p - \bar{p}}{\bar{p}_s - \bar{p}} \right\}$$

where \bar{p} is the pressure of the first model level below that corresponding to z_c .

The values of $\tau_w(p)$ and $\tau_{pr}(p)$ are then summed to give the complete profile.

4.2.4 The tendencies

These are incremented by the expressions

$$\left(\frac{\partial u}{\partial t} \right)_k^{sw} = -g \frac{U_L}{|\bar{V}_L|} \frac{(\tau_{k+\frac{1}{2}} - \tau_{k-\frac{1}{2}})}{(p_{k+\frac{1}{2}} - p_{k-\frac{1}{2}})}$$

$$\left(\frac{\partial v}{\partial t} \right)_k^{sw} = -g \frac{V_L}{|\bar{V}_L|} \frac{(\tau_{k+\frac{1}{2}} - \tau_{k-\frac{1}{2}})}{(p_{k+\frac{1}{2}} - p_{k-\frac{1}{2}})}$$

(4.13)

$$\left(\frac{\partial T}{\partial t} \right)_k^{sw} = \frac{1}{4C_{pd}\Delta t} \left\{ U_k^2 + V_k^2 - \left[U_k + 2\Delta t \left(\frac{\partial u}{\partial t} \right)_k^{sw} \right]^2 - \left[V_k + 2\Delta t \left(\frac{\partial v}{\partial t} \right)_k^{sw} \right]^2 \right\}$$

4.2.5 Diagnostics

A limited number of print statements provide information on the output from the scheme for selected gridpoints.

Code for postprocessing, zonal mean and mask diagnostics and global budgets is described elsewhere in the documentation.

4.2.6 Implicitness

Since the computation of the low-level stress uses the low-level winds, the computation of the tendencies is done implicitly (for the three lowest model levels).

References

Palmer, T.N., G.J. Shutts, R. Swinbank, 1986: Alleviation of a systematic westerly bias in general circulation and numerical weather prediction models through an orographic gravity wave drag parameterization. *Quart.J.Roy.Met.Soc.*, 112, 1001-1031.

Peltier, W.R., and T.L. Clark, 1987: Nonlinear mountain waves and wave-mean flow interaction: elements of a drag parametrization. ECMWF Seminar/Workshop on Observation, Theory and Modelling of Orographic Effects, ECMWF, Shinfield Park, Reading, 15-20 September 1986, Vol.1, 223-249.

CHAPTER 5
Convection

5.1 CUMULUS CONVECTION

Cumulus convection is parametrized by a mass flux scheme which is described in detail (including numerical aspects) in *Tiedtke* (1989). The scheme considers penetrative convection, shallow convection and mid-level convection. Clouds are represented by a bulk model and include updraft and downdraft mass fluxes. Momentum transport by convective circulations is also included following the proposal by *Schneider and Lindzen* (1976).

5.1.1 Large-scale budget equations

The contributions from cumulus convection to the large-scale budget equations of heat moisture and momentum are

$$\left. \begin{aligned}
 \left(\frac{\partial \bar{s}}{\partial t} \right)_{cu} &= - \frac{1}{\rho} \frac{\partial}{\partial z} [M_u s_u + M_d s_d - (M_u + M_d) \bar{s}] \\
 &\quad + L(c_u - e_d - \bar{e}_i - \bar{e}_p) - (L_s - L_v)m \\
 \left(\frac{\partial \bar{q}}{\partial t} \right)_{cu} &= - \frac{1}{\rho} \frac{\partial}{\partial z} [M_u q_u + M_d q_d - (M_u + M_d) \bar{q}] \\
 &\quad - (c_u - e_d - \bar{e}_i - \bar{e}_p) \\
 \left(\frac{\partial \bar{u}}{\partial t} \right)_{cu} &= - \frac{1}{\rho} \frac{\partial}{\partial z} [M_u u_u + M_d u_d - (M_u + M_d) \bar{u}] \\
 \left(\frac{\partial \bar{v}}{\partial t} \right)_{cu} &= - \frac{1}{\rho} \frac{\partial}{\partial z} [M_u v_u + M_d v_d - (M_u + M_d) \bar{v}]
 \end{aligned} \right\} \quad (5.1)$$

where M_u , M_d , c_u , and e are the net contributions from all clouds to the upward mass flux, downward mass flux, condensation/sublimation and evaporation respectively, and s_u , s_d , q_u , q_d , u_u , u_d , v_u and v_d are the weighted averages of s , q , u and v from all updrafts and downdrafts. Here \bar{e}_i is the evaporation of cloud air that has been detrained into the environment, \bar{e}_p is the evaporation of precipitation in the unsaturated subcloud layer and m is the melting of snow. In addition to (5.1) we consider the equations for precipitation

$$\left. \begin{aligned} P^W(z) &= \int (G_p^W - e_d^W + \bar{e}_p^W + m) \bar{\rho} dz \\ P^I(z) &= \int (G_p^I - e_d^I - \bar{e}_p^I - m) \bar{\rho} dz \end{aligned} \right\} \quad (5.2)$$

where $P^W(z)$, $P^I(z)$ are the fluxes of rain water and snow at height z and G_p^W and G_p^I are the conversion rates from cloud ice and cloud water into precipitation, respectively.

5.1.2 Cloud model equations

The updraft of the cloud ensemble is assumed to be in a steady state. Then the bulk equations for mass, heat, moisture, cloud water content and momentum are

$$\left. \begin{aligned} \frac{\partial M_u}{\partial z} &= E_u - D_u \\ \frac{\partial (M_u \bar{s})}{\partial z} &= E_u \bar{s} - D_u \bar{s}_u + L \bar{\rho} c_u \\ \frac{\partial (M_u \bar{q})}{\partial z} &= E_u \bar{q} - D_u \bar{q}_u - \bar{\rho} c_u \\ \frac{\partial (M_u l)}{\partial z} &= D_u l + \bar{\rho} c_u - \bar{\rho} G_p \\ \frac{\partial (M_u \bar{u}_u)}{\partial z} &= E_u \bar{u} - D_u \bar{u}_u \\ \frac{\partial (M_u \bar{v}_u)}{\partial z} &= E_u \bar{v} - D_u \bar{v}_u \end{aligned} \right\} \quad (5.3)$$

where E and D are the rates of mass entrainment and detrainment per unit length l is the cloud water content (water/ice) and c_u is the net condensation/sublimation in the updrafts.

Cloud air is assumed to be saturated and cloud processes are crudely represented. Freezing and melting processes are not considered and the conversion from cloud droplets to rain/snow is assumed to be proportional to the cloud water content as

$$\bar{\rho} G_p = K(z) l M_u \quad (5.4)$$

where $K(z)$ is an empirical function that varies with height. This simple parametrization yields rather reasonable vertical distributions of the generation of raindrops (Yanai *et al.*, 1973). Here K is assumed to be zero near cloud base and constant at higher levels:

$$K(z) = \begin{cases} 0, & \text{if } z \leq Z_B + \Delta Z \\ 2.10^{-3} m^{-1}, & \text{if } z > Z_B + \Delta Z \end{cases} \quad (5.5)$$

where Δz is 1500m over sea and 3000m over land. The choice of $K = 0$ at lower levels ensures that shallow cumuli do not produce precipitation, noting that a sizeable portion of the liquid water content in nonprecipitating cumuli is of precipitation-sized drops.

We further note that the cloud water detrained into the environmental air is assumed to evaporate there instantaneously; then

$$\bar{e}_t = \frac{1}{\rho} D_w l \quad (5.6)$$

The vertical integration of (5.3) requires the knowledge of cloud base mass flux and mass entrainment and detrainment. Cloud-base mass flux is determined for the various types of convection from the parametrization assumptions discussed below. Entrainment of mass into convective plumes is assumed to occur through (i) turbulence exchange of mass through cloud edges and (ii) through organized inflow associated with large-scale convergence, detrainment through turbulent exchange and as organized outflow at cloud top:

$$E_w = E_w^{(1)} + E_w^{(2)}, \quad D_w = D_w^{(1)} + D_w^{(2)} \quad (5.7)$$

Turbulent entrainment and detrainment are parametrized as

$$E_w^{(1)} = \epsilon_w M_w, \quad D_w^{(1)} = \delta_w M_w \quad (5.8)$$

where the fractional entrainment/detrainment rates depend inversely on cloud radii (Simpson and Wiggert, 1969; Simpson, 1971):

$$\epsilon_w = \frac{0.2}{R_w}, \quad \delta_w = \frac{0.2}{R_w} \quad (5.9)$$

By assuming typical cloud sizes for the various types of convection, average values of entrainment/detrainment rates are defined: in the presence of synoptic scale flow convergence, large clouds which contribute most to the convective heating and moistening are assumed to exist and consequently small values for the entrainment/detrainment rates are imposed whereas in the absence of flow convergence clouds of smaller sizes with larger entrainment rates prevail. In order to keep the scheme simple we use fixed values of turbulent entrainment/detrainment rates for each of the various types of convection:

$$e_u - \delta_u = \begin{cases} 1 \times 10^{-4} \text{ m}^{-1}, & \text{for penetrative and midlevel} \\ & \text{convergence in the presence} \\ & \text{of large-scale flow convergence} \\ 3 \times 10^{-4} \text{ m}^{-1}, & \text{for shallow convection in} \\ & \text{suppressed conditions.} \end{cases} \quad (5.10)$$

For penetrative convection and midlevel convection we deliberately impose a very small value typical for tropical thunder clouds (*Simpson, 1971*) so as not to inhibit the penetration of clouds to large heights. For shallow convection we use a value typical for the larger trade wind cumuli (*Nitta, 1975*), noting that small clouds with much larger entrainment/detrainment rates which detrain immediately above cloud base are not represented in our parametrization.

The parametrization of organized entrainment and detrainment is discussed below.

Below cloud base, the net convective fluxes of heat and moisture due to updraft and compensating subsidence in the environment are assumed to decrease linearly from their values at cloud base towards zero at the surface so as not to alter the vertical structure of the subcloud layer and in particular not its well-mixed character.

Downdrafts are considered to be associated with convective precipitation from the updrafts and originate from cloud air influenced by the injection of environmental air. Following *Fritsch and Chappell (1980)* and *Foster (1958)*, the Level of Free Sinking (LFS) is assumed to be the highest model level where a mixture of equal parts of cloud air and saturated environmental air at wet-bulb temperature becomes negative buoyant with respect to the environmental air. The downdraft mass flux is assumed to be directly proportional to the upward mass flux. Following *Johnson (1976, 1980)* the mass flux at the LFS is specified from the updraft mass flux at cloud base as

$$(M_d)_{LFS} = \gamma (M_u)_{base} \quad \text{with } \gamma = -0.3 \quad (5.11)$$

The coefficient γ is a disposable parameter.

The vertical distribution of the downdraft mass flux, dry static energy and moisture below the LFS is determined by the equations for mass, dry static energy and moisture content as

$$\left. \begin{aligned}
-\frac{\partial M_d}{\partial z} &= E_d - D_d \\
-\frac{\partial(M_d s_d)}{\partial z} &= E_d \bar{s} - D_d s_d + L \bar{\rho} e_d \\
-\frac{\partial(M_d q_d)}{\partial z} &= E_d \bar{q} - D_d q_d + \bar{\rho} e_d \\
-\frac{\partial(M_d u_d)}{\partial z} &= E_d \bar{u} - D_d u_d \\
-\frac{\partial(M_d v_d)}{\partial z} &= E_d \bar{v} - D_d v_d
\end{aligned} \right\} \quad (5.12)$$

We note that cumulus downdrafts are viewed as updrafts but upside-down. Entrainment and detrainment in downdrafts are highly uncertain as relevant data are not available. Numerical experiments show, however, that the results are rather insensitive to changes in the entrainment and detrainment rates. We use

$$e_d = \delta_d = 2 \cdot 10^{-4} \text{ m}^{-1} \quad (5.13)$$

This gives a mass flux which is independent of height and which effectively detrains into the environment in the subcloud layer. We also note that e_d is the evaporation of convective rain to maintain a saturated descent and that the moistening and cooling of the environmental air injected at LFS is also due to evaporating rain. As the downdrafts are determined from the updrafts the remaining parametrization task is to specify the updraft. This is done by means of closures defined below for the various types of convection.

a. Penetrative convection

Many diagnostic studies show that penetrative convection predominantly occurs in disturbed situations and strongly depends on low-level synoptic scale convergence. Various parametrization schemes are based on this relationship one way or another. Here, we apply a moisture convergence hypothesis; following *Kuo* (1965, 1974) and *Lindzen* (1981), we postulate that when there is a deep layer of conditional instability and large-scale moisture convergence, cumulus clouds exist that entrain environmental air through their base and through their sides directly proportional to the supply of moisture and detrain cloud air at higher levels.

The injection of mass into the clouds through their base is determined by imposing a moisture balance for the subcloud layer such that the moisture content is maintained in the presence of large-scale transports, turbulent transports and convective transports. This balance may be written as

$$[M_n (q_n - \bar{q}) + M_d (q_d - \bar{q})]_B = - \int_0^B \left(\bar{V} \cdot \nabla \bar{q} + \bar{w} \frac{\partial \bar{q}}{\partial z} + \frac{1}{\bar{\rho}} \frac{\partial}{\partial z} (\bar{\rho} \bar{w} \bar{q}_n) \right) \bar{\rho} dz \quad (5.14)$$

where B denotes the cloud base height defined as the condensation level for surface air. The vertical

distribution of the updraft mass flux above cloud base is determined using similar arguments as for the subcloud layer; that is, we postulate that there is organized entrainment which is directly proportional to the large-scale moisture convergence as

$$E_u^{(2)} = - \frac{\bar{\rho}}{\bar{q}} \left(\bar{V} \cdot \nabla \bar{q} + \bar{w} \frac{\partial \bar{q}}{\partial z} \right) \quad (5.15)$$

Organized entrainment is only considered in the lower part of the cloud layer where large-scale convergence is encountered, that is, below the level of strongest vertical ascent. The idea to link the cloud mass flux directly to the large-scale moisture convergence has first been advocated as a parametrization by *Lindzen* (1981) who indicated that it may provide vertical profiles of mass flux and convective heating in good agreement with observations. The assumption (5.15) ensures that the vertical distribution of the convective mass flux follows that of the large-scale ascent which is partly supported by diagnostic studies for tropical convection (e.g. *Cheng et al.*, 1980; *Johnson*, 1980). Equation (5.15) forms, together with the assumption (5.14), for the cloud base mass flux, the basic closure and as such is crucial for the performance of the parametrization of penetrative convection. The verification of the scheme during periods of tropical convection confirms that the closure provides realistic profiles of convective mass fluxes and convective heating (see *Tiedtke*, 1989).

In addition to organized entrainment we consider turbulent entrainment and detrainment by (5.8) and (5.9).

Cumulus clouds detrain effectively at levels near to their zero-buoyancy level by means of organized outflow. Therefore, the vertical distribution of the total detrainment from all clouds depends on the spectral cloud distribution. Since spectral cloud distribution is not available, however, organized outflow is assumed to occur only in the model layer which contains the zero-buoyancy level of the deepest clouds. Our detrainment assumption implies a unimodal cloud distribution with large detrainment from the deepest clouds and little detrainment from shallow clouds and medium deep clouds.

The effect from shallow cumuli in the presence of penetrative convection has been neglected because their parametrization is a still unsolved problem. This is because the role of shallow cumuli in connection with penetrative convection is not well understood, particularly when cumulus downdraft occur simultaneously as these compete with shallow convection having similar effects on the environment as shallow cumuli (*Johnson*, 1976). The results obtained with this scheme indicate, however, that neglecting the contributions from shallow cumuli when penetrative convection is encountered does not introduce large errors in the convective heating and drying.

b. Shallow convection

Here we consider cumulus convection, which predominantly occurs in undisturbed flow, that is in the absence of large-scale convergent flow. Typical examples are tradewind cumuli under a subsidence inversion, convection occurring in the ridge region of tropical easterly waves and daytime convection over land. This type of convection seems to be effectively controlled by subcloud layer turbulence. In fact, most of the diagnostic studies carried out for tradewind cumuli show that the net upward moisture flux at cloud base level is nearly equal to the turbulent moisture flux at the surface (*Le Mone and Pennell, 1976*). As this implies a quasi-steady moisture balance, we shall apply the same moisture budget equation (5.14) as for penetrative convection. The difference, however, is that the moisture supply to cumulus clouds is now largely through surface evaporation as the contributions from large-scale convergence are either small or even negative, such as in the undisturbed trades where dry air is transported downward to lower levels.

Under typical tradewind conditions the vertical distribution of the total convective fluxes above cloud base is dominated by two types of clouds: very small cumuli, which in large numbers detrain immediately above cloud base, and deeper clouds, which detrain just beneath and above the trade inversion. The intrusion of cumulus clouds into the stable layer above the inversion is through overshooting of cumuli above their level of zero-buoyancy (*Nitta, 1975*). Because of the coarse resolution employed in large-scale models, where the vertical gridlength is typically 50hPa to 100hPa, it is difficult to represent these two types. The scheme presented here ignores the effect of very small cumuli but tentatively accounts for the effects of overshooting cumuli, as we assume that a given fraction of the cloud ensemble penetrates into the inversion layer and detrains there into the environment. Thus, cloud air shall only partly detrain into the environment within the model layer that contains the zero-buoyancy level: the remaining fraction shall intrude into the next layer above and detrain there:

$$\left. \begin{aligned}
 D_u^{(2)} &= (1 - \beta) (M_u)_{k+1/2} / \Delta z && \text{for top layer } k \\
 D_u^{(2)} &= \beta (M_u)_{k+1/2} / \Delta z && \text{for layer } k - 1 \\
 \beta &= 0.3
 \end{aligned} \right\} \quad (5.16)$$

Although this parametrization is very crude, it clearly reproduces more realistic trade inversions than when the effect from overshooting cumuli is ignored ($\beta = 0$), as then the inversion becomes too strong in the simulation and the cloud layer below the inversion too moist (see *Tiedtke, 1989*). The value 0.3 for the disposable parameter β provides the best results and, because there is no other information available, is adopted here.

c. *Midlevel convection*

Midlevel convection, that is, convective cells which have their roots not in the boundary layer but originate at levels above the boundary layer, often occur at rainbands at warm fronts and in the warm sector of extra-tropical cyclones (*Browning et al., 1973; Houze et al., 1976; Herzegh and Hobbs, 1980*). These cells are probably formed by the lifting of low level air until it becomes saturated (*Wexler and Atlas, 1959*) and the primary moisture source for the clouds is from low-level large-scale convergence (*Houze et al., 1976*). Often a low-level temperature inversion exists that inhibits convection from starting freely from the surface; therefore convection seems to be initiated by lifting low-level air dynamically to the level of free convection. This occurs often in connection with mesoscale circulations which might be related to conditionally symmetric instability (*Bennets and Hoskins, 1979; Bennets and Sharp, 1982*) or a wave-CISK mechanism (*Emanuel, 1982*).

Although it is not clear how significant the organization of convection in mesoscale rainbands is for the large-scale flow, a parametrization should ideally account for both convective and mesoscale circulations. Such a parametrization, however, is presently not available and we must therefore rely on simplified schemes. Here we use a parametrization which in a simple way considers the finding of the diagnostic studies mentioned above. We assume that convection is activated when there is a large-scale ascent at lower levels, the environmental air is sufficiently moist, i.e., of relative humidity in excess of 90%, and convectively unstable layer exists above. The free convection level is determined by lifting a parcel of environmental temperature and moisture content,

$$T_u = \bar{T}, \quad q_u = \bar{q} \tag{5.17}$$

adiabatically, allowing for condensational heating, and then checking for buoyancy. The upwards mass flux is set equal to the vertical mass transport by the large-scale flow at that level:

$$(M_v)_B = \bar{\rho}_B \bar{w}_B \tag{5.18}$$

which ensures that the amount of moisture which is vertically advected through cloud base by the large-scale ascent is fully available for generation of convective cells.

In addition to the injection of mass through cloud base, we assume again that cloud air is produced by moisture convergence above cloud base through lateral entrainment in the same way as for penetrative convection as given by (5.15).

5.1.3 Discretization of the model equations

The flux divergence in the large-scale budget equations (5.1) and in the cloud equations (5.3) and (5.12) are

approximated by centered finite differences as

$$-\frac{1}{\rho} \frac{\partial(Ma)}{\partial z} = g \frac{M_{k+\frac{1}{2}} a_{k+\frac{1}{2}} - M_{k-\frac{1}{2}} a_{k-\frac{1}{2}}}{p_{k+\frac{1}{2}} - p_{k-\frac{1}{2}}} \quad (5.19)$$

The definition of the large-scale variables at half levels pose a problem, when the half-level values defined by linear interpolation of full-level values [e.g., $\bar{s}_{k+\frac{1}{2}} = 0.5(\bar{s}_k + \bar{s}_{k+1})$] very noisy profiles evolve in time particularly with regard to humidity. Much smoother profiles are obtained when the half-level values are determined by downward extrapolation from the next full level above along a cloud-ascent through that level:

$$\left. \begin{aligned} \bar{T}_{k+\frac{1}{2}} &= \bar{T}_k + \left(\frac{\partial T}{\partial p} \right)_{h_{sat}} (p_{k+\frac{1}{2}} - p_k) \\ \bar{q}_{k+\frac{1}{2}} &= \bar{q}_k + \left(\frac{\partial q}{\partial p} \right)_{h_{sat}} (p_{k+\frac{1}{2}} - p_k) \end{aligned} \right\} \quad (5.20)$$

where $h_{sat} = s + Lq_{sat}$ is the saturation moist static energy. Using an extrapolation like (5.20) for calculating the downward transports is also more consistent with the calculation of the updrafts where cloud air is transported upwards through level $k + \frac{1}{2}$ with the thermal state below that level and equally with the downdrafts which depend only on values of s and q above that level. Similarly, because of (5.20) the downward transport of environmental air through the same level accounts now only for thermal properties above that level. The choice of a moist adiabat for extrapolation is dictated by the property of the moist static energy which is, by convection in the absence of downdrafts, only changed through the fluxes of moist static energy

$$\left(\frac{\partial \bar{h}}{\partial z} \right)_{env} = -\frac{1}{\rho} \frac{\partial}{\partial z} [M_u(h_u - \bar{h})] \quad (5.21)$$

As the lines of the saturation moist static energy h_{sat} through point $(P_{k+\frac{1}{2}}, \bar{T}_{k-\frac{1}{2}})$ and the updraft moist static energy are almost parallel, apart from entrainment effects, the difference $h_u - \bar{h}$ is little affected by the vertical discretization.

The ascent in the updrafts is obtained by vertical integration of (5.3). Starting at the surface the condensation level (= lowest half-level which is saturated or supersaturated and where buoyancy is met) is determined from an adiabatic ascent. The cloud profile above cloud base is determined layer by layer by first doing a dry adiabatic ascent with entrainment and detrainment included and then adjusting temperature and moisture towards a saturated state. The cloud parcel is finally checked for positive buoyancy, that is, for excess of

the virtual static energy in the cloud over the environmental value

$$(\bar{S}_v)_u \geq \bar{S}_v = s + C_p T \delta 0.608q \quad (5.22)$$

and cloud top is defined as the level where the parcel loses buoyancy.

Finally, we mention that for numerical reasons the environmental air must not be convectively unstably stratified:

$$\bar{S}_{k-\Delta k} \geq \bar{S}_{k+\Delta k} \quad (5.23)$$

In fact, one of the forecasts with the ECMWF global model became numerically unstable when (5.23) was not imposed.

5.1.4 Melting of snow

Melting of snow is parametrized as stratiform precipitation (see 6.1.5)

5.1.5 Evaporation of rain

The evaporation of convective rain is parametrized following a proposal of *Kessler* (1969), where the evaporation is assumed to be proportional to the saturation deficit $q_{sat} - q$ and to be dependent on the density of rain M_R (g/m^3)

$$E = \alpha_1 (q_{sat} - q) M_R^{13/20}$$

where V_0 is a constant being zero for $q > q_{sat}$

As the density of rain M_R is not given by the model it is convenient to express it in terms of the rain intensity R [$g/(m^2sec)$] as

$$R = M_R (V_0 + w) = M_R \cdot V_0$$

where α_1 is the mean fall speed of rain drops which again is parametrized following *Kessler* (1969).

$$V_0 = \alpha_2 M_R^{1/8} / \sqrt{p/p_s}$$

Thus we have

$$E = \alpha_1 (q_{sat} - q) \left[\left(\frac{\sqrt{p/p_s}}{\alpha_2} R \right)^{13/20} \right]^{8/9}$$

Since the convective rain takes place only over a fraction C_c of the grid area the evaporation rate at

level k becomes

$$E = C_c \cdot \alpha_1 (q_{sat} - q) \left[\frac{\sqrt{p/p_s}}{\alpha_2} \frac{R}{C_c} \right]^{\alpha_3}$$

where the constants have the following values (Kessler, 1969)

$$\alpha_1 = 5.44 \cdot 10^{-4}, \quad \alpha_2 = 5.09 \cdot 10^{-3} \quad \alpha_3 = 0.5777$$

In order to save computing time (with $\alpha_3 = 1/2$) we use slightly different values.

In view of the uncertainty of the fractional area of precipitating clouds a constant value of

$$C_c = 0.05$$

is assumed.

The evaporation rate is calculated implicitly in the model by means of

$$2g \frac{\partial R^{\alpha_3}}{\partial p} = -A$$

which follows from

$$E = AR^{\alpha_3} \quad A = \alpha_1 (q_{sat} - q) \left(\frac{\sqrt{p/p_s}}{\alpha_2} \frac{1}{C_c} \right)^{\alpha_3}$$

and

$$E = \frac{1}{\rho} \frac{\partial R}{\partial z} = -g \frac{\partial R}{\partial p}$$

5.2 STRATOCUMULUS

Stratocumulus convection is parametrized by means of a vertical diffusion scheme (Tiedtke *et al.*, 1988). It is only applied in the boundary layer where it provides a net upward transport of moisture to avoid the generation of saturated layers within a convective boundary layer. We assume that

- the time change and the advection of liquid cloud water are typically small
- the balance is between the turbulent transport of liquid cloud water and condensational processes

$$\frac{1}{\rho} \frac{\partial}{\partial z} (\overline{\rho w l}) = C - E$$

The effects of stratocumulus on the large-scale flow can then be described by the turbulent fluxes of heat

moisture and liquid cloud water:

$$\left(\frac{\partial \bar{s}}{\partial t}\right)_{Ck} - \frac{1}{\rho} \frac{\partial}{\partial z} (\bar{\rho}(\bar{w}'s' - L\bar{w}'l'))$$

$$\left(\frac{\partial \bar{q}}{\partial t}\right)_{Ck} - \frac{1}{\rho} \frac{\partial}{\partial z} (\bar{\rho}(\bar{w}'q' + \bar{w}'l'))$$

In the present scheme we ignore the effects from the turbulent transports of liquid cloud water. The net effect of stratocumulus convection is then given by the turbulent fluxes of heat and moisture, which are parametrized on the bases of the mixing length theory:

$$\left(\frac{\partial \bar{s}}{\partial t}\right)_{Ck} - \frac{1}{\rho} \frac{\partial}{\partial z} \left(\bar{\rho} K \frac{\partial \bar{s}}{\partial z}\right)$$

$$\left(\frac{\partial \bar{q}}{\partial t}\right)_{Ck} - \frac{1}{\rho} \frac{\partial}{\partial z} \left(\bar{\rho} K \frac{\partial \bar{q}}{\partial z}\right) \tag{5.24}$$

Equations (5.24) are only applied below 900hPa and when the convection scheme was not activated, i.e., failed because convection did not penetrate over at least on larger depth. Cloud base is the condensation level for surface air. Then (5.24) is applied considering the fluxes through cloud base and cloud top.

At present we use the following values for determining fluxes between level k and $k+1$

$$K = \begin{cases} 10 m^2/sec & \text{cloud layers and cloud base} \\ 10 \frac{(RH)_k - 0.8}{1 - 0.8} ((RH)_{k-1} - (RH)_k) & \text{top entrainment} \\ 0 & \text{elsewhere} \end{cases}$$

5.3 CODE

The parametrization of cumulus convection and stratocumulus is performed in subroutines shown in Fig. 5.1.

CUCALL Provides interface of routines for cumulus parametrization, convective clouds (for radiation) and stratocumulus. It takes the input values through arguments from PHYSC and returns updated tendencies of T , q , u and v as well as convective precipitation rates and cloud parameter for radiation calculation.

CUMASTR Master routine for convection scheme

CUINI Initializes variables for convection scheme

CUBASE Calculates condensation level for surface air

CUASC Calculates ascent in updrafts, CUASC is called twice, the second time after downdrafts have been calculated

CUDLFS Calculates the level of free sinking for downdrafts

CUDDRAF Calculates the downdraft descent

CUFLX Calculates final convective fluxes

CUDTDQ Calculates the tendencies of T and q from convection as well as precipitation rates

CUDUDV Calculates the tendencies of u and v from convection

STRATCU Does vertical diffusion of heat and moisture for stratocumulus. Input values T , q , q_c , and Flag signifying convective points are passed on from CUMASTR.

The solution of the vertical diffusion equation is identical to that described in 3.2 for the turbulent fluxes.

CUADJQ Calculates super/sub saturation and adjusts T and q accordingly.

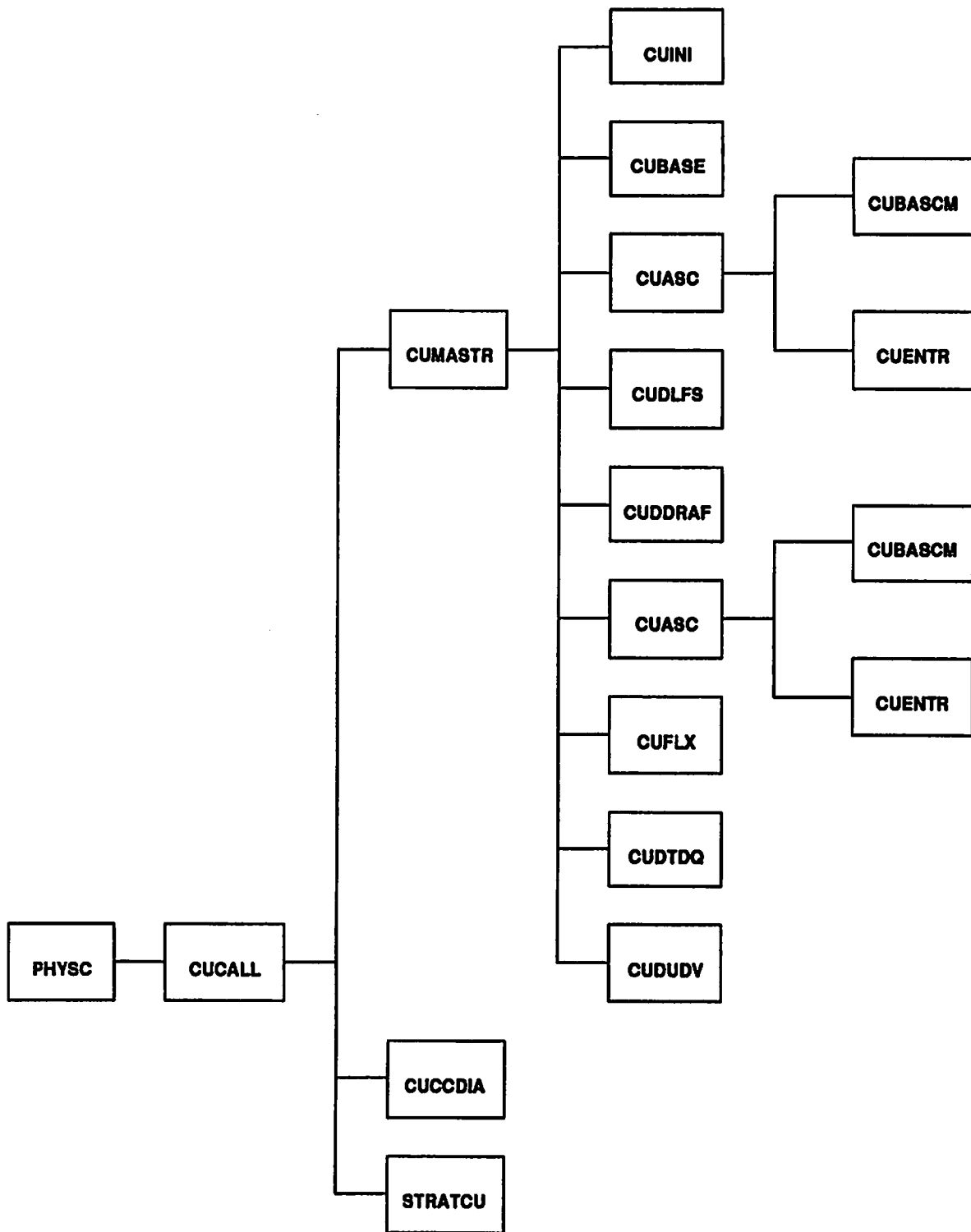


Fig. 1 Subroutines for convection scheme

EXTERNALS

Subroutine **QUADJTG** for calculating super (sub) saturation and adjusting T and q accordingly.

PARAMETERS are defined in SUBROUTINE **CUPARAM** called from **INIPHY**

REFERENCES

- Bennets, D. A., and B. J. Hoskins, 1979: Conditional symmetric instability - a possible explanation for frontal rainbands. *Quart.J.Roy.Meteor.Soc.*, 105, 945-962.
- Bennets, D. A., and J. C. Sharp, 1982: The relevance of conditional symmetric instability to the prediction of meso-scale frontal rainbands. *Quart.J.Roy.Meteor.Soc.*, 108, 595-602.
- Browning, K.A., M. E. Hardman, T. W. Harrold and C. W. Pardoc, 1973: The structure of rainbands within a mid-latitude depression. *Quart.J.Roy.Meteor.Soc.*, 99, 215-231.
- Cheng, L., T.-C. Yip and H.-R. Cho, 1980: Determination of mean cumulus cloud vorticity from GATE A/B-scale potential vorticity budget. *J.Atmos.Sci.*, 37, 797-811.
- Emanuel, K. A., 1982: Inertial instability and mesoscale convective systems. Part II: Symmetric CISK in a baroclinic flow. *J.Atmos.Sci.*, 39, 1080-1097.
- Foster, D. S., 1958: Thunderstorm gusts compared with computed downdraft speeds. *Mon.Wea.Rev.*, 86, 91-94.
- Fritsch, J.M., and C. G. Chappell, 1980: Numerical prediction of convectively driven mesoscale pressure systems. Part I: Convective parametrization. *J.Atmos.Sci.*, 37, 1722-1733.
- Herzogh, P. H., and P. V. Hobbs, 1980: The mesoscale and microscale structure and organization of clouds and precipitation in mid-latitude cyclones. Part II: Warm frontal clouds. *J.Atmos.Sci.*, 37, 597-611.
- Houze, R. A., J. D. Locatelli and P. V. Hobbs, 1976: Dynamics and cloud microphysics of the rainbands in an occluded frontal system. *J.Atmos.Sci.*, 35, 1921-1936.
- Johnson, R. H., 1976: The role of convective-scale precipitation downdrafts in cumulus and synoptic scale interactions. *J.Atmos.Sci.*, 33, 1890-1910.
- Johnson, R. H., 1980: Diagnosis of convective and mesoscale motions during Phase III of GATE. *J.Atmos.Sci.*, 37, 733-753.
- Kessler, E., 1969: On the distribution and continuity of water substance in atmospheric circulation. *Meteorological Monographs*, 10, Americ.Meteor.Soc., Boston, MA.
- Le Mone, M. A., and W. T. Pennell, 1976: The relationship of trade wind cumulus distribution to subcloud layer fluxes and structure. *Mon.Wea.Rev.*, 104, 524-539.
- Lindzen, R. S., 1981: Some remarks on cumulus parametrization. Rep. on NASA-GISS Workshop: Clouds in Climate: Modelling and Satellite Observational Studies, 42-51.
- Nitta, T., 1975: Observational determination of cloud mass flux distributions. *J.Atmos.Sci.*, 32, 73-91.
- Schneider, E. K., and R. S. Lindzen, 1976: A discussion of the parametrization of momentum exchange of cumulus convection. *J.Geophys.Res.*, 81, 3158-3160.
- Simpson, J., 1971: On cumulus entrainment and one-dimensional models. *J.Atmos.Sci.*, 28, 449-455.

Simpson, J., and V. Wiggert, 1969: Models of precipitating cumulus towers. *Mon.Wea.Rev.*, 97, 471-489.

Tiedtke, M., 1989: A comprehensive mass flux scheme for cumulus parameterization in large-scale models. *Mon.Wea.Rev.*, 117, 1779-1800.

Tiedtke, M., W. A. Heckley, and J. Slingo, 1988: Tropical forecasting at ECMWF: On the influence of physical parametrization on the mean structure of forecasts and analyses. *Quart.J.Roy.Meteor.Soc.*, 114, 639-664.

Wexler, R., and D. Atlas, 1959: Precipitation generating cells. *J.Meteor.*, 16, 327-332.

Yanai, M., S. Esbensen and J.-H. Chu, 1973: Determination of bulk properties of tropical cloud clusters from large-scale heat and moisture budgets. *J.Atmos.Sci.*, 30, 611-627.

CHAPTER 6
Stratiform precipitation

6.1 THEORY

6.1.1 Definition of the saturation specific humidity

We use the Tetens formula for the calculation of the saturation pressure $e_s(T)$ (Lowe, 1977):

$$e_s(T) = a_1 e^{a_2 \left(\frac{T-T_0}{T-a_3} \right)} \quad (6.1)$$

in which a_3 and a_4 are different depending on the sign of $(T-T_0)$ (i.e. water or ice phase with $T_0 = 273.16$ K). The saturation specific humidity q_{SAT} being the mass ratio of water vapour to moist air we have

$$q_{SAT} = \varepsilon e_s(T) / [p - (1-\varepsilon)e_s(T)] \quad (6.2)$$

with $\varepsilon = R_d/R_v$, where R_d and R_v are the gas constants for dry air and water vapour respectively.

6.1.2 Equilibrium values T^* , q^* at saturation starting from T and q

When only phase changes between water vapour and either liquid water or ice crystals are considered, the changes of T and q are obtained in the following way:

First, the initial supersaturated state (T, q) is modified in a new supersaturated state (T^*, q) . This is obtained by solving:

$$C_{pd} (1 + (\delta - 1)q) \Delta T - L \Delta q \quad (6.3)$$

where $q = q^* + \Delta q$, q^* being the saturated value at (T^*, p)

We can define a quantity L/C_p effective:

$$\left(\frac{L}{C_p} \right)_{eff} = \frac{L}{C_{pd}(1 + (\delta - 1)q)} \quad (6.4)$$

where L is either L_v or L_i depending on the sign of $(T-T_0)$. We can then rewrite (6.3):

$$\Delta T - \left(\frac{L}{C_p} \right)_{eff} \Delta q \quad (6.5)$$

Starting from a couple of T , q values we are seeking to find another two values T^* , q^* with the two

conditions:

$$T^* - T = \left(\frac{L}{C_p} \right)_{\text{eff}} (q - q^*)$$

and

$$q^* = Q_{\text{SAT}}(T^*, p) \quad (6.6)$$

Since we only know T and q beforehand we compute $\left(\frac{L}{C_p} \right)_{\text{eff}}$ first with the sole use of these two

quantities. Then we approximate $Q_{\text{SAT}}(T^*, p)$ by:

$$q^* = q_{\text{SAT}}(T, p) + \frac{dq_{\text{SAT}}(T, p)}{dT} (T^* - T) \quad (6.7)$$

Thus we have

$$q^* - q = \frac{q_{\text{SAT}}(T, p) - q}{1 + \left(\frac{L}{C_p} \right)_{\text{eff}} \frac{dq_{\text{SAT}}(T, p)}{dT}} \quad (6.8)$$

Secondly, we remove $\Delta W = q - q^*$ from the layer as precipitation as rain or snow depending on the sign of $(T - T_0)$ and we set

$$\frac{\partial T}{\partial t} = \frac{T^* - T}{\Delta t} \quad \text{and} \quad \frac{\partial q}{\partial t} = \frac{q - q^*}{\Delta t}$$

6.1.3 Derivative of $q_{\text{SAT}}(T, p)$ with respect to T

$$\frac{dq_{\text{SAT}}}{dT} = \frac{d}{dT} \left(\frac{e e_s(T)}{p - (1-e)e_s(T)} \right) \quad (6.9)$$

Using (6.1) it is easy to compute:

$$\frac{dq_{\text{SAT}}}{dT} = \frac{a_3 (T_0 - a_4) q_{\text{SAT}}(T, p)}{(T - a_4)^2 \left(1 - (1-e) \frac{e_s(T)}{p} \right)} \quad (6.10)$$

Combining (6.6), (6.8) and (6.10) allows the determination of q^* and T^* .

6.1.4 Evaporation of precipitation

Parametrization of evaporation is rather uncertain. The previous scheme was based on Kessler's approach (Kessler, 1969), using, however, different values for the disposable parameters in previous versions of the operational model, giving significantly different evaporation rates. In view of this uncertainty it was therefore decided to base the parametrization on the observation that the subcloud layer below precipitating non convective clouds is always almost saturated. We therefore impose that the rain/snow effectively evaporates to saturate a layer before reaching the next layer below.

6.1.5 Melting of snow

Melting of snow is parametrized considering observational data summarized by Mason (1971). Melting occurs in a thin layer of a few 100 m below the freezing level. We therefore assume that the snow can melt in each layer whenever the temperature exceeds 2°C. The melting is limited not only by the snow amount but also by keeping the induced cooling of the layer such that the temperature of the layer after melting occurs is not less than the 2°C threshold.

6.2 CODE: SUBROUTINE COND

COND is the last routine to be called for the diabatic processes in the atmosphere. It takes as input the provisional values T , q and p at all levels and corresponding Δp thickness at $(t+1)$, i.e. as a result of the explicit part of the adiabatic calculations and the rest of the diabatic effects (radiation, vertical diffusion and moist convection).

The purpose of COND is then an instantaneous adaption of these values.

We assume that no liquid water or ice are stored in the clouds; if $q > q_{SAT}(T, p)$ then q brought back to q^* and the quantity

$$\frac{(q - q^*)}{2\Delta t} \frac{\Delta p}{g}$$

increases either the rain flux from top to bottom of the layer or the snow flux, depending on the sign of $(T - T_0)$.

The result of the large scale condensation/evaporation melting process is the divergence of the snow/rain flux within each layer k . This divergence is the difference between the incoming flux at the top of the layer $R^T = R_{k,u}$ and the outgoing flux at the bottom of the layer $R^B = R_{k,v}$.

[2.1] At the top of the atmosphere there is no precipitation flux and therefore no evaporation or snow melting can occur within the first layer.

[3.1] The input values for T and q are provisional values obtained by incrementation of $T(t-1)$ and $q(t-1)$ by tendencies due to other than large scale condensation processes

$$\tilde{\psi}_k(t+1) = \tilde{\psi}_k(t-1) + \Delta \tilde{\psi}_k \quad \psi = T, q$$

For sake of simplicity the tilde will be omitted further on. The computation of $\left(\frac{L}{C_p}\right)_{eff}$ is performed

according to Eqn. (6.4) distinguishing between ice and liquid water phase.

[3.2] Depending on the layer temperature being larger than 2°C , snow melting occurs with respect to the constraints of 6.1.5 and modifies the incoming flux R_R^T and R_S^T . Let $\Delta_k S$ be the snow amount melted in layer k . Then

$$R_R^T = R_R^T + \Delta_k S$$

$$R_S^T = R_S^T - \Delta_k S$$

The index R and S refers to rain and snow flux, respectively.

The provisional temperature T_k of the layer is modified to account for the cooling:

$$T_k = T_k - \Delta_k S \frac{\Delta p_k}{2g\Delta t} \left(\frac{C_p}{L} \right)_{f_{\sigma}}$$

where

$$\left(\frac{L}{C_p} \right)_{f_{\sigma}} = \left(\frac{L}{C_p} \right)_{l_{\sigma}} - \left(\frac{L}{C_p} \right)_{v_{\sigma}}$$

This new temperature is then used for the saturation computation.

[3.3] In supersaturated layers within the rain or the snow, flux increases by

$$\Delta_k R = \frac{q_k - q_k^*}{2\Delta t} \cdot \frac{\Delta p_k}{g}$$

The quantity $(q_k - q_k^*)$ representing the distance from equilibrium is computed using Eqn. (6.8) of the theoretical part. In supersaturated layers we have then at the bottom:

$$\begin{aligned} R_S^B = R_S^T & \quad ; \quad R_R^B = R_R^T + \Delta_k R & \text{for} & \quad T_k > T_o \\ R_S^B = R_S^T + \Delta_k R & \quad ; \quad R_R^B = R_R^T & \text{for} & \quad T_k < T_o \end{aligned}$$

[3.4] Avoid evaporation computation if no precipitation.

[4.] If the incoming flux is not equal to zero, there may occur evaporation in the case of unsaturated layers. For unsaturated layers the instantaneous, provisional flux is equal to the incoming flux R^T since there was no incrementation due to condensation. We obtain

$$R^B = \text{MAX} (0, R^T + \text{MIN} (0, \Delta_k R_p \cdot 0.95))$$

which insures that there is no supersaturation in the considered layer due to evaporation.

[6.2] The divergence of snow and rain flux within the layer changes the T and q tendencies:

$$\left(\frac{\Delta q_K}{2\Delta t}\right)_{COND} = \frac{g}{\Delta p} [(R_R^B - R_R^T) + (R_S^B - R_S^T)]$$

and

$$\left(\frac{\Delta T_K}{2\Delta t}\right)_{COND} = -\frac{g}{\Delta p} \left[\left(\frac{L}{C-p}\right)_{v,d} (R_R^B - R_R^T) + \left(\frac{L}{C_p}\right)_{l,w} (R_S^B - R_S^T) \right]$$

[6.4] The bottom fluxes for the layer considered become the top fluxes for the next one and the bottom fluxes at the surface are stored for later use in subroutine SURF.

6.3 REMOVAL OF NEGATIVE MOISTURE VALUES: SUBROUTINE QNEGAT

The purpose of this routine is not to answer a parameterisation need but to remedy some weakness in the discretised dynamical and diffusion equations. If any negative value of q predicted at (t+1) occurs (i.e. from explicit dynamical tendencies plus vertical diffusion plus convection and large scale precipitation) or, more precisely, if q is smaller than a limit value arbitrarily fixed at 10^{-12} , it is brought back to this limit value and the necessary amount of water to perform this change is taken from the layer underneath. This layer is then checked for the same criterion and if an adjustment of the lowest layer is necessary, water is assumed to be available from the ground, although no contribution to the evaporation flux is computed.

References

Kessler, E., 1969: On the distribution and continuity of water substance in atmospheric circulations. Amer.Meteor.Soc. Met.Monogr., 10, 1-84. Americ.Meteor.Soc., Boston, MA.

Mason, B.J., (1971): The physics of clouds. Oxford Univ.Press, 671 pp.

CHAPTER 7

Soil Processes

7.1 THEORY

In the grid point space, the points are divided in two categories land and sea points. A sea point corresponds to a percentage of open water in the mesh greater than 50%. Inland lakes can be sea.

7.1.1 Sea points

Over the sea the surface temperatures are pre-assigned depending on SST analysis and are kept constant during the forecast period.

$$T_{s,t} = T_{s,t-0}$$

This assumption is made for open water as well as for ice covered water which concerns points where $T_{s,t-0} < -2^{\circ}C$ and on which snow cannot accumulate.

The surface humidity is equal to the saturation value at the given surface temperature and pressure.

Accordingly the relative humidity at the surface h (Eq. 3.16) is 1.

$$q_s = q_{sat}(T_s, P_s), h=1$$

7.1.2 Land points

The soil is represented by a three-layer model as shown in Fig. 7.1. The depths of the layers ($D_1 = 7$ cm, $D_2 = D_3 = 6 D_1$) have been chosen so that the system responds to the daily cycle, as well as to medium term forcing. The climate value imposed in the bottom layer is changed monthly, but stays constant during a 10-day forecast.

a) *Temperature*

The temperature evolution obeys a simple diffusion equation (Fourrier's law) with the turbulent heat and radiation fluxes at the surface as boundary conditions.

The equations for temperature are:

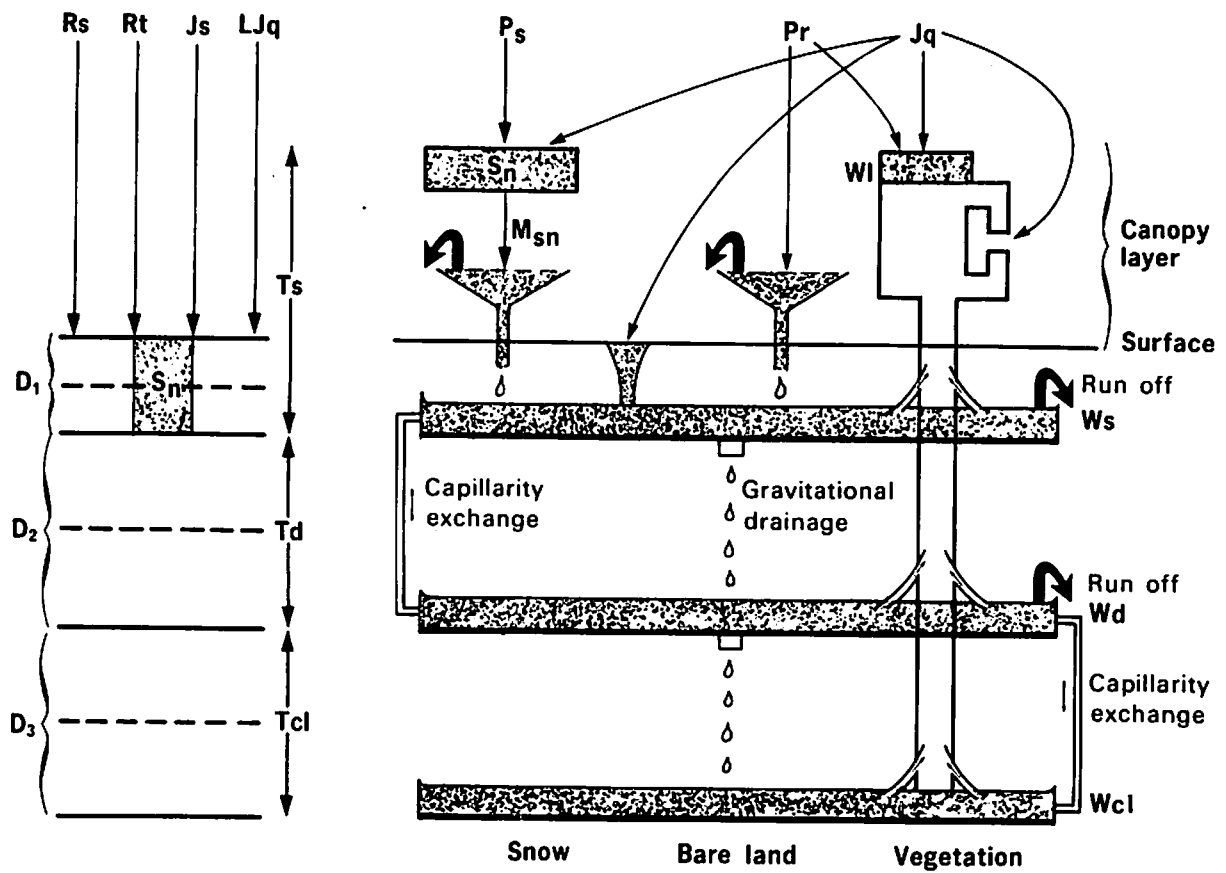


Fig. 7.1 Schematic representation of the surface and sub-surface parametrization in the ECMWF model.

$$\frac{\partial T_s}{\partial t} = \frac{\Sigma F}{\rho_s C_s D_1} + \frac{(T_d - T_s) \kappa^*}{0.5 D_1 (D_1 + D_2)} \quad (7.1)$$

$$\frac{\partial T_d}{\partial t} = \frac{(T_d - T_s) \kappa^*}{0.5 D_2 (D_1 + D_2)} + \frac{(T_{cl} - T_d) \kappa}{0.5 D_2 (D_2 + D_3)} \quad (7.2)$$

The symbol ΣF represents the sum of all the surface heat fluxes: solar (R_s) and thermal (R_T) radiation fluxes, sensible (J) and latent (LJ) heat fluxes. All these fluxes are taken positive downward. The soil characteristics are imposed as follows:

An effective snow cover over land, CVS , taking into account the masking by the vegetation, is defined as

$$CVS = \text{Min} \left(1, \frac{Sn}{D_1} \right) * [(1 - C_v) + C_v * C_{v_{sn}}]$$

(see chapter 2 for definition of $C_{v_{sn}}$)

The heat capacity per unit volume is defined as:

$$\rho_s C_s = [1 - CVS] \rho_g C_g + CVS \rho_l C_l \quad (7.3)$$

with $\rho_g C_g = 2.4 \times 10^6 J m^{-3} K^{-1}$, and $\rho_l C_l = 2.09 \times 10^6 J m^{-3} K^{-1}$

and the heat diffusivity using:

$$\kappa^* = \{[1 - CVS] + a CVS\} \kappa$$

with $\kappa = 7.5 \times 10^{-7} m^2 s^{-1}$ and $a = 0.3$

The shading of the canopy is accounted for simply by modifying κ^* in the following way:

$$\begin{cases} \kappa^* = \kappa^* \text{ if } R_s = 0 \\ \kappa^* = \kappa^* (1 - 0.5 C_v) \text{ if } R_s > 0 \end{cases}$$

b) Moisture

We distinguish between a skin reservoir which evolves under the action of its own evaporation and its ability to collect dew and intercept precipitation and the soil reservoirs (see Fig. 7.1).

The moisture flux J_g is split in three parts:

$$J_g = J_{gl} + J_{qv} + J_{qG} \quad (7.4)$$

where J_{gl} is the part of the evaporation coming from the skin reservoir itself (see chapter 3 for definition of these quantities).

The skin reservoir content W_l evolves according to:

$$\frac{\partial W_l}{\partial t} = (J_{gl} + CIP \cdot C_v \cdot P_R) / \rho_{H_2O} \quad (7.5)$$

C_v is the percentage of vegetation, P_R is the initial rain flux at the surface, CIP is the coefficient of efficiency of interception of rain, taken as 25%.

The computation of the interception of precipitation is done separately for the convective and large-scale rain. For convective rain, it is assumed that the precipitation (CP) falls in an area $1/C_A$ with an intensity $CA * CP$ ($C_A = 0.5$, see *Entekhabi and Eagleson, 1989*)

We impose also

$$0 \leq W_l \leq W_{lmax} \quad (7.6)$$

with W_{lmax} as in Eq 3.7.

After this step, the remaining moisture flux ($J_{qv} + J_{qG}$) and the rain P_R are modified in order to represent what has not been used in the skin reservoir. $J_{qv}/(J_{qv} + J_{qG})$ is not modified.

The moisture evolution in the soil obeys a simple diffusion equation modified to account for the effect of gravity (Darcy's law) and with an additional sinking term for each layer, corresponding to the root uptake by vegetation. The top boundary conditions are given by infiltration of rain water and snow melt, I_f , and evaporation J_{qv} , as modified after the skin reservoir has been dealt with.

$$\frac{\partial W_s}{\partial t} = \frac{J_{qv}}{\rho_{H_2O}} + I_f + \frac{(W_d - W_s)\lambda}{0.5D_1(D_1 + D_2)} - \gamma - \frac{Ext_1}{\rho_{H_2O}} \quad (7.7)$$

$$\frac{\partial W_d}{\partial t} = \frac{(W_d - W_s)\lambda}{0.5D_2(D_1 + D_2)} + \frac{(W_{Cl} - W_d)\lambda}{0.5 * D_2(D_2 + D_3)} - \frac{Ext_2 D_1}{\rho_{H_2O} D_2} \quad (7.8)$$

λ is the hydraulic diffusivity taken as $10^{-7} m^2 s^{-1}$ and γ is the hydraulic conductivity taken as $10^{-10} m s^{-1}$. The quantity W_s is the amount of water present in top layer reservoir of the ground model. It is measured in metres of water. To be consistent W_d must also be scaled to the same depth D_1 .

The root uptake Ext_i are linked by:

$$J_{qv} = Ext_1 + Ext_2 + Ext_3$$

The partitioning of the water pumping by the vegetation in the reservoirs is given by:

$$Ext_i = \frac{R_i W_i \lambda |J_{qv}|}{\sum \lambda R_i W_i}; W_i = W_s, W_d, W_{cl}$$

I_f represents the infiltration of water.

In order to compute it, a maximum infiltration rate, I_{fmax} is defined as

$$I_{fmax} = \left[\lambda \frac{W_{sat} - W_s}{0.5 D_1 D_1} + \gamma \right] \quad (7.11)$$

where W_{sat} is the soil wetness at the soil porosity ($W_{sat} = 0.44 * D_1$)

The surface runoff due to sloping terrain, RO_1 , is computed as

$$RO_1 = (P_r + M_{sn}) * R_{SR}$$

where the fraction R_{SR} is given by

$$R_{SR} = \text{Max} [0, (Vor - Vor_{min}) / (Vor_{min} + Vor_{max})] \quad (7.12)$$

Vor is the non-directional variance of orography, $Vor_{min} = 50^2 m^2$, $Vor_{max} = 750^2 m^2$. M_{sn} is the melting of snow (to be specified later).

A second contribution to surface runoff is computed as

$$RO_2 = \text{Max} \{0, [(P_r + M_{sn}) - RO_1] - I_{fmax}\}$$

In this last computation we use again the assumption that the convective precipitation doesn't occupy the entire grid-box. The infiltration I_f is finally defined as

$$I_f = (P_r + M_{sn}) - (RO_1 + RO_2) \quad (7.13)$$

In addition to (7.7) and (7.8) we have the conditions

$$0 \leq W_s \leq W_{scap} \text{ and } 0 \leq W_d \leq W_{scap} \quad (7.14)$$

If the value W_{scap} (0.02m) is exceeded, runoff is assumed to take place.

If one or both of the reservoir contents become negative, a rearrangement of soil wetness takes place, one reservoir borrowing the needed water from the adjacent reservoir below it.

c) *Snow*

The snow depth is measured in meters of equivalent liquid water, and obeys the equation:

$$\frac{\partial S_n}{\partial t} = \frac{J_{qS_n}}{\rho_{H_2O}} + P_s - M_{S_n} \quad (7.15)$$

where P_s is the amount of precipitation as snow and M_{S_n} represents the melting of snow (see paragraph d). The area fraction covered by snow is defined as

$$C_{S_n} = \min \left(\frac{S_n}{S_{n_{cr}}}, 1 \right) \quad (7.16)$$

with $S_{n_{cr}} = 0.015m$

A correction to avoid negative values of S_n is applied.

d) *Snow melting*

In snow melting episodes the surface layer (snow free and snow covered part) and the deep layer directly underneath the snow covered part exchange energy. A distinction is made between "surface" melting and "deep" melting. For the former, the water melted by the surface fluxes is assumed to refreeze inside the snow pack, no changes in the snow depth occur. For "deep" melting, the energy to melt the snow pack is borrowed from the ground directly.

We will call \bar{T}_s , \bar{T}_p , \bar{W}_s , \bar{W}_d and \bar{S}_n the values obtained after integration of (7.1 - 7.2), (7.7 - 7.8) and (7.9), without the melting term.

Because of (7.3) (see also fig 7.1) \bar{T}_s represents a mean surface temperature in the grid box,

$$\rho_s C_s \bar{T}_s = CVS * \rho_l C_l T_{s_{sn}} + (1-CVS) * \rho_g C_g * T_{s_g}$$

where T_{s_m} and T_{s_o} are, respectively, the (unknown) temperatures of the snow mantle and the snow free part of the ground

- (i) If $\bar{T}_s < T_o$ provisional values become the final one.
- (ii) If $\bar{T}_s > T_o$, it is assumed that this reflects a mean state with $T_{s_m} = T_o$ (melting snow).

An equilibrium temperature of the ground part of the grid box, T_s^e , is found by solving

$$\rho_s C_s \bar{T}_s + \rho_g C_g * CVS * \bar{T}_d - \rho_g C_g * T_s^e + CVS * \rho_l C_l * T_o,$$

giving

$$T_s^e = \bar{T}_s + CVS * \left[\bar{T}_d - \bar{T}_s + \frac{\rho_l C_l}{\rho_g C_g} (\bar{T}_s - T_o) \right]$$

(ii-1) If $T_s^e < T_o$ we have conditions for surface melting. The final temperature of the ice pack is T_o . No change occurs in S_n , but the energy released in refreezing the water inside the snow mantle is assumed to be gained by the deep layer, corresponding to a temperature difference

$$\Delta T_d = \frac{\rho_l C_l}{\rho_g C_g} (\bar{T}_s - T_o)$$

Conservation of total energy in this redistribution implies

$$\rho_s C_s \bar{T}_s + \rho_g C_g * CVS * \bar{T}_d = \rho_s C_s T_s + \rho_g C_g * CVS * (\bar{T}_d + \Delta T_d)$$

where T_s is the new surface temperature.

Solving for T_s gives

$$T_s = [CVS * \rho_l C_l * T_o + (1-CVS) * \rho_g C_g * \bar{T}_s] / \rho_s C_s$$

while the new deep temperature T_d is given by

$$T_d = \bar{T}_d + \frac{D_1}{D_2} CVS \frac{\rho_l C_l}{\rho_g C_g} (\bar{T}_s - T_o)$$

(ii-2) If $T_s^e > T_o$ "deep" melting occurs. The whole layer is now involved in the melting. The amount of snow melted is proportional to $(T_s - T_o)$, where T_o is assumed to be the final temperature of the part of the deep layer in contact with the snow.

$$\Delta S_n = \min \left\{ \bar{S}_n, CVS * \frac{\rho_g C_g}{L_f \rho_{H_2O}} D_1 (T_e - T_d) \right\}$$

A new snow amount is computed as

$$S_n = \bar{S}_n - \Delta S_n$$

corresponding to a new snow cover

$$CVS^* = \min \left(1, \frac{S_n}{D_1} \right) * [(1 - C_v) + C_v * C_{v,s}]$$

The energy conservation reads now

$$\begin{aligned} & \rho_g C_g T_s^e + CVS * \rho_l C_l T_o + (CVS^* - CVS) * \rho_l C_l T_o + CVS * \rho_g C_g * (T_o - T_s^e) \\ & - (\rho_s C_s)^* T_s + CVS^* \rho_g C_g T_o \end{aligned}$$

In the previous equation the terms in the left-hand side represent the initial energy of the ground part (including the deep soil part involved in the melting), the initial energy of the snow mantle, the energy involved in the change in snow cover and the energy for the temperature change of the deep layer. On the right-hand side we have the final energy of the surface layer (with $(\rho_s C_s)^*$ the heat capacity corresponding to the snow cover CVS^*) and the final energy of the deep layer in contact with the snow.

Solving for T_s gives

$$T_s = \left[CVS^* * \rho_l C_l T_o + (CVS - CVS^*) \rho_g C_g T_o + (1 - CVS) * \rho_g C_g T_s^e \right] / (\rho_s C_s)^*$$

while the new deep temperature is

$$T_d = \bar{T}_d + CVS * \frac{D_1}{D_2} (T_o - \bar{T}_d)$$

(iii) Finally the water available from melting is used to wet the soil after interception by the skin reservoir and runoff have taken place.

e) Time-stepping

(7.1), (7.2), (7.5), (7.7), (7.8) and (7.15) are solved implicitly in the following manner. Let us write these equations in a general way as

$$\frac{\partial \psi}{\partial t} = \phi(\psi) \tag{7.17}$$

where ψ represents T_s , W_s , or S_n and ϕ is the flux divergence, precipitation or snow melt. ϕ can be linearized in terms of ψ so that

$$\phi^{t+1} = \phi^{t-1} + \frac{\partial \phi^{t-1}}{\partial \psi} (\psi^{t+1} - \psi^{t-1}) \quad (7.18)$$

where the superscript indicates the time level. If now (7.17) is written as a centred implicit time step:

$$\frac{\psi^{t+1} - \psi^{t-1}}{2\Delta t} = \frac{1}{2} (\phi^{t-1} + \phi^{t+1}) - \phi^{t-1} + \frac{1}{2} \frac{\partial \phi}{\partial \psi} (\psi^{t+1} - \psi^{t-1}) \quad (7.19)$$

From this we obtain:

$$\psi^{t+1} - \psi^{t-1} = \frac{2\Delta t \cdot \phi^{t-1}}{1 - \Delta t \cdot \frac{\partial \phi^{t-1}}{\partial \psi}} \quad (7.20)$$

In addition to this implicit procedure we use a time filter to connect the odd time steps to the even ones. This filter uses only the forward part of the operator used for the atmospheric variables:

$$\psi_{filtered}^t = \psi^t + \epsilon_f [\psi^{t+1} - \psi^t] \quad (7.21)$$

The reason for using the forward operator only is to allow the snow to melt completely and soil moisture to reach saturation.

7.2 CODE - SUBROUTINE SURF

Subroutine SURF drives the surface computations in the model.

[2.] No calculations are performed for grid-points over the sea.

[3.1] Temperature changes are computed in routine SRFT. The sensible and latent heat fluxes together form the total heat flux which, with its derivative with respect to T_s , is a result of subroutine VDIFF.

The solar radiation flux at the surface is independent of T_s and is a result of RADHEAT. The thermal radiation and its derivative are recomputed using the Stefan-Boltzmann formula:

$$F_T = \epsilon_e \sigma T_s^4$$
$$\frac{\partial F_T}{\partial T_s} = 4 \epsilon_e \sigma T_s^3$$

where σ is the Stefan-Boltzmann constant and ϵ_e the effective soil emissivity computed during the full radiation time step.

According to Eq. (7.1) these quantities are used for the computation of $T_s(t+1)$. We also compute $T_d(t+1)$ using Eq. (7.2).

[3.3] Changes in moisture associated to the skin reservoir are computed in routine SRFWL. In the following order, evaporation, collection of dew ($J_q > 0$) and interception of precipitation (P_R) are considered. The precipitation and moisture fluxes are adjusted.

[3.4] Surface and deep soil moisture changes are dealt with in SRFW. The surface runoff due to sloping terrain and then due to water not allowed to infiltrate is calculated and stored in RO_s .

Then the soil moisture changes are considered without melting, allowing the reservoirs to be in excess of the field capacity. The evapotranspiration over the vegetated part is converted in root-uptake for the different reservoirs. The calculations are performed as for the temperatures using Eqs. 7.7 and 7.8.

[3.6] Snow changes prior to melting are dealt with in SRFSN. Depending on C_{sn} either the snow depth or the water content is affected. Equation 7.15 (without the term M_{sn}) is solved.

[4.1] Routine SRFSML controls the melting computations and the correction to negative values of

snow. From the new provisional values of soil temperature \bar{T}_s , \bar{W}_s and \bar{S}_n snow melting is computed (if $\bar{T}_s > T_o$).

First, snow depth is corrected to avoid negative values. This correction term will be considered similar to a "melting" from an energetic point of view.

New values of T_s , T_d and S_n are obtained following what was described in section 7.1.2 (d). The water available from melting is used to wet the soil. First the skin reservoir intercepts it. The remaining part is then checked for surface runoff due to orography and the maximum infiltration of the ground. The remaining water is used to wet the surface reservoir.

Finally the water used in the correction for negative snow depth is borrowed from the surface reservoir.

[5.] Routine SRFWNG controls the adjustment needed in order to obtain properly bounded soil wetness. A correction is performed for the water content due to the runoff

$$RO_s = W_s - W_{s_{max}} \text{ if } W_s > W_{s_{max}}$$

$$RO_d = W_d - W_{d_{max}} \text{ if } W_d > W_{d_{max}}$$

and to avoid negative values for W_s and W_d .

[6.] The application of the forward time filter is then performed.

References

Entekhabi, D. and P.S. Eagleson, 1989: Land surface hydrology parametrization for atmospheric general circulation models including subgrid scale spatial variability. *J.Climate*, **2**, 816-831.

APPENDIX 1

Climatological data used in the model

In addition to the physical constants already listed in Table 1, the model uses a number of physical and climate fields. The derivation of surface climate fields are described in more detail by *Branković and Van Maanen (1985)* and only a brief account of these fields is given here. The maps of all surface fields shown are in T213 resolution. For the surface geopotential height also other resolutions are shown (Fig.A1a-d).

1. OROGRAPHY

Orography, or geopotential of terrain height, was derived from the US Navy dataset, provided by NCAR. This dataset, with a resolution of 10' of arc on a regular latitude-longitude grid, contains the average terrain heights of each grid element, as well as maximum and minimum height, number and orientation of significant ridges, and the percentages of water and urban areas.

The model orography is represented in terms of an envelope orography. It is calculated according to the expression

$$\phi_s = g(H_m + \alpha\sigma)$$

where $g = 9.80665$ is the acceleration of the earth's gravity, H_m is the mean height on the T213 Gaussian grid retrieved from the US Navy dataset, α is the proportion of standard deviation to be added to the mean height over land points, and σ is the standard deviation of mean height defined for the same grid as H_m . For the operational orography $\alpha=1$ (Figs. A.1-A.5).

The operational orography is smoothed using a Gaussian filter with a radius of 25 km. The filtering smooths a field interpolated from the 10' grid. Then, the spectral fit is applied to the filtered orography. The purpose of spectral fitting is to ensure consistency in spectral resolution between the orography field and model resolution of upper air fields. Orography ripples appear as a consequence of spectral fitting.

2. LAND-SEA MASK

Each grid-point of the model is defined as a land or sea point depending on whether the grid square contains more or equal to, or less than 50% of land fraction at the T213 Gaussian grid derived from the US Navy dataset (Fig. A.6).

3. ROUGHNESS LENGTH

The total roughness length is a combination of the roughness length due to vegetation, which has been interpolated from original to the T213 Gaussian grid, and the roughness length derived from orography parameters on the same grid as described by *Tibaldi and Geleyn (1981)*.

The procedure to compute roughness length z_o was the following:

- a) z_o data on vegetation obtained on a 5° x 5° grid from München University (*Baumgartner et al., 1977*) were interpolated to a T213 Gaussian grid.
- b) Information was extracted from the US Navy data about urbanisation. A value proportional to 2.5 metres for 100% town area was assumed.
- c) Information was also extracted from the same source about the number of significant ridges and of topography maximum excursion in a 10'x10' box. This was combined with an analysis of the variance and number of extremes of the 10' grid topography with respect to the mean T213 value into the following formula for z_o (roughness height α to variance x slope):

$$z_o = \sqrt{\frac{N}{F} (\sum p_i \bar{h}_i^2 - (\sum p_i \bar{h}_i)^2)} + \sum \sqrt{\frac{n_i}{f_i}} p_i \frac{(\bar{h}_i - h_i^{\min})(h_i^{\max} - \bar{h}_i)}{4}$$

- where:
- N = number of relative \bar{h}_i maxima in the ECMWF grid square
 - F = surface area of the ECMWF grid square
 - n_i = number of significant ridges in the 10' grid square
 - \bar{h}_i = mean height in the 10' grid square
 - h_i^{\max} = maximum height in the 10' grid square
 - h_i^{\min} = minimum height in the 10' grid square
 - f_i = surface area of the 10' grid square
 - p_i = proportion of the ECMWF grid square occupied by the i'th 10' grid square

A blended z_o is derived by using a root mean square average of a), b) and c). The logarithm of the blended roughness length is then smoothed by the same Gaussian filter as used in the orography filtering. Over sea and sea ice points it is set to 0.001 m. Fig A.7 shows the roughness length field up to 50 cm with fine contouring and Fig. A.8 shows the roughness length above 50 cm with coarser contouring.

4. ALBEDO

The original data on the albedo on a 1° x 1° grid corresponds to Dorman and Sellers (1989), and was then interpolated to the model grid.

Over yearly averaged sea ice the albedo was set to 0.55, over water points to 0.07, over land the minimum is 0.07 and overall maximum cannot exceed 0.80.

This is a background yearly climate field and model alters it during the run according to snow cover (Fig. A.9).

5. DEEP-LAYER SOIL TEMPERATURE

This field was derived from surface temperature which has been obtained by the procedure described by *Branković and Van Maanen (1985)*. From the surface temperature deep-layer temperature is calculated using the expression

$$T_d^{(n)} = (1-c) T_o + c (aT_s^{(n)} + bT_s^{(n-1)})$$

where T_o denotes the mean annual surface temperature, $T_s^{(n)}$ and $T_s^{(n-1)}$ are the surface temperatures for month n and previous month $n-1$, a and b are constants defining the temperature phase lag and c is a constant describing the amplitude damping. Currently $a = b = 0.5$ and $c = 0.77$. The above formula applies only over land points, so Figs. A.10 to A.21 display, besides the deep-layer temperature over land, the actual sea surface temperature over water points.

6. DEEP-LAYER SOIL MOISTURE

This climate field is derived from the original data of *Mintz and Serafini (1981)*. The original soil moisture is first interpolated to the operational Gaussian grid. The depth of the model's deep (third) ground layer is 42 cm and the maximum water content in this layer is assumed to be 12 cm. Since values used in the forecast model are scaled to the depth of the first ground layer (which is 7 cm deep), all original data are therefore scaled accordingly. In Figs. A.22 to A.33 the deep-layer soil moisture is shown as a percentage of the total field capacity.

7. VEGETATION

This field is derived from Henderson-Sellers' dataset containing information primarily gathered by *Mathews (1983)*, then revised and widened by *Wilson and Henderson-Sellers (1985)*. The basic information is vegetation types with corresponding surface coverage on a 1°x1° regular grid. This allows

to compute on the same grid a fractional coverage of vegetation. This basic information is then interpolated or extrapolated to give a vegetation ratio at various model resolution. Its distribution for the operational resolution is shown in Fig. A.34.

8. OZONE DISTRIBUTION

The total amount of ozone was taken from *London et al. (1976)*, while the altitude of the maximum concentration was derived from *Wilcox and Belmont (1977)*. These two quantities correspond to the parameters a and b in (2.36). Heights of the maximum ozone concentration and its distribution are shown in Figs. A.35 and A.36.

References

Baumgartner, A., Mayer, H. and Metz, W., 1977: Weltweite Verteilung des Rauigkeitsparameters Z_0 mit Anwendung auf die Energiedissipation an der Erdoberfläche. Meteorolog.Rdsch., 30, 43-48.

Branković, Č., and J. Van Maanen, 1985: The ECMWF climate system. ECMWF Tech.Memo.No. 109, 51 pp + Figs.

Dorman, J.L., and P.J. Sellers, 1989: A global climatology of albedo, roughness length and stomal resistance for atmospheric general circulation models as represented by a simple biosphere model (SiB). J.Appl.Meteor., 28, 833-855.

London, J., Bojkov, R.D., Oltmans, S. Kelley, J.I. 1976: Atlas of the global distribution of total ozone, July 1957 - June 1967. NCAR Technical Note 113+STR.

Matthews, E., 1983: Global vegetation and land use: New high-resolution data bases for climate studies. J.Clim.Appl.Meteor., 22, 474-487.

Mintz, Y., and Y. Serafini, 1981: Global fields of soil moisture and land-surface evapotranspiration. NASA Goddard Flight Center Tech.Memo. 83907, Research Review - 1980/81, 178-180.

Tibaldi, S., and J.F. Geleyn, 1981: The production of a new orography, land-sea mask and associated climatological surface fields for operational purposes. ECMWF Tech.Memo.No. 40, 93 pp.

Wilcox, R.W. and A.D. Belmont, 1977: Ozone concentration by latitude, altitude and month, near 80°W. Report, Control Data Corporation, Contract No.DOT- FA77WA-3999.

Wilson, M.F., and A. Henderson-Sellers, 1985: Cover and soils data sets for use in general circulation climate models, J.Climatol., 5, 119-143.

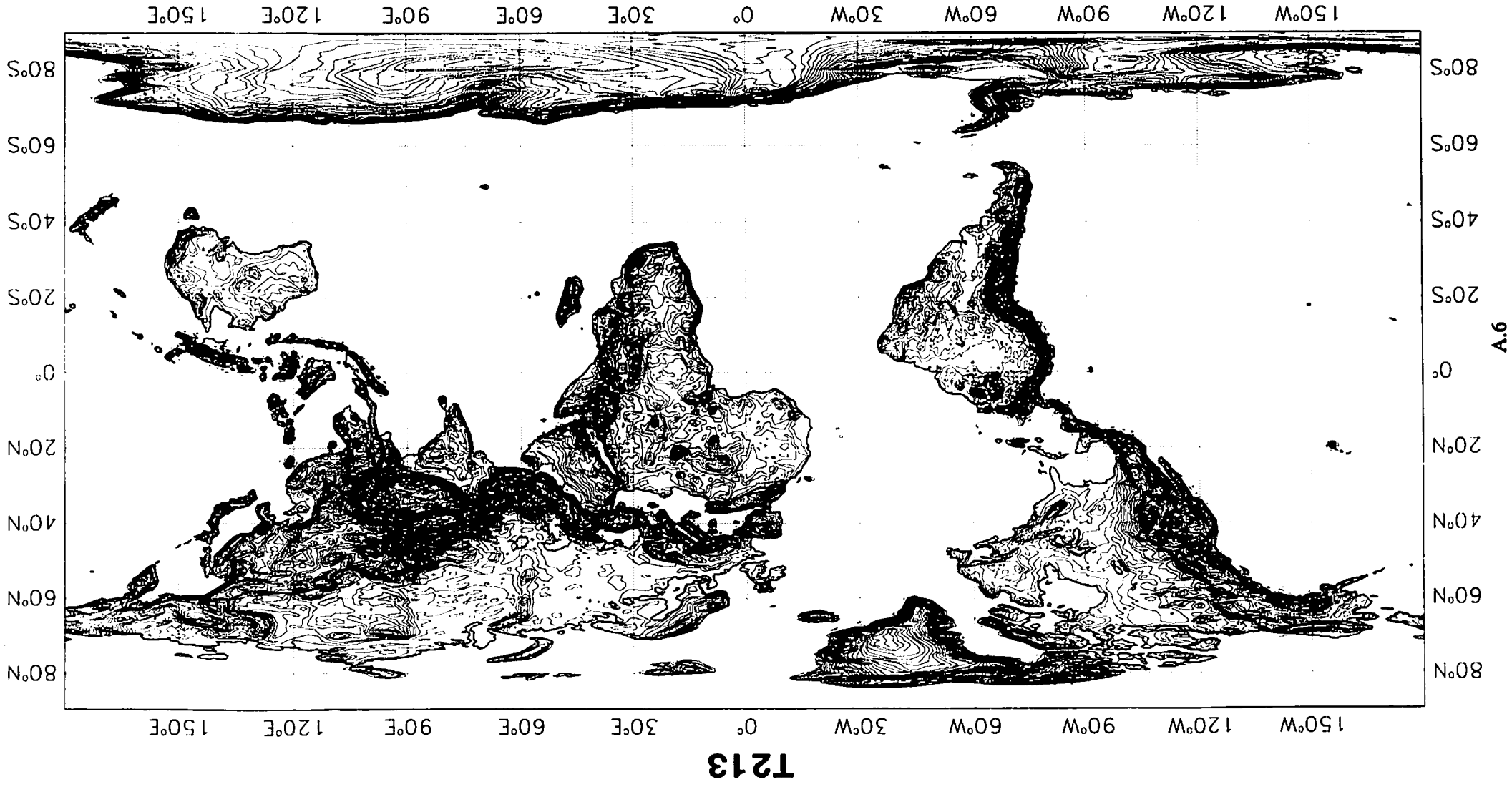


Fig. A.1 Surface geopotential height (terrain height). Contour interval 10 dam.

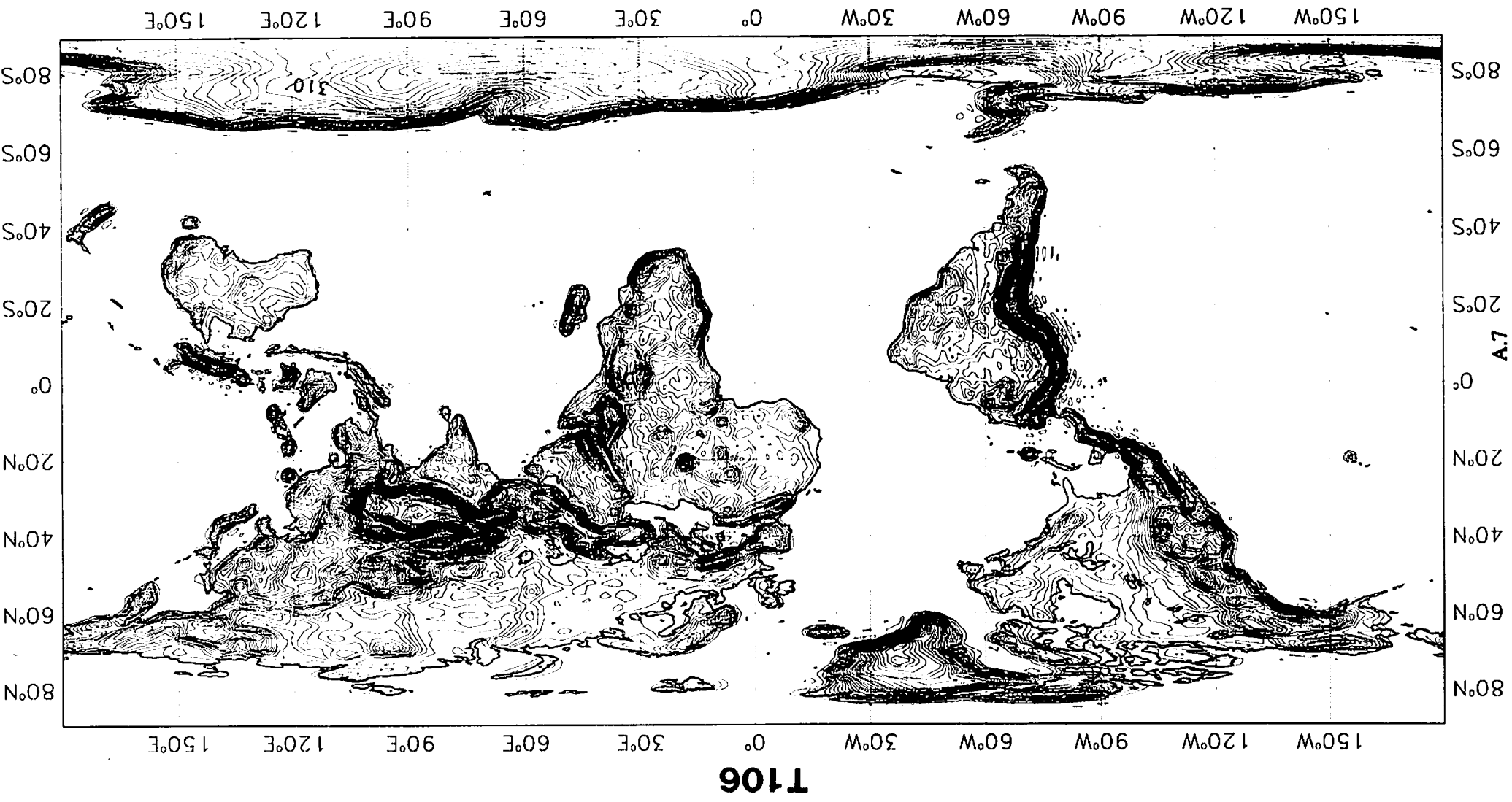


Fig. A.1.a Surface geopotential height (terrain height). Contour interval 10 dam.

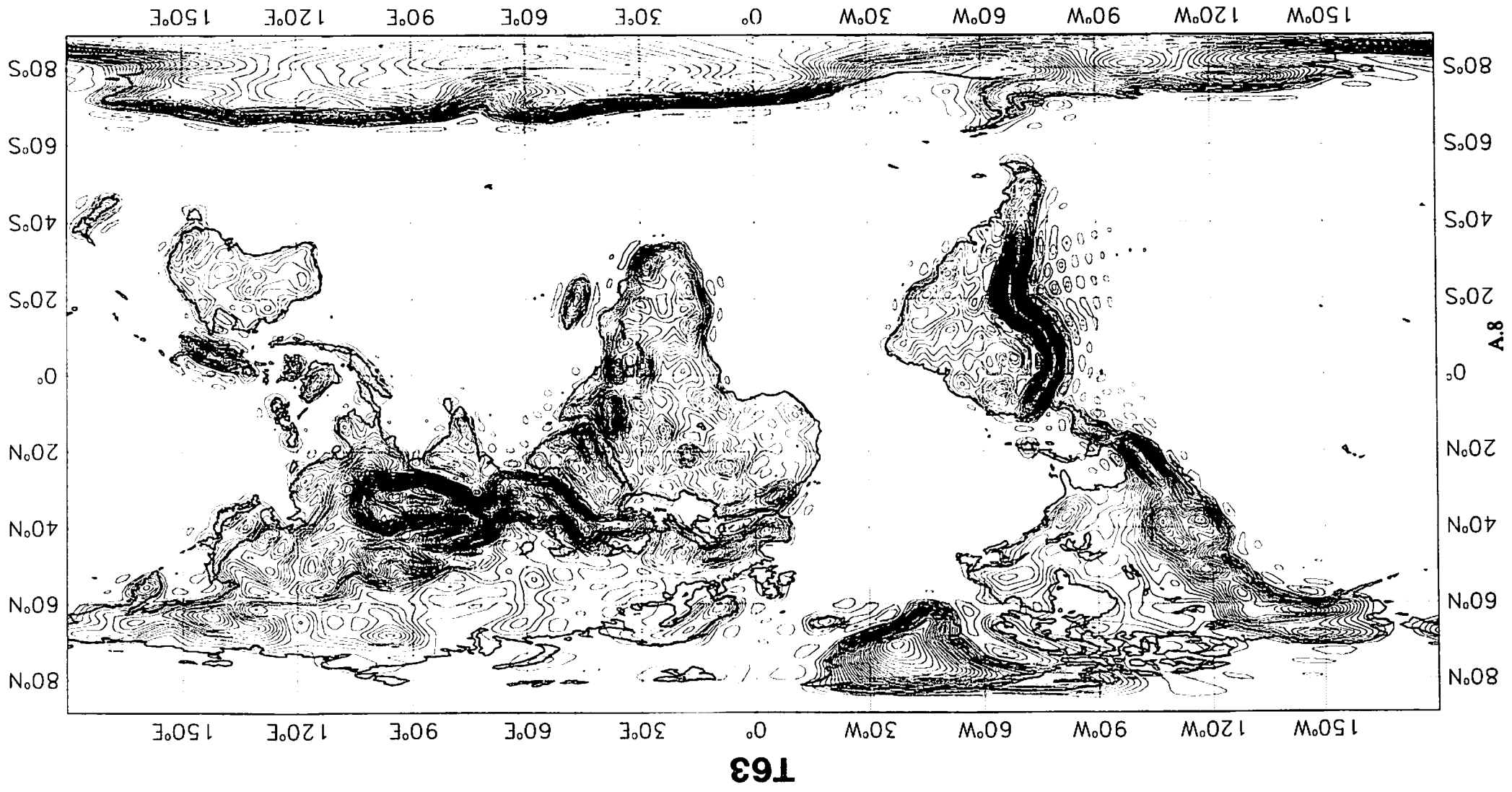


Fig. A.1.b Surface geopotential height (terrain height). Contour interval 10 dam.

T63

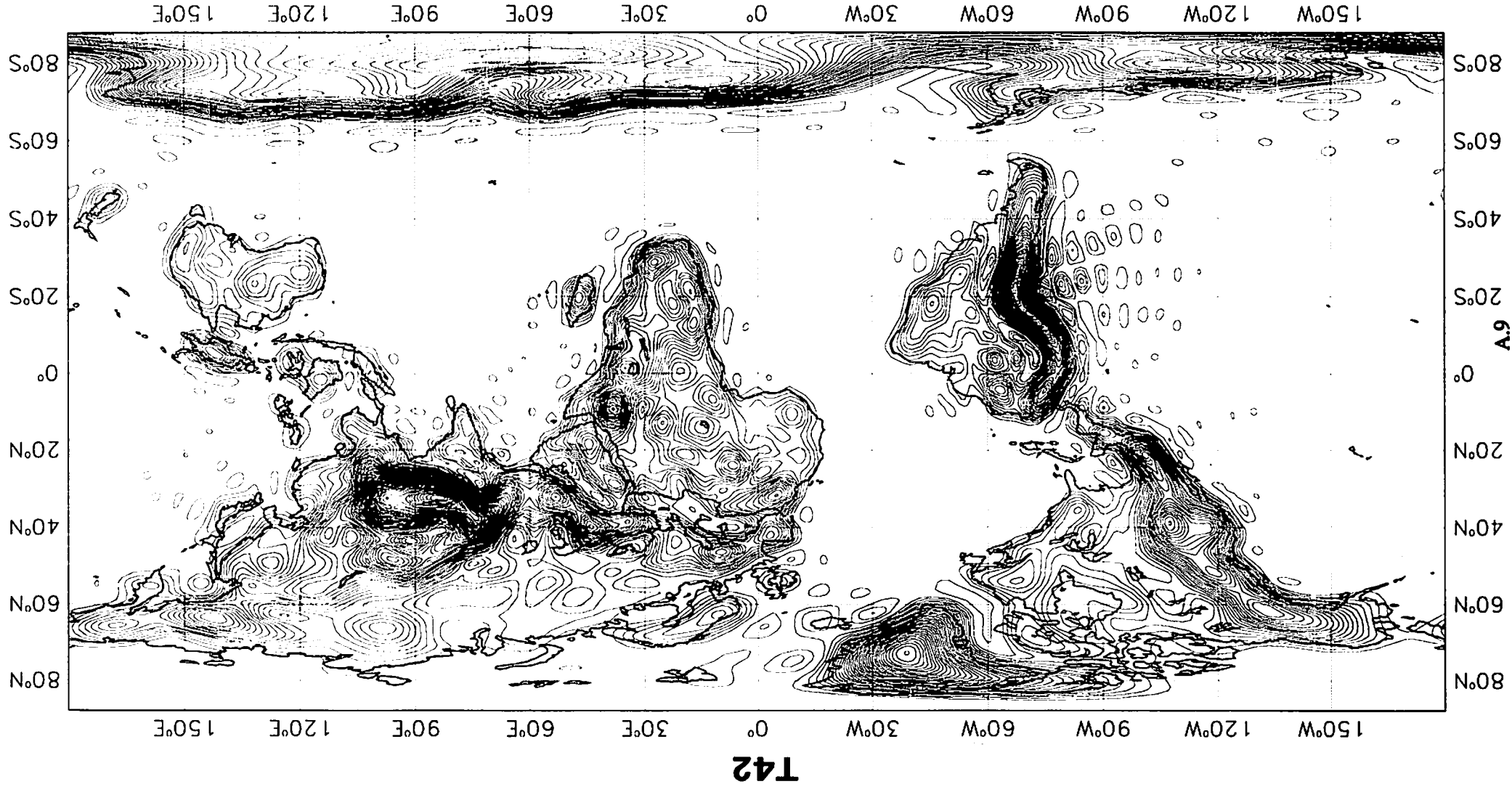


Fig. A.1.c Surface geopotential height (terrain height). Contour interval 10 dam.

T21

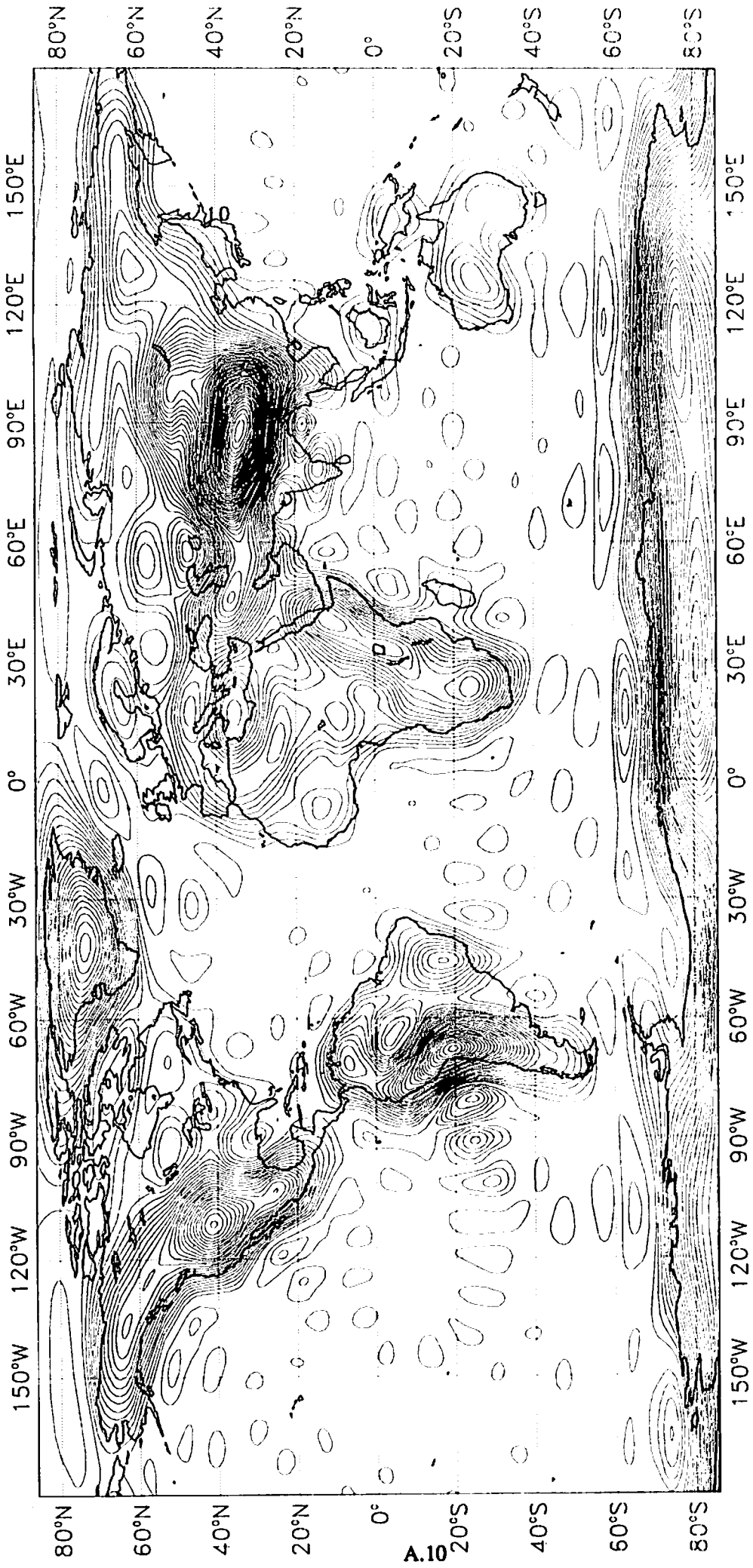


Fig. A.1.d Surface geopotential height (terrain height). Contour interval 10 dam.

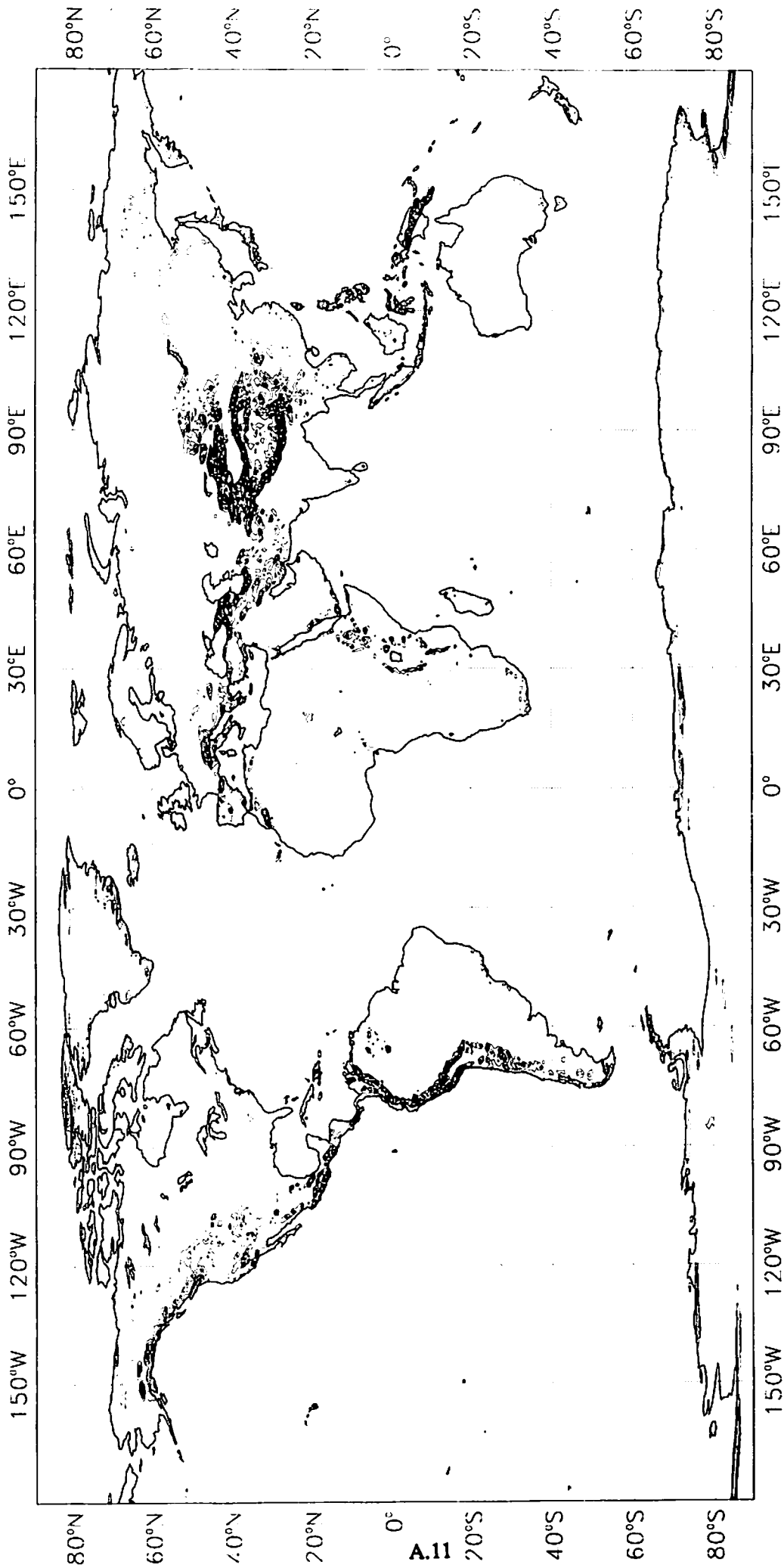


Fig. A.2 North south orographic variance. Contour interval 50,000 m²/s².

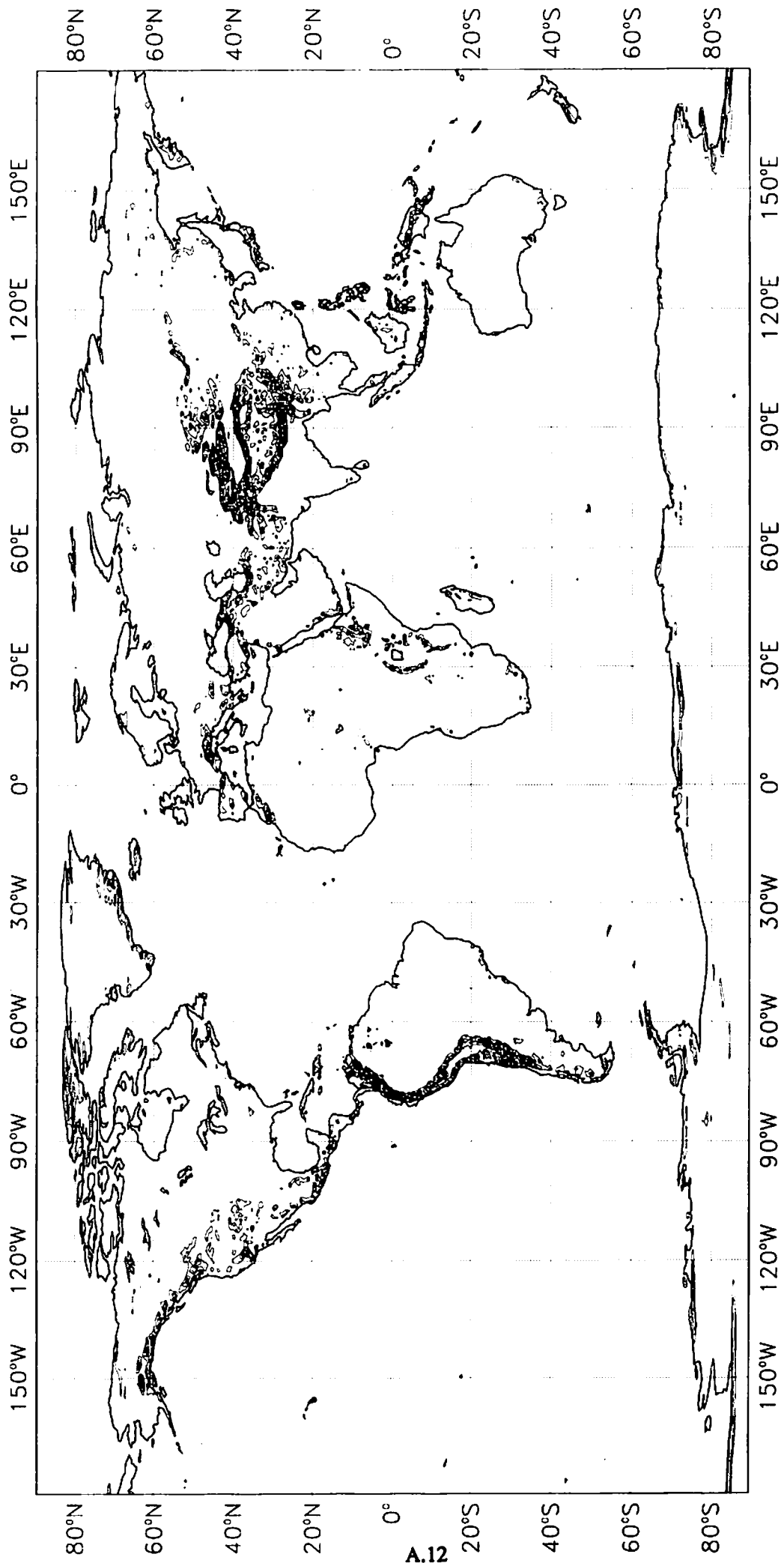


Fig. A.3 North west south east orographic variance. Contour interval 50,000 m²/s⁴.

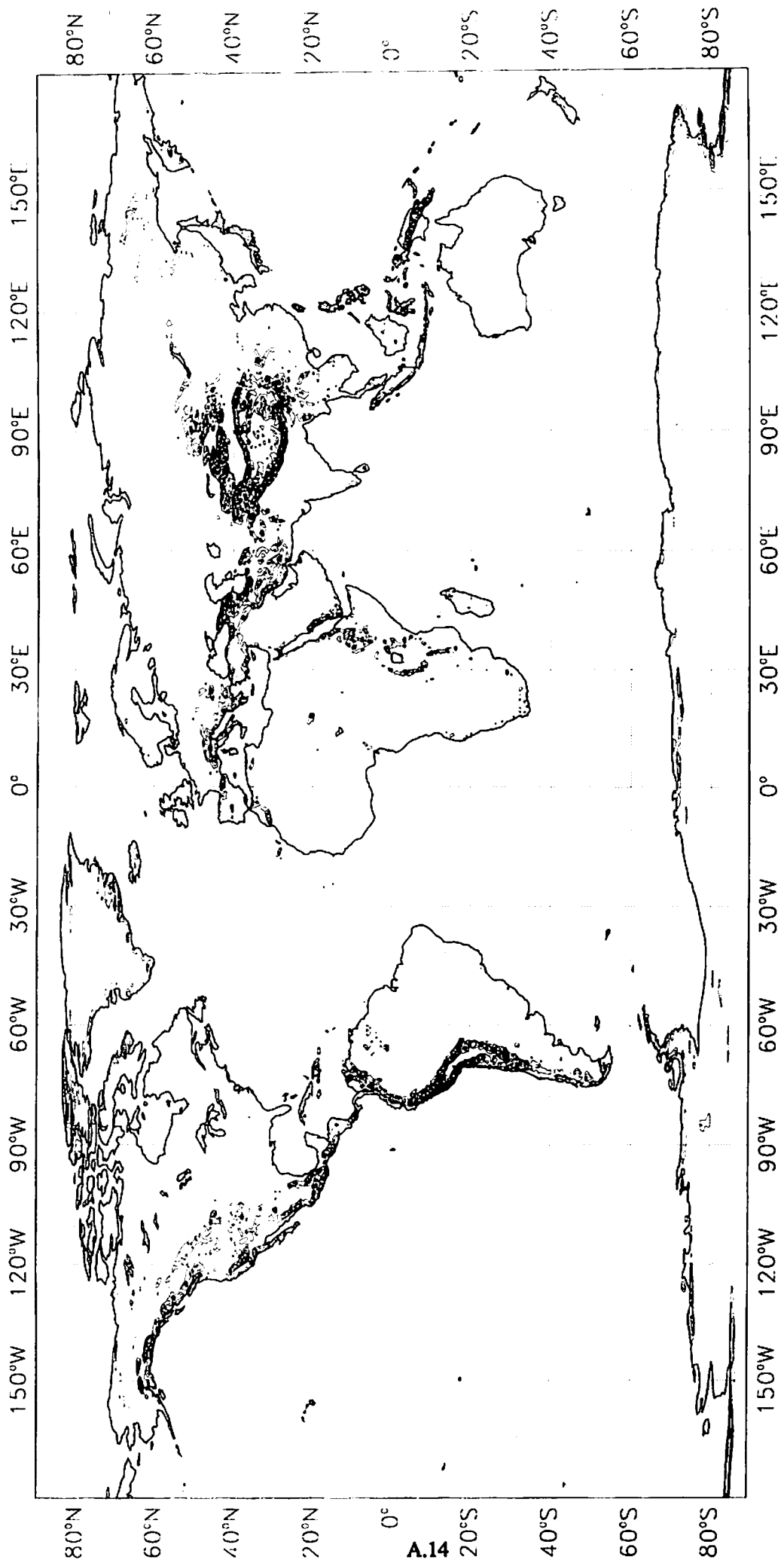


Fig. A.5 North east south west orographic variance. Contour interval 50,000 m²/s⁴.

The T213 reduced Gaussian grid

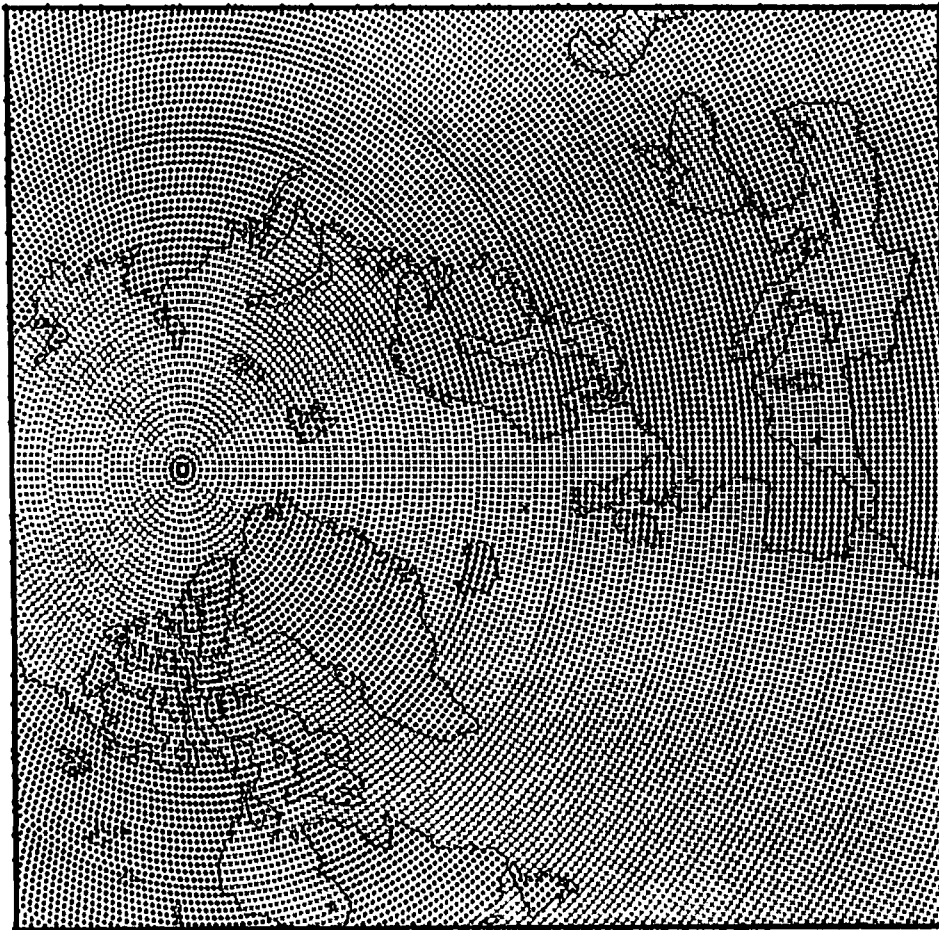


Fig. A.6.1 Land-sea mask Europe.

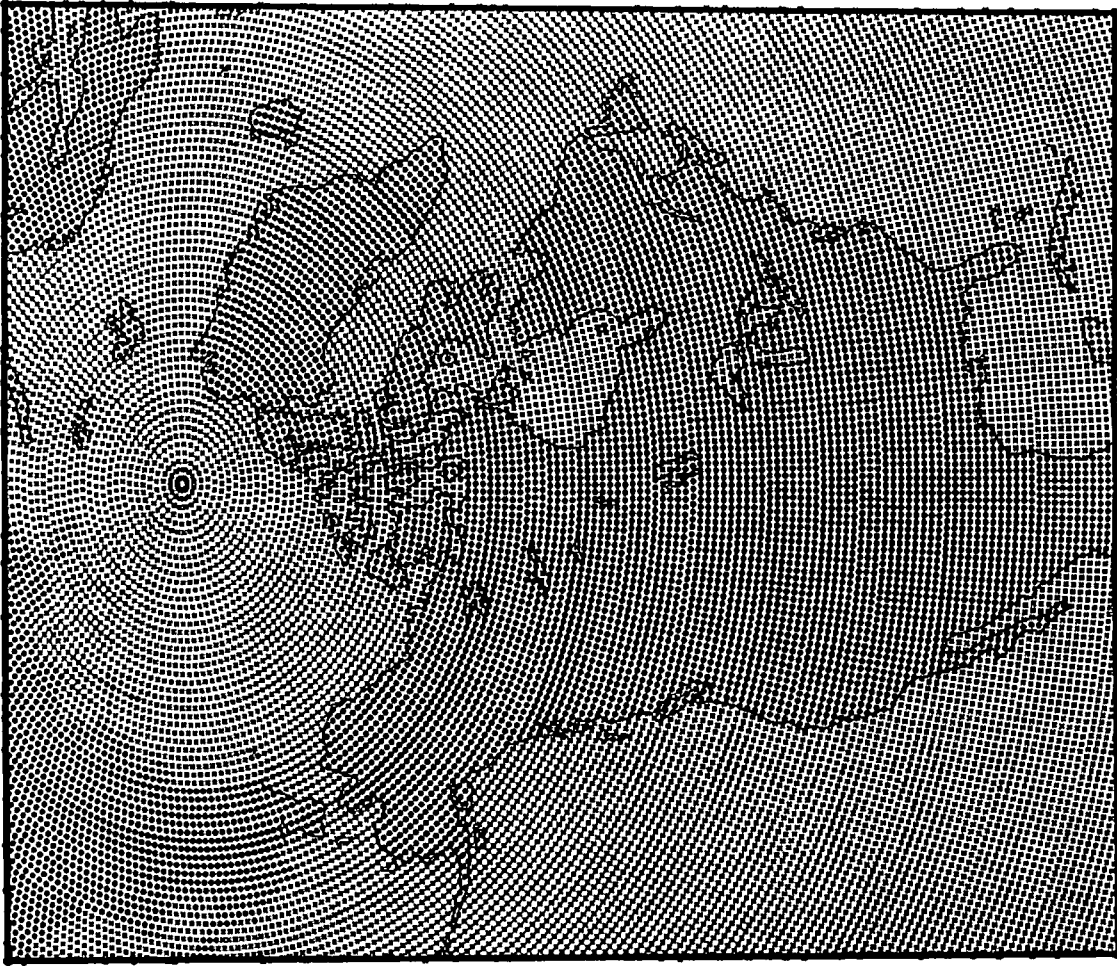
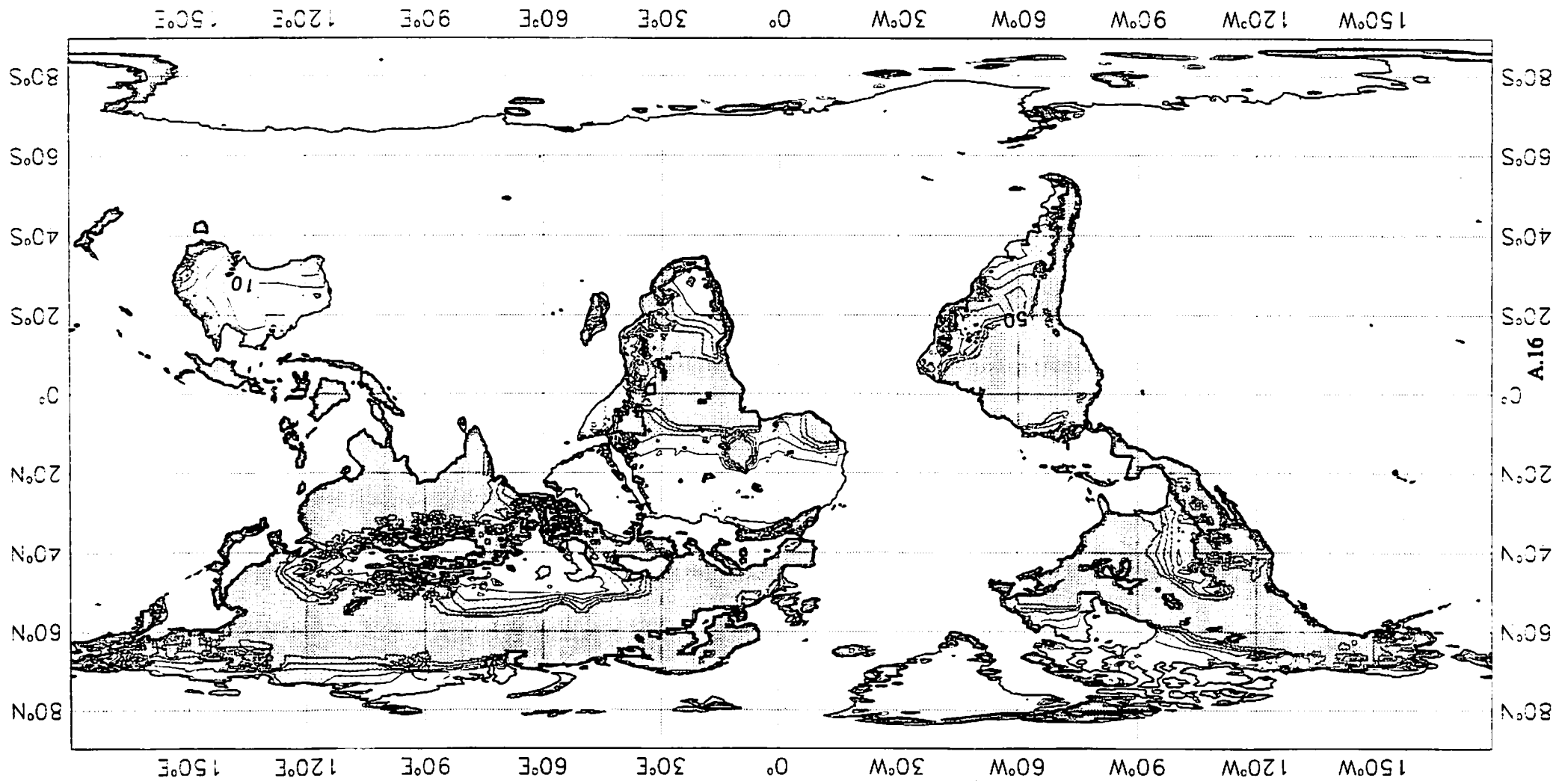


Fig. A.6.2 Land-sea mask North America.

Fig. A.7 Roughness length below 50 cm. Contour interval 10 cm.



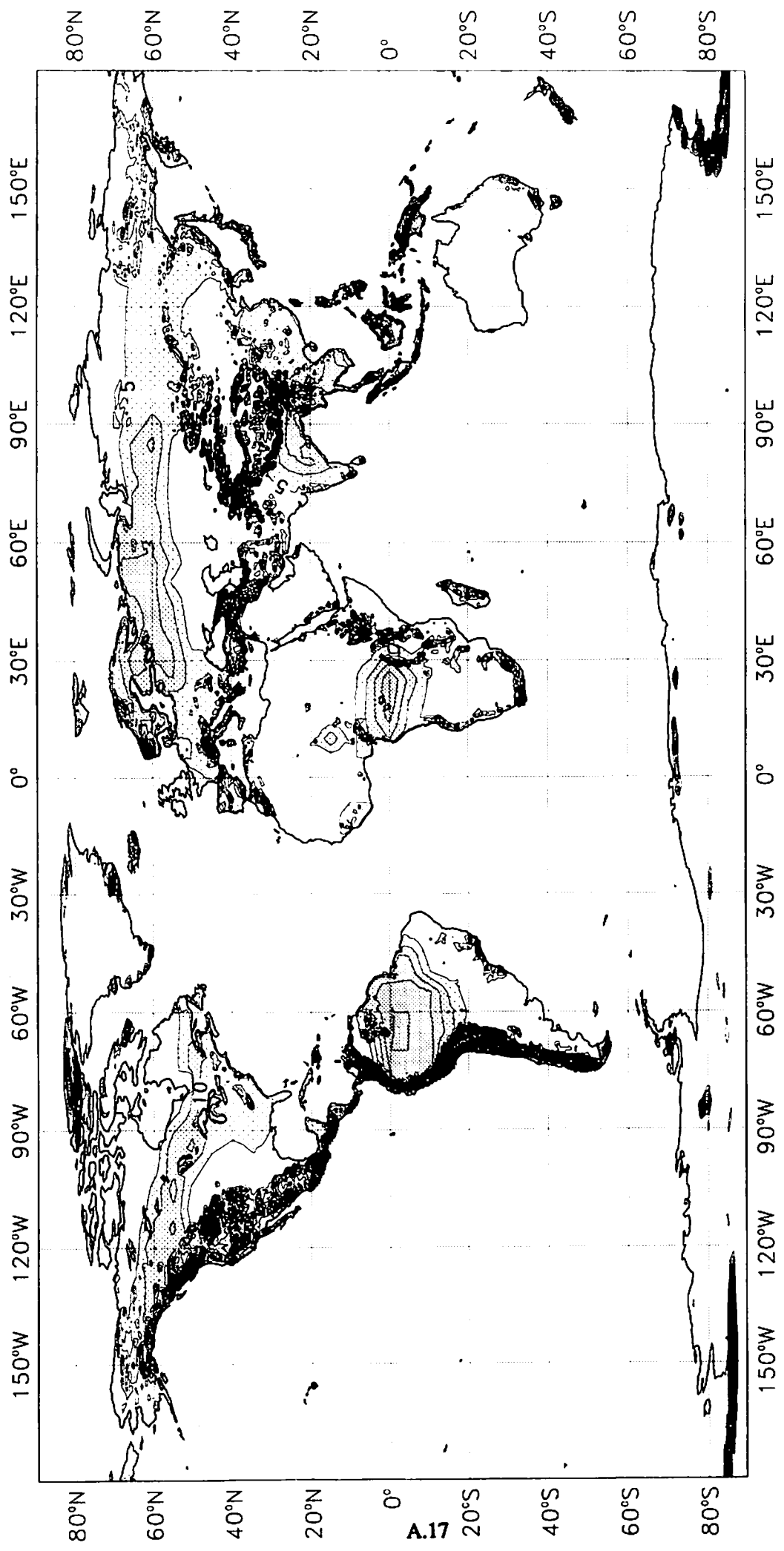


Fig. A.8 Roughness length above 50 cm. Contour interval 50 cm.

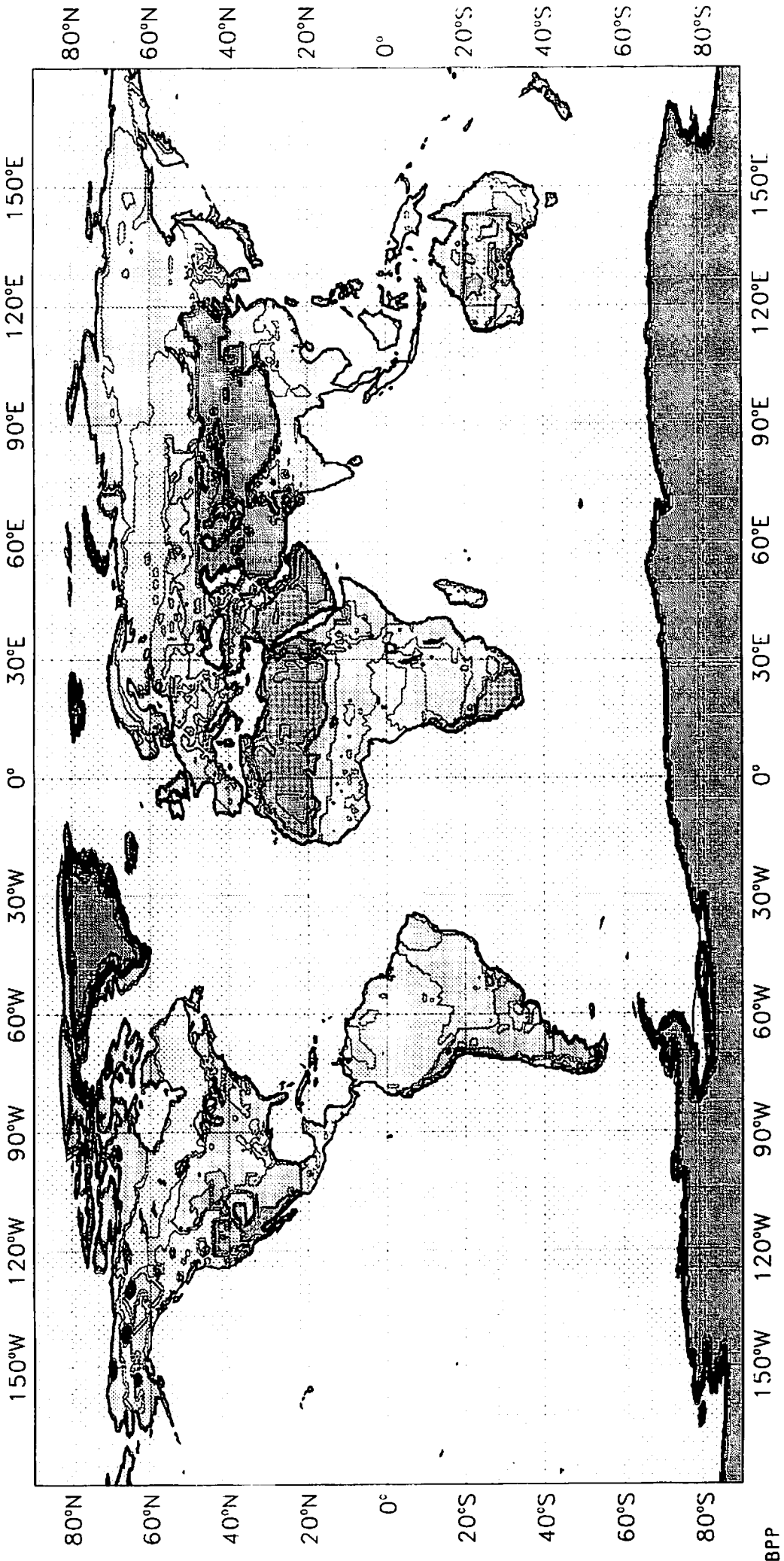


Fig. A.9 Albedo. Contour interval 4 %.

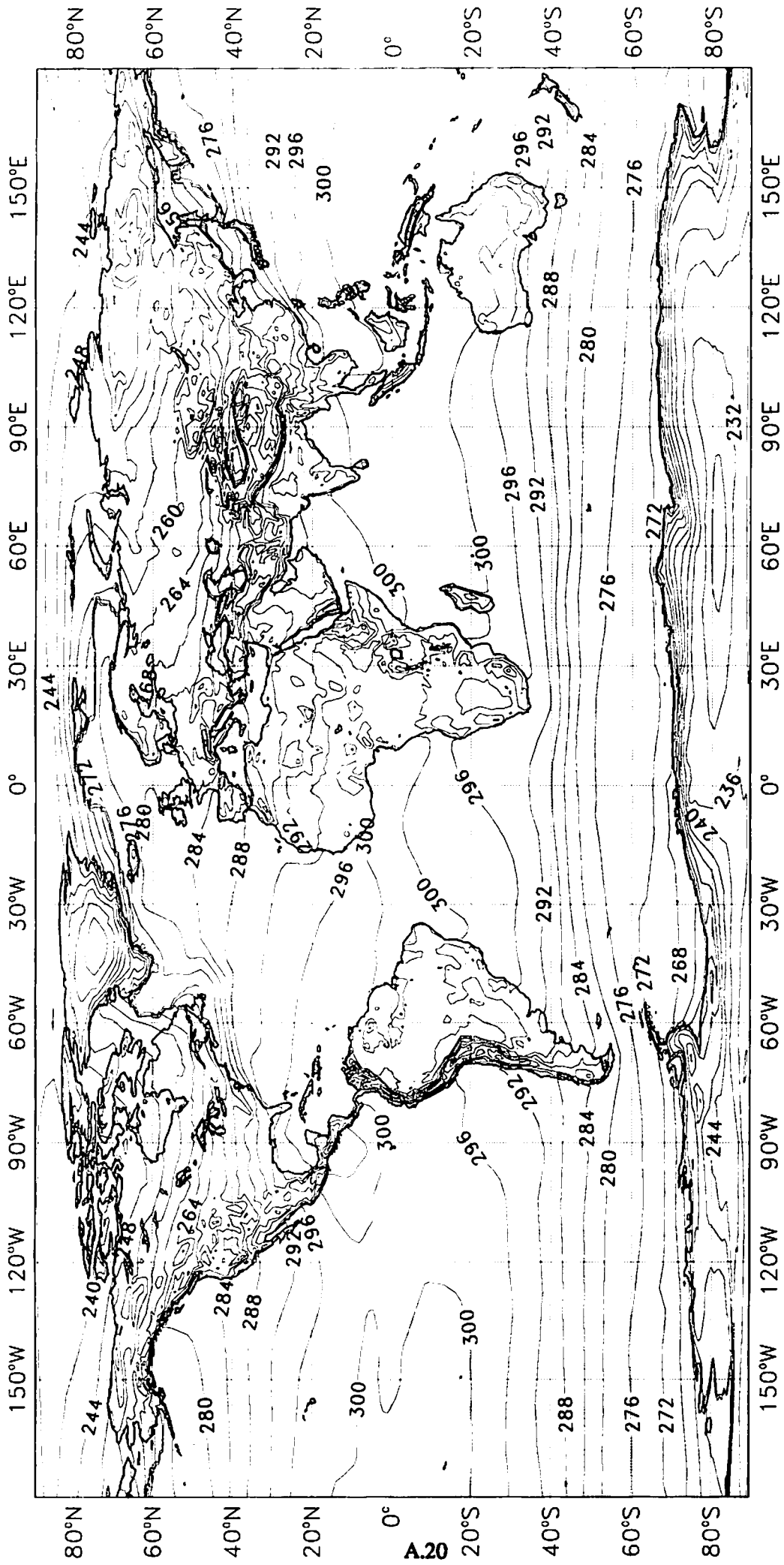


Fig. A.11 Climate deep soil temperature - February 1990.

Fig. A.12 Climate deep soil temperature - March 1990.

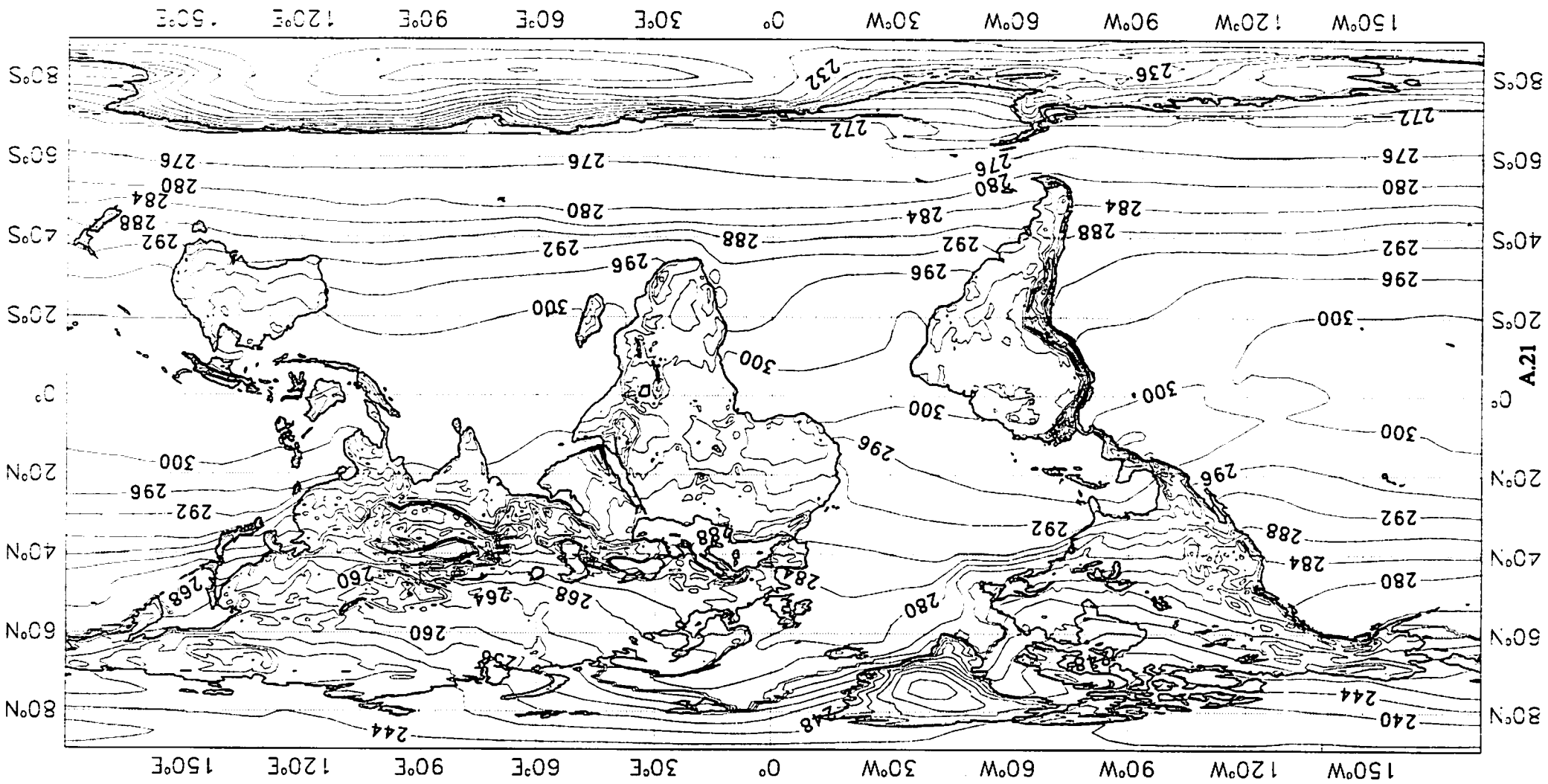
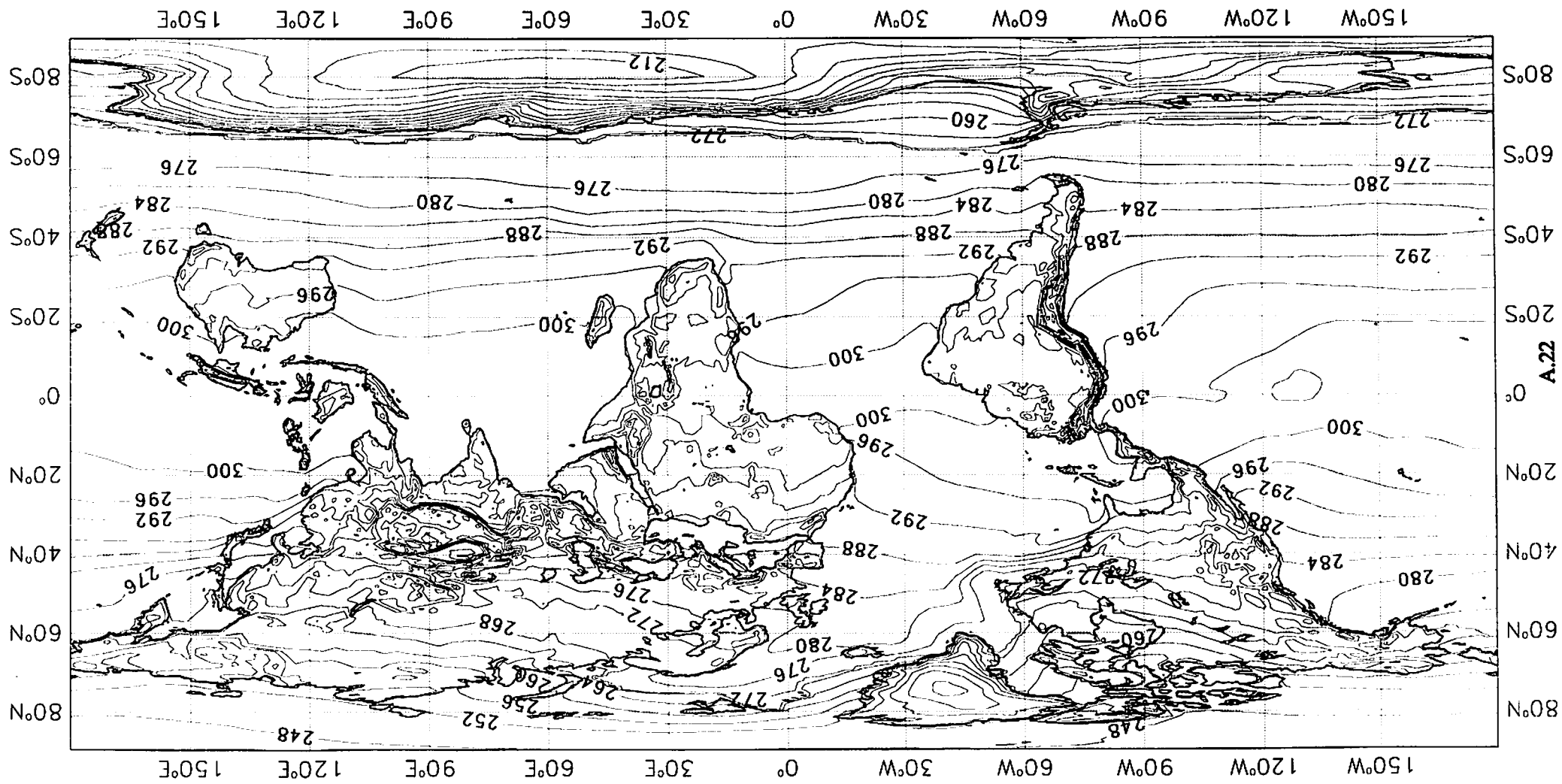


Fig. A.13 Climate deep soil temperature - April 1990.



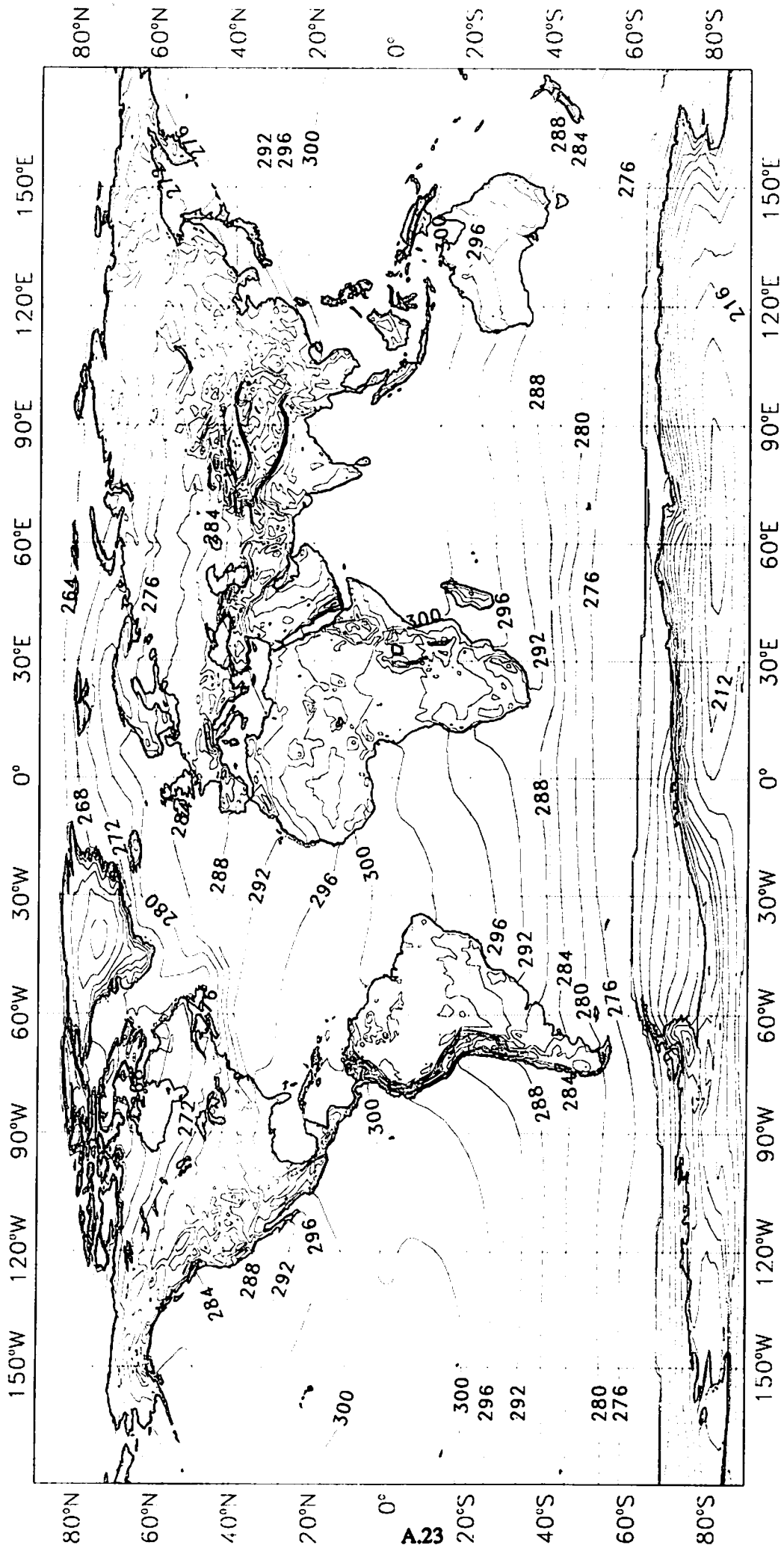


Fig. A.14 Climate deep soil temperature - May 1990.

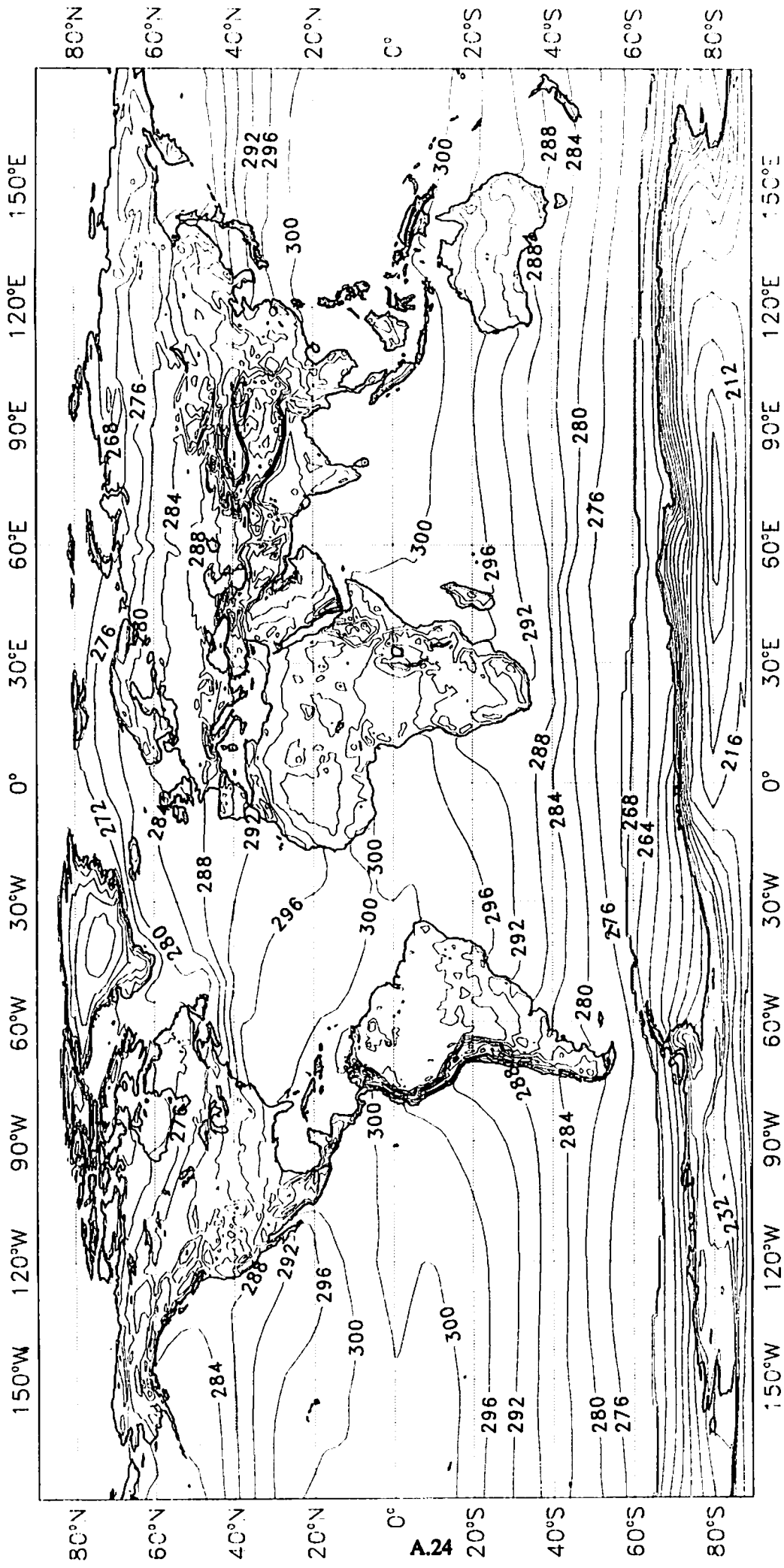


Fig. A.15 Climate deep soil temperature - June 1990.

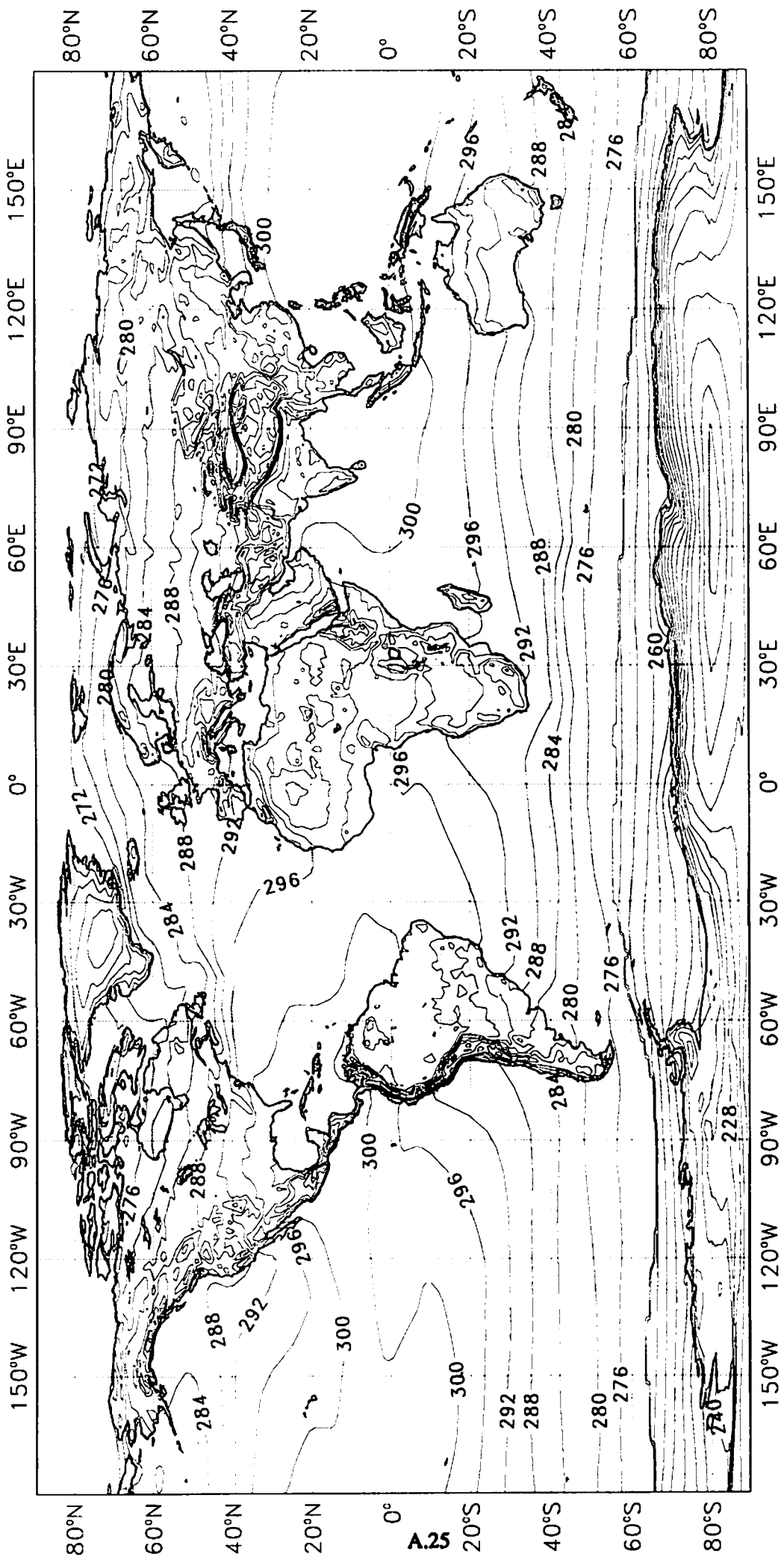
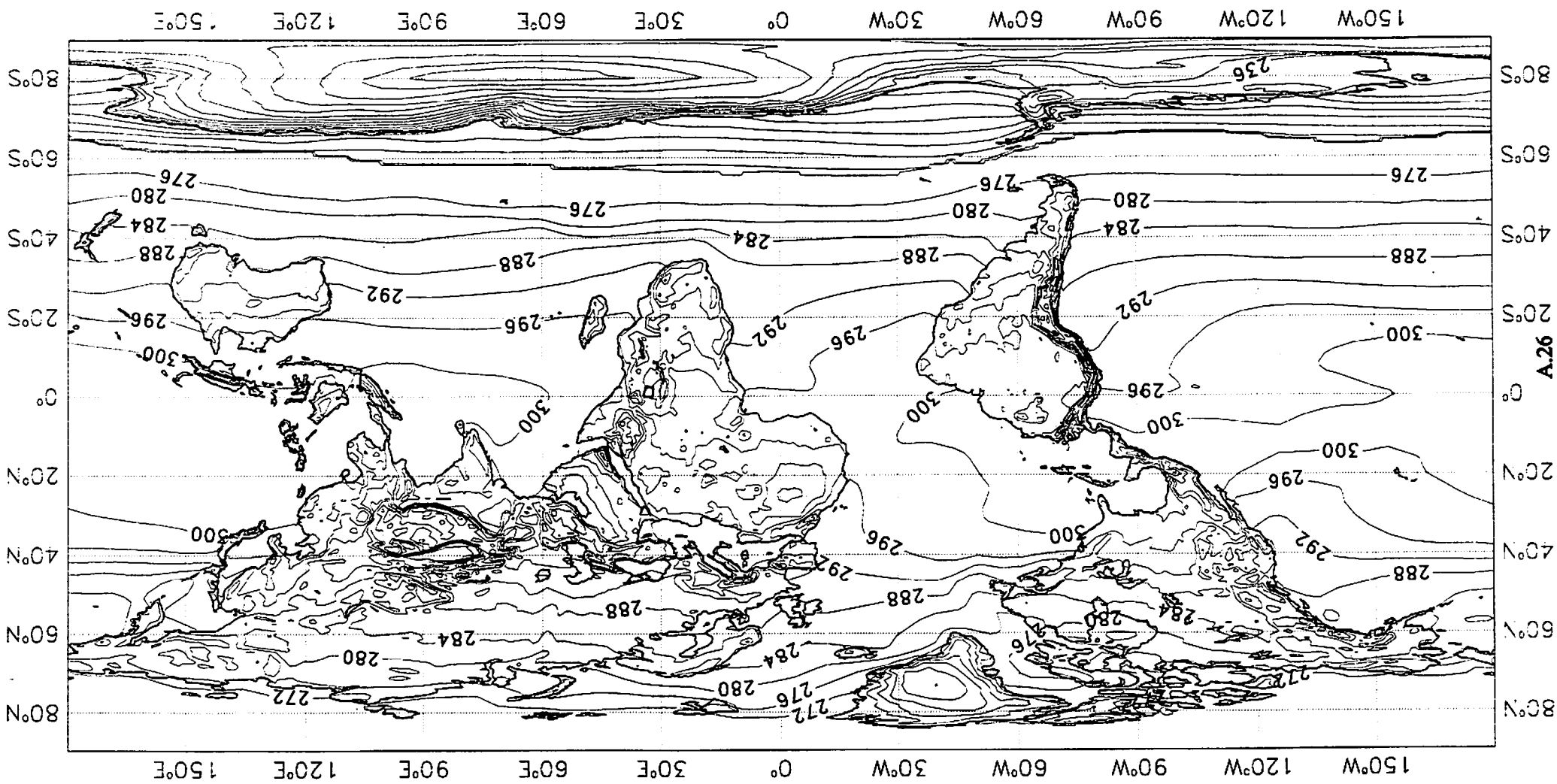


Fig. A.16 Climate deep soil temperature - July 1990.

Fig. A.17 Climate deep soil temperature - August 1990.



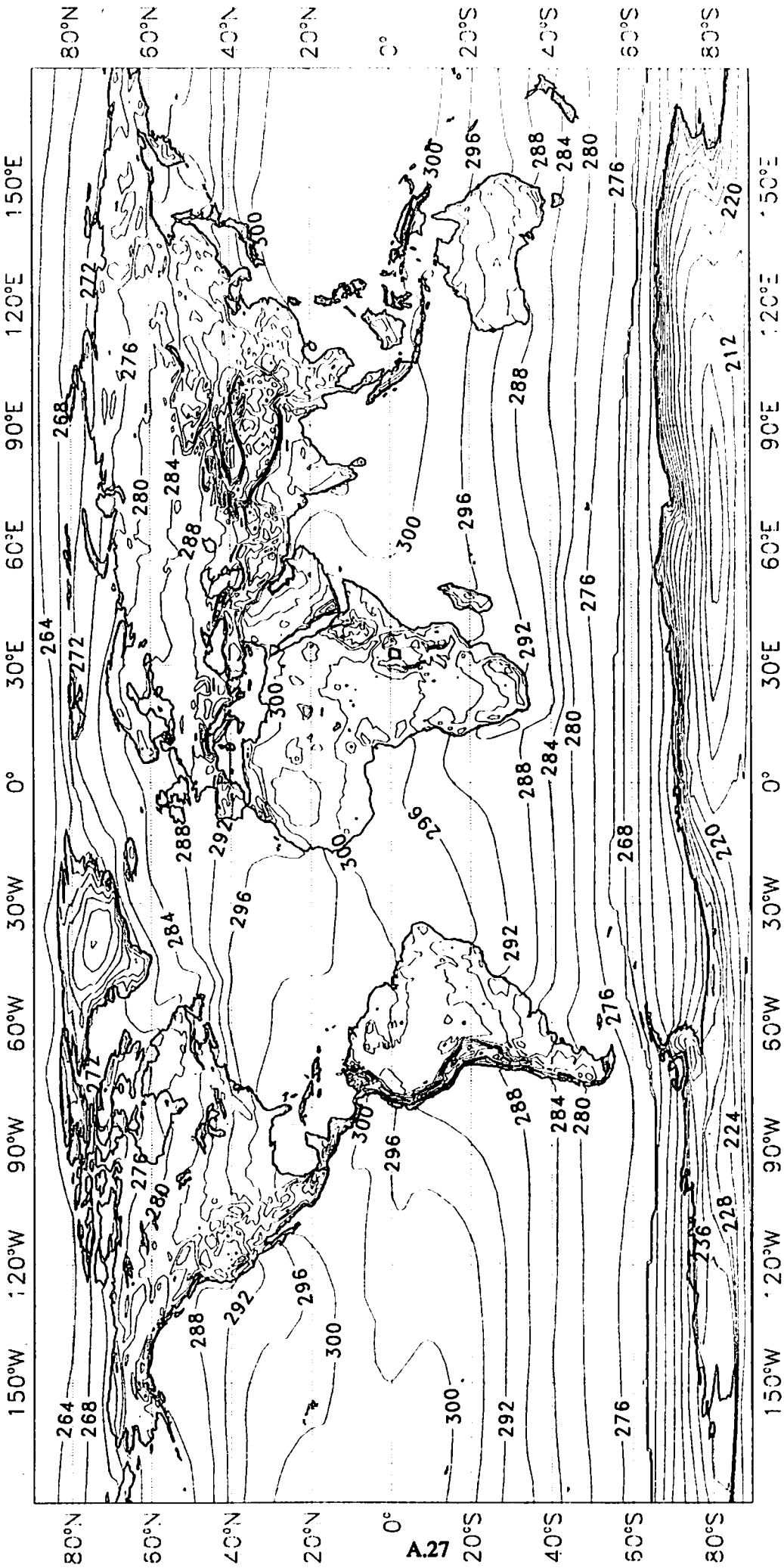


Fig. A.18 Climate deep soil temperature - September 1990.

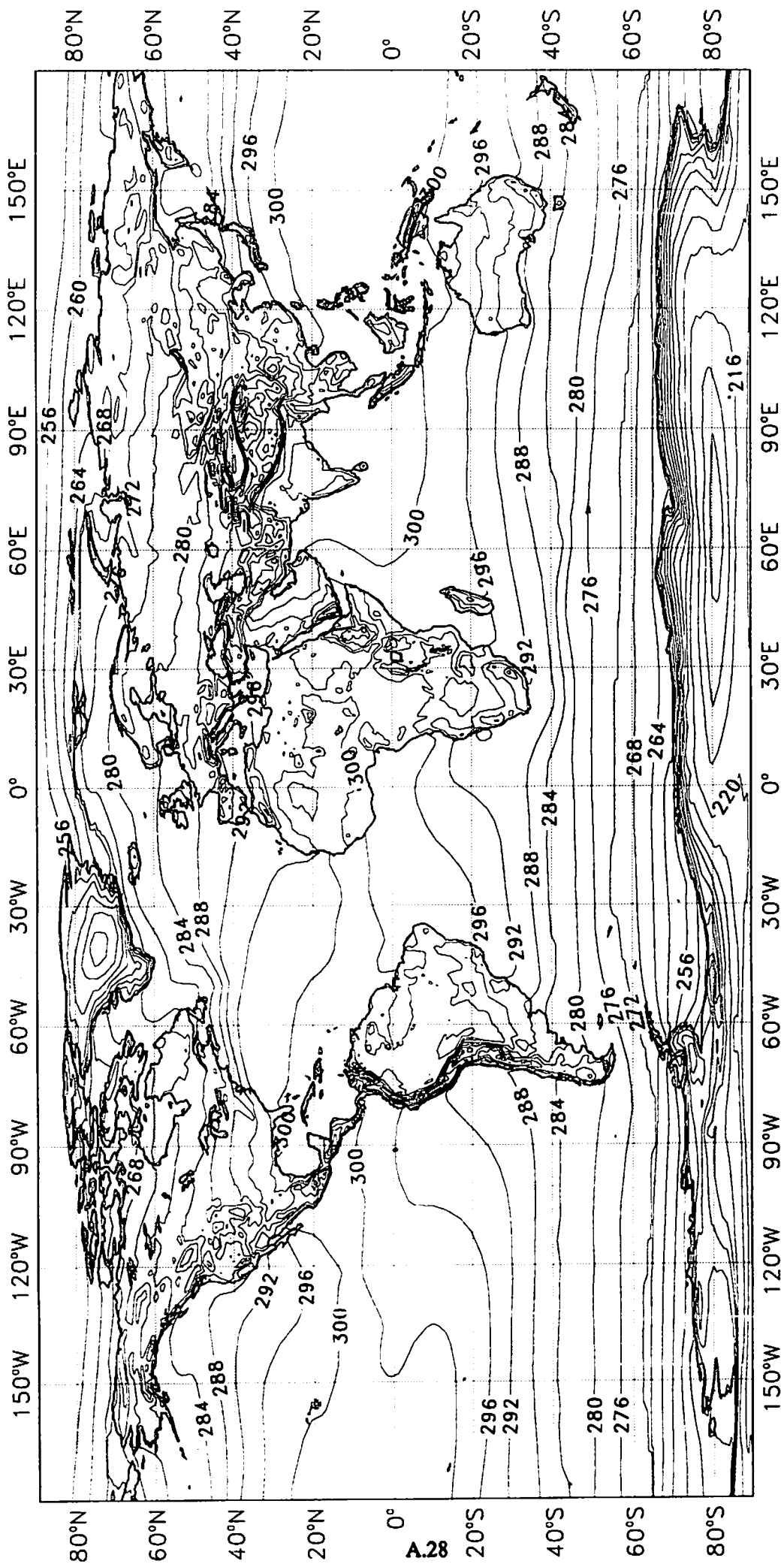


Fig. A.19 Climate deep soil temperature - October 1990.

A.28

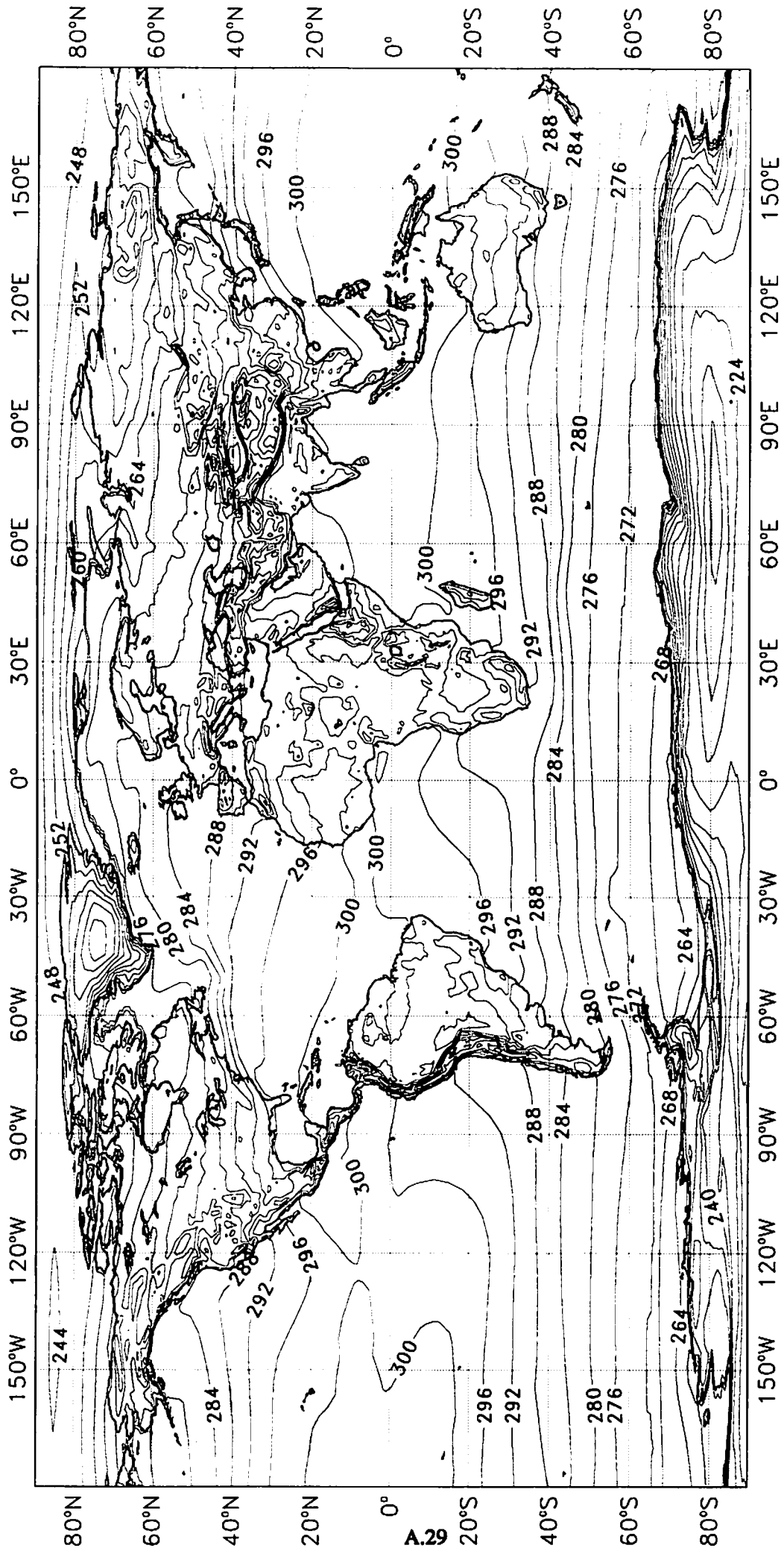


Fig. A.20 Climate deep soil temperature - November 1990.

Fig. A.22 Climate deep soil wetness - January 1990. Contour interval 1 mm.

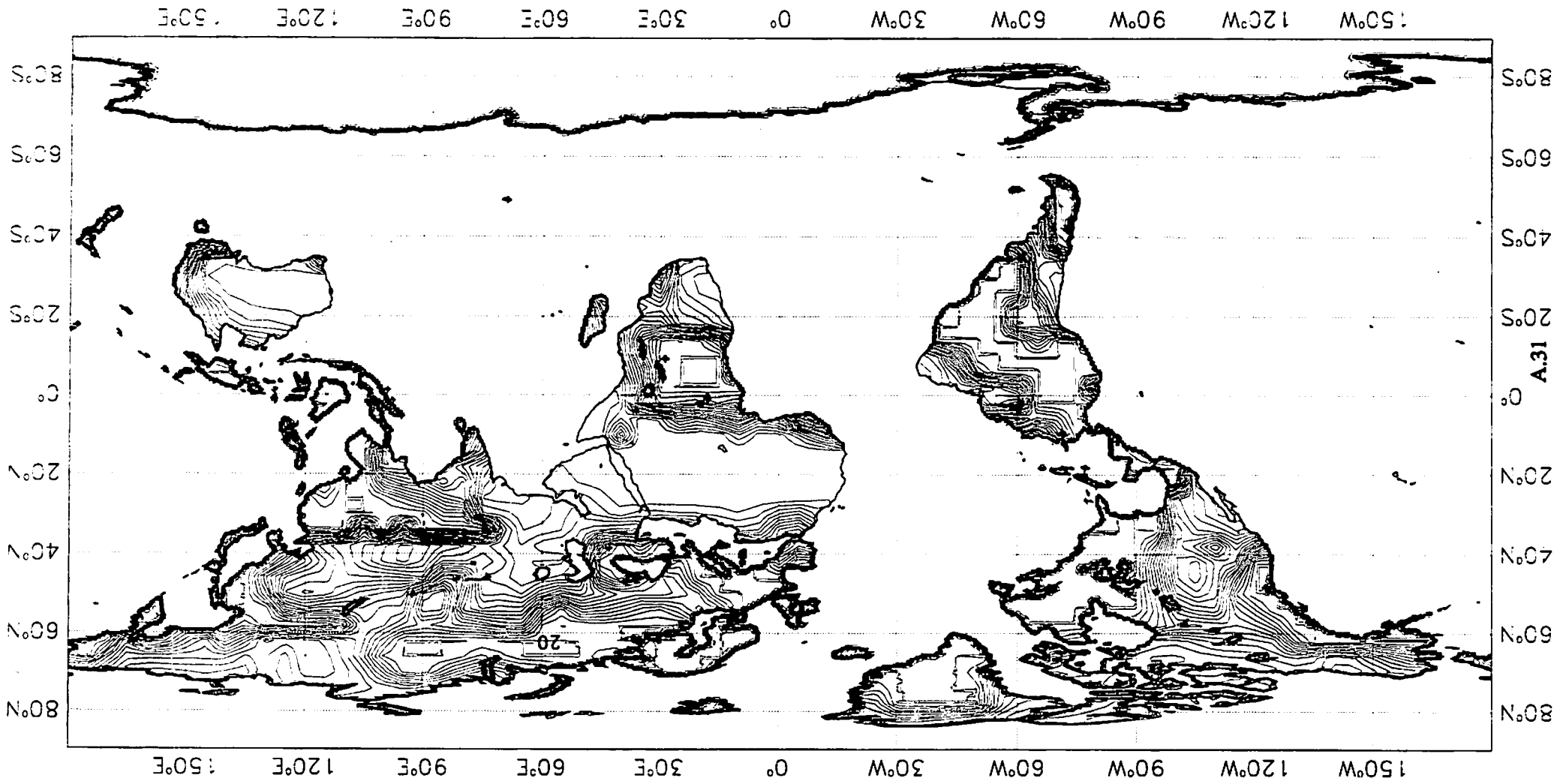


Fig. A.23 Climate deep soil wetness - February 1990. Contour interval 1 mm.

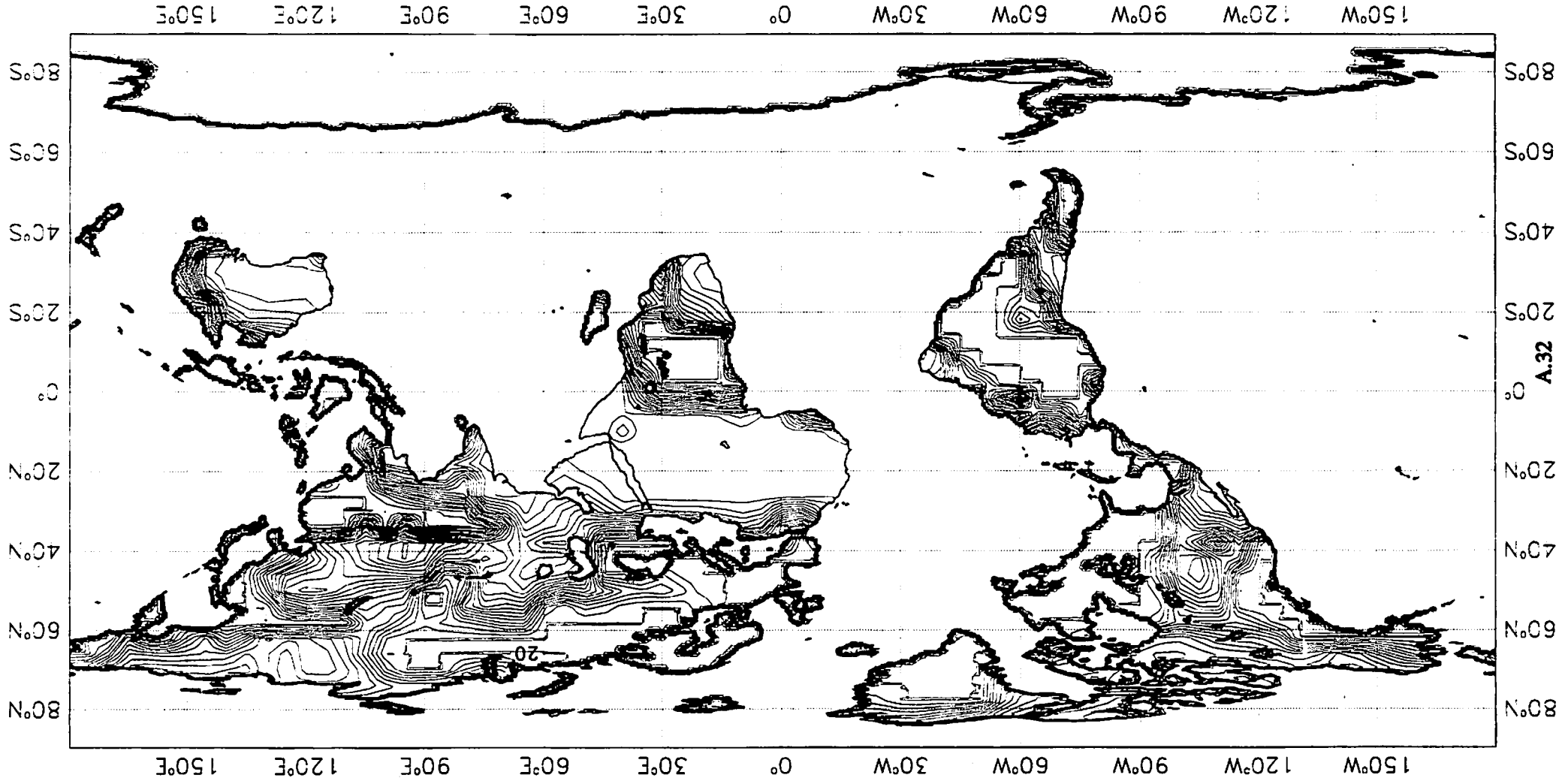
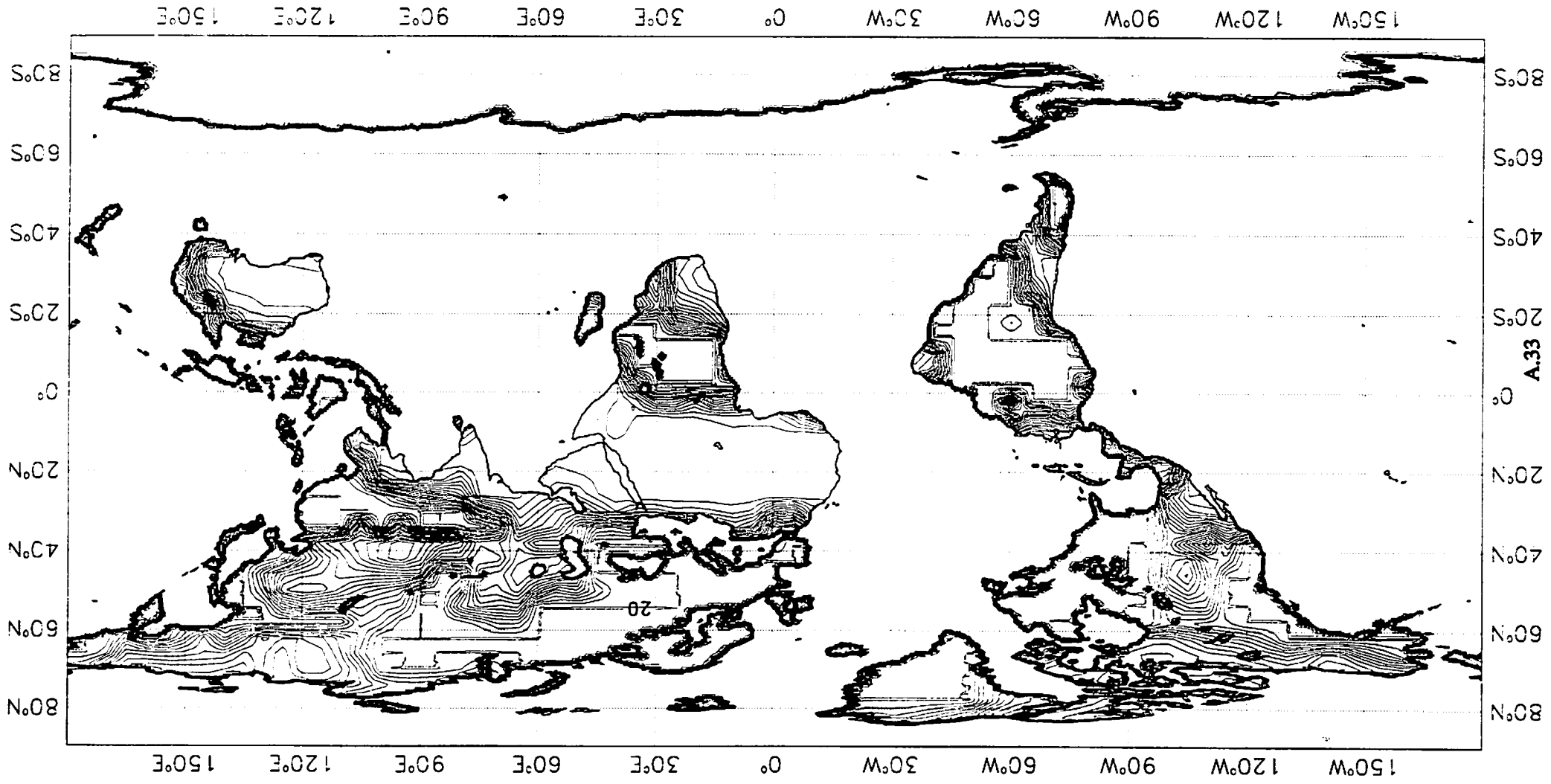
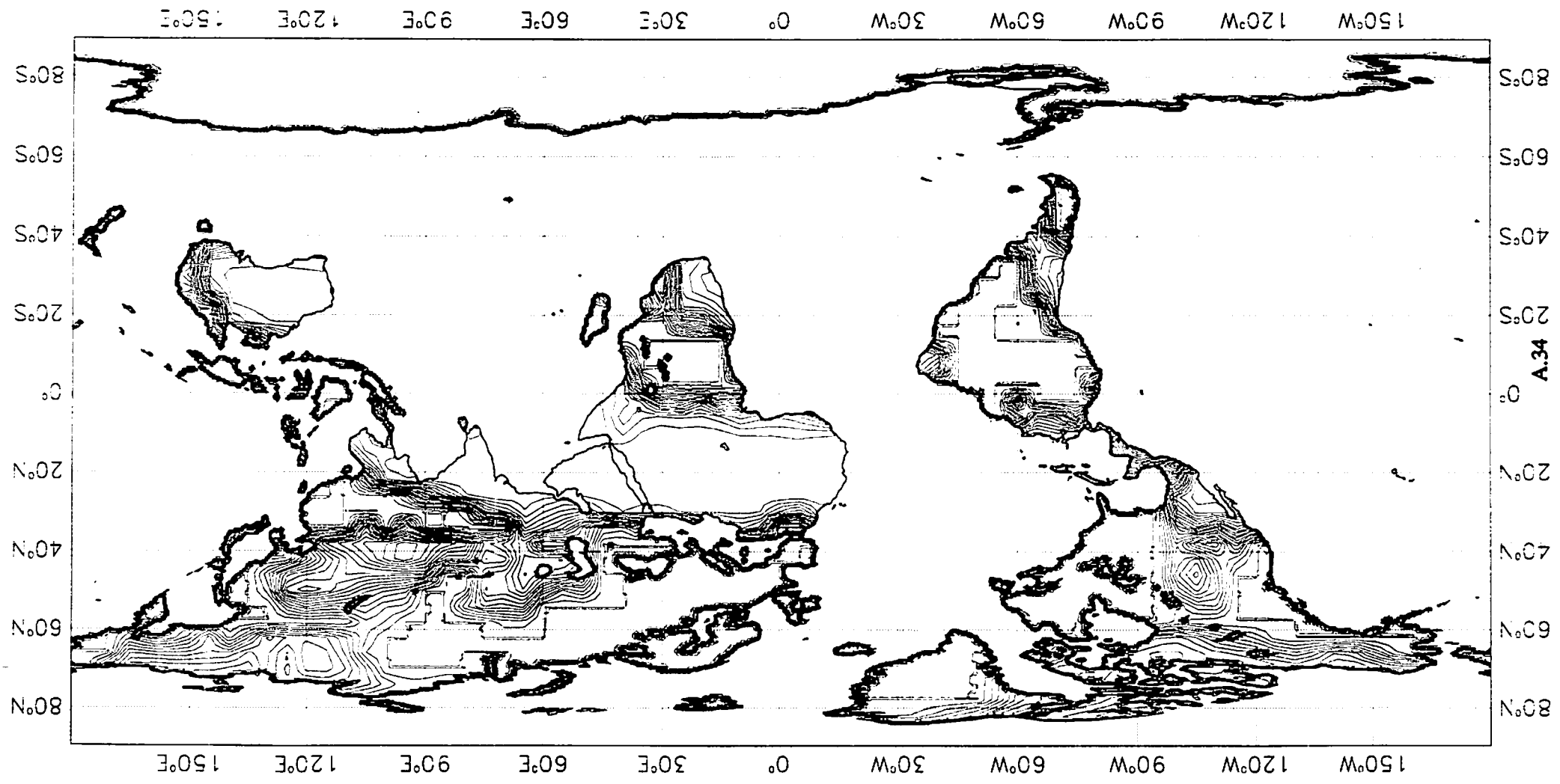


Fig. A.24 Climate deep soil wetness - March 1990. Contour interval 1 mm.



A.33

Fig. A.25 Climate deep soil wetness - April 1990. Contour interval 1 mm.



A.34

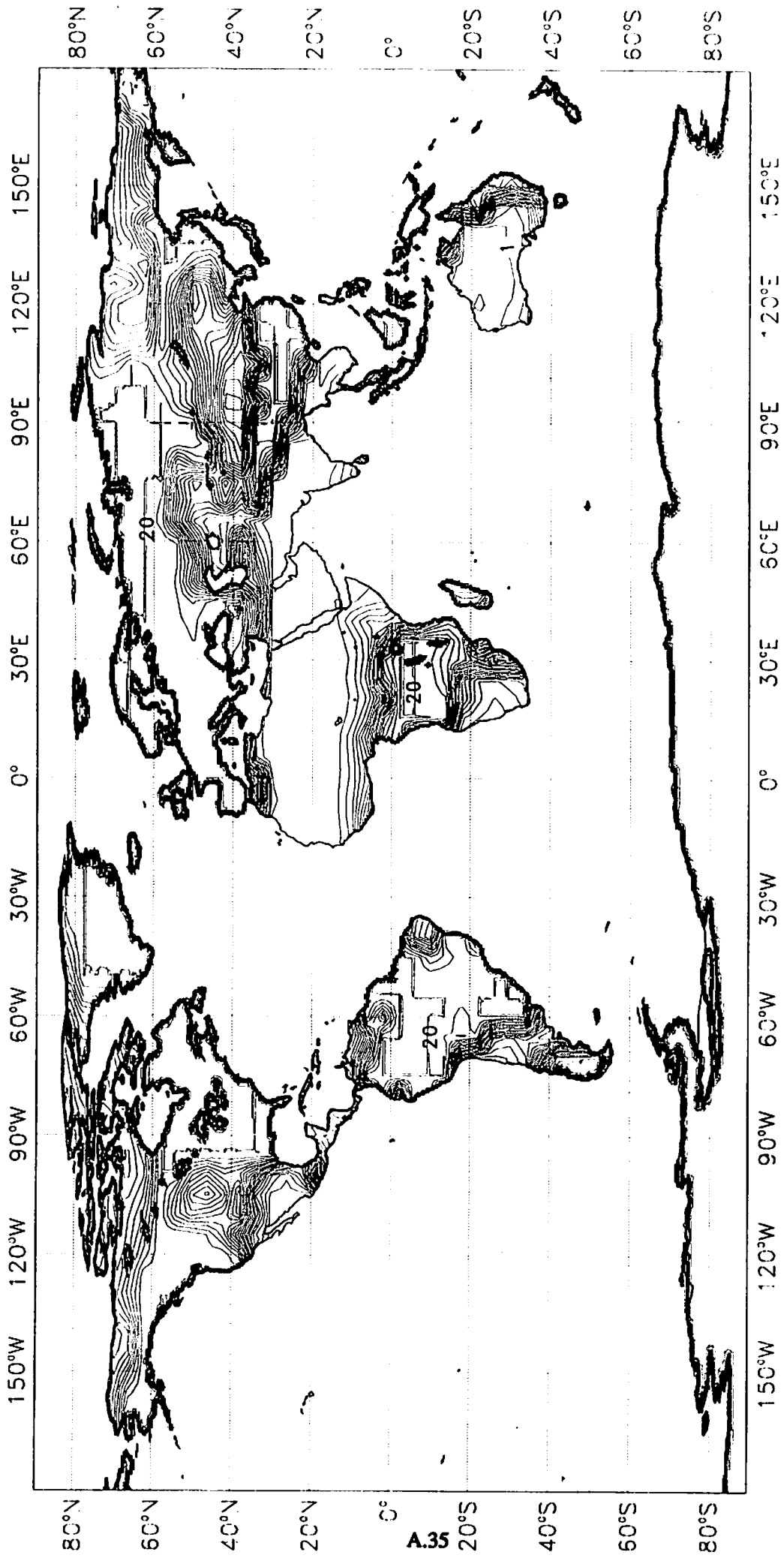


Fig. A.26 Climate deep soil wetness - May 1990. Contour interval 1 mm.

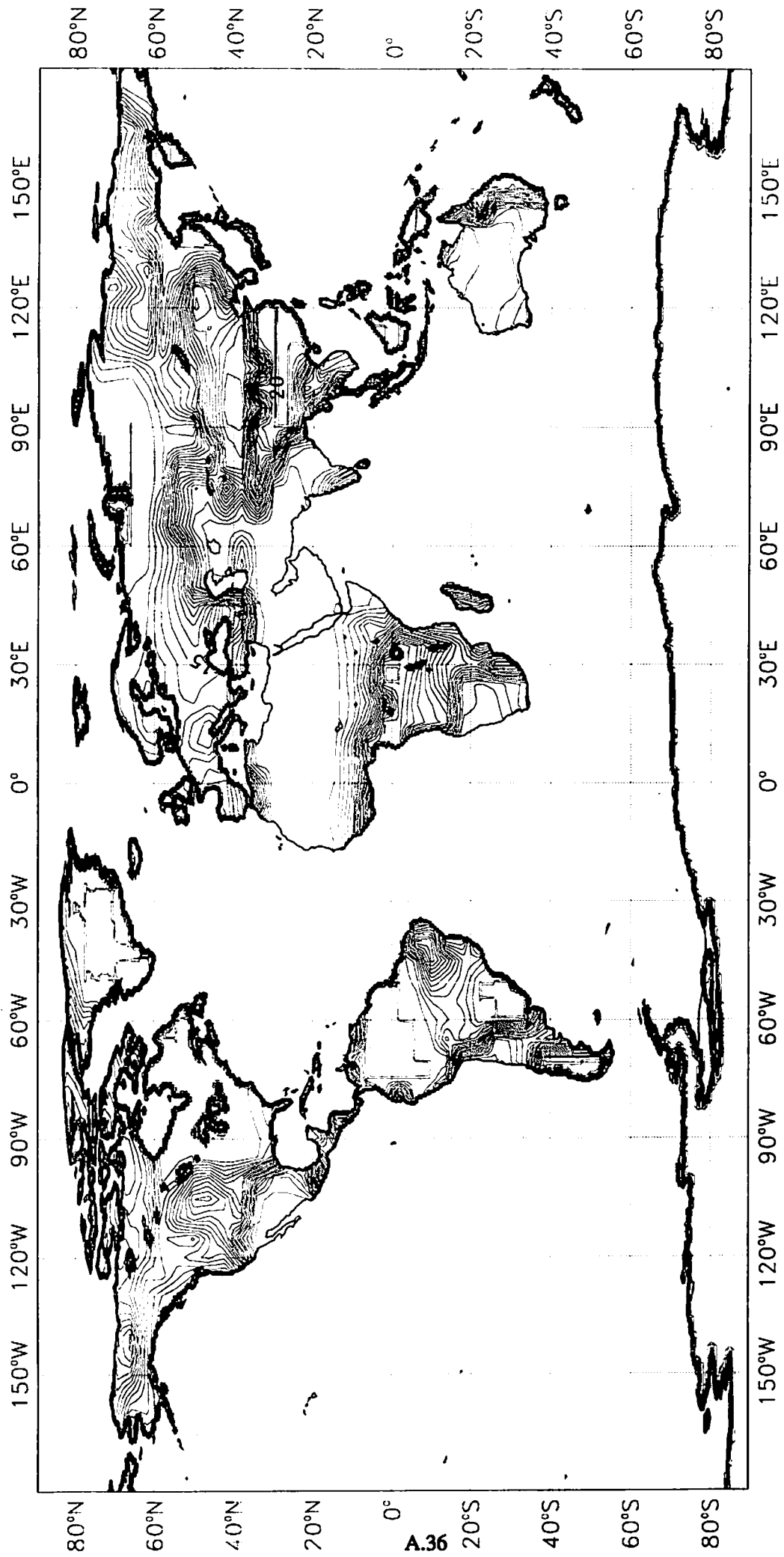


Fig. A.27 Climate deep soil wetness - June 1990. Contour interval 1 mm.

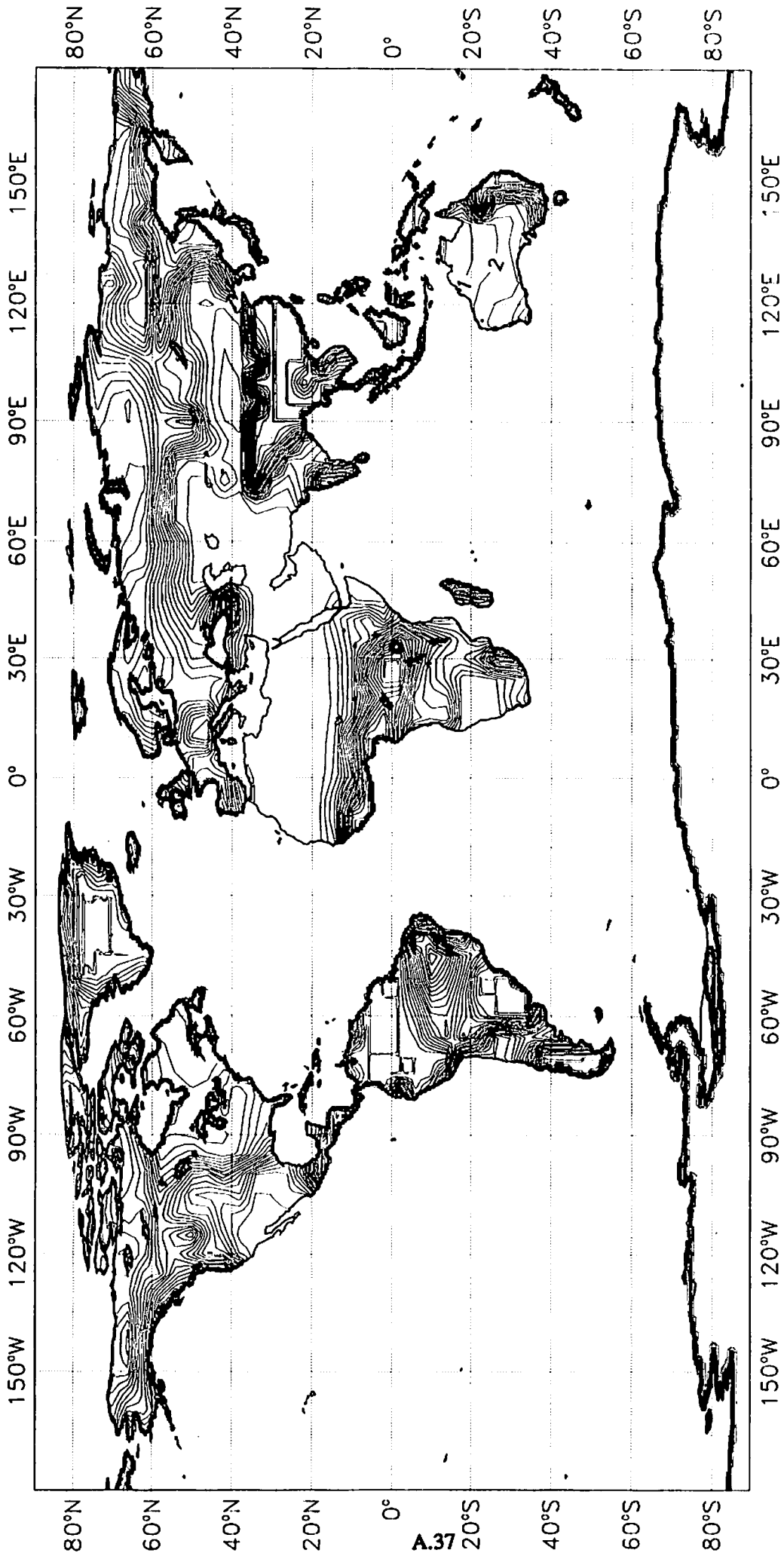


Fig. A.28 Climate deep soil wetness - July 1990. Contour interval 1 mm.

Fig. A.29 Climate deep soil wetness - August 1990. Contour Interval 1 mm.

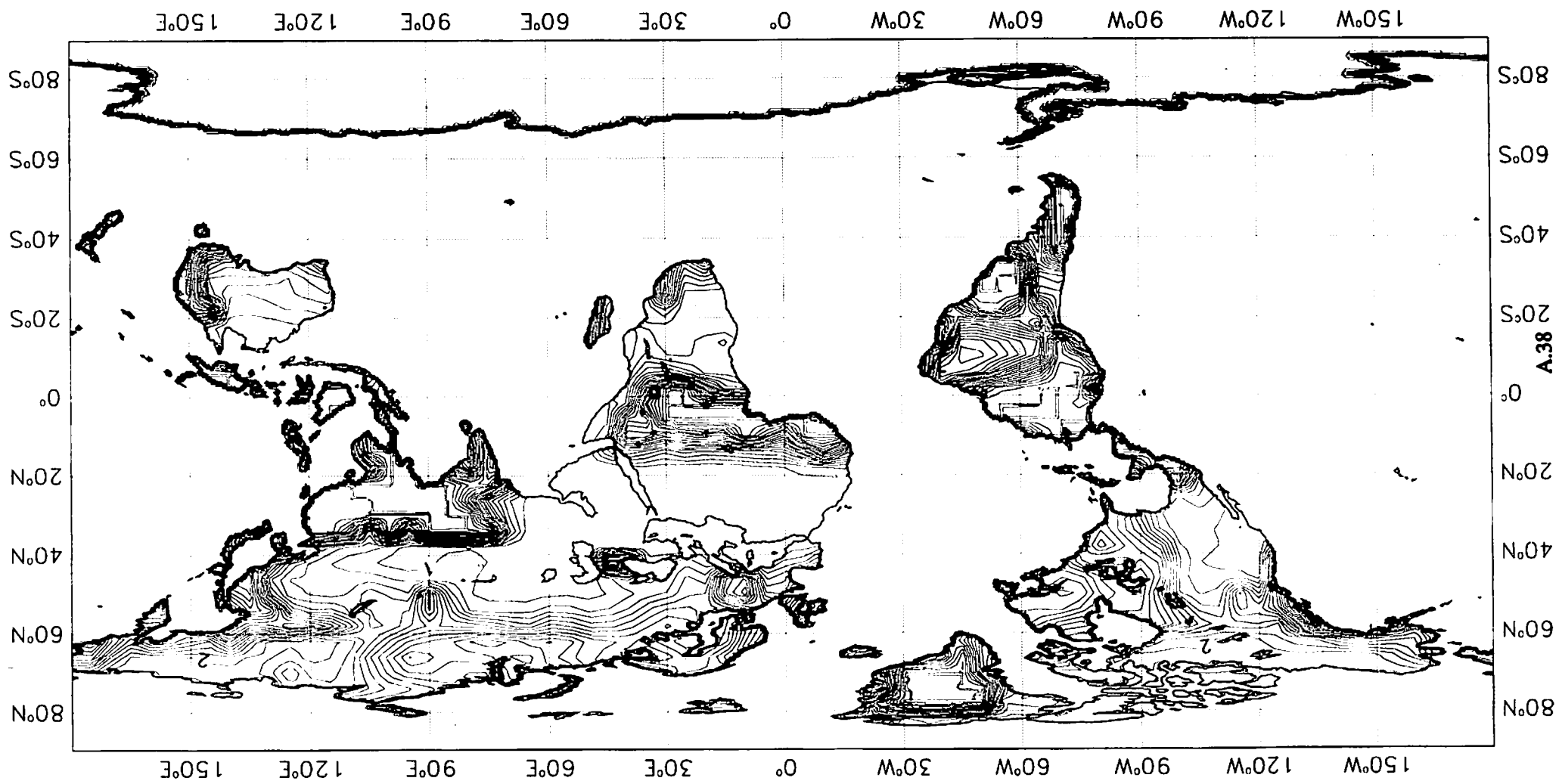
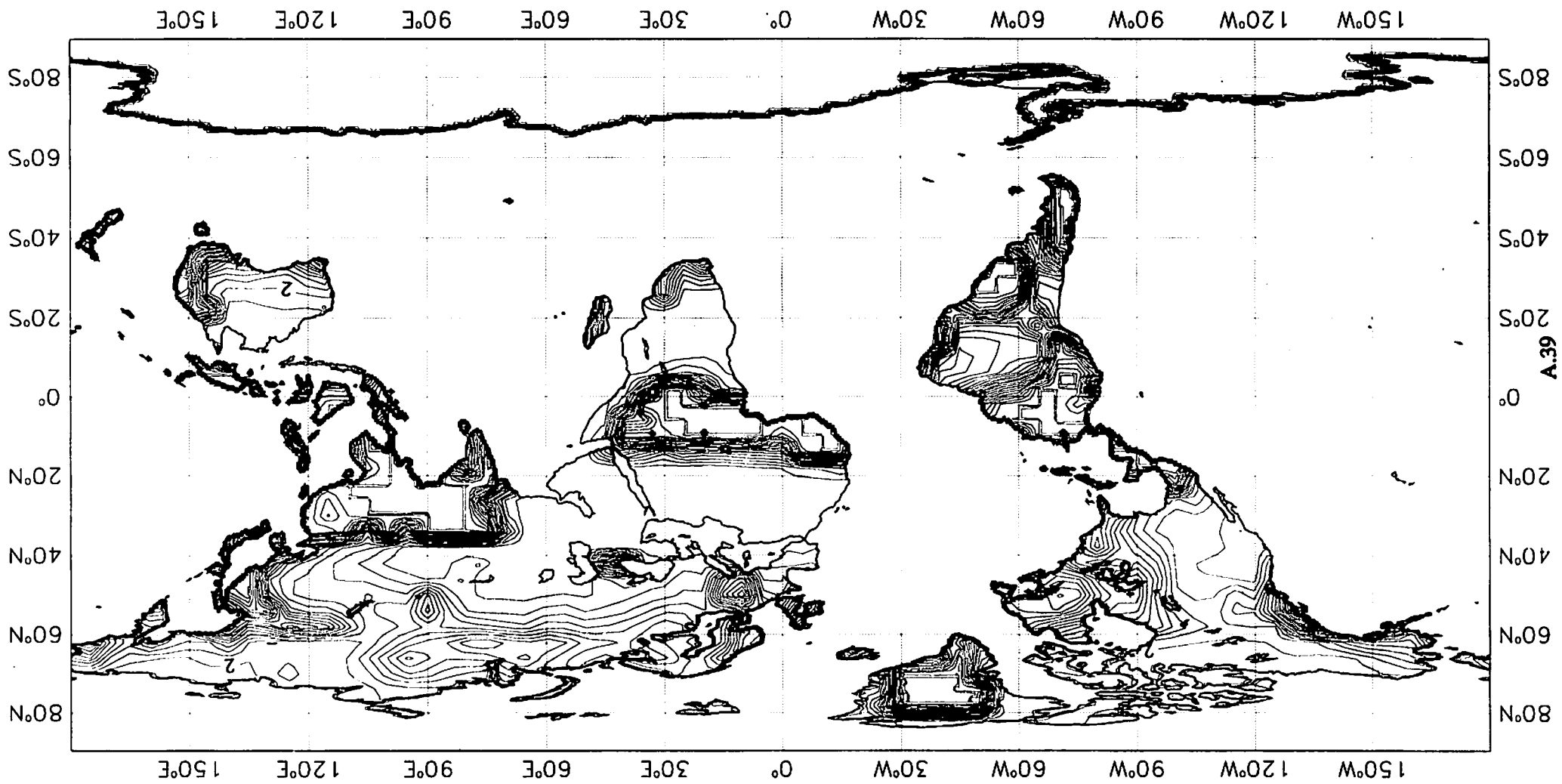


Fig. A.30 Climate deep soil wetness - September 1990. Contour interval 1 mm.



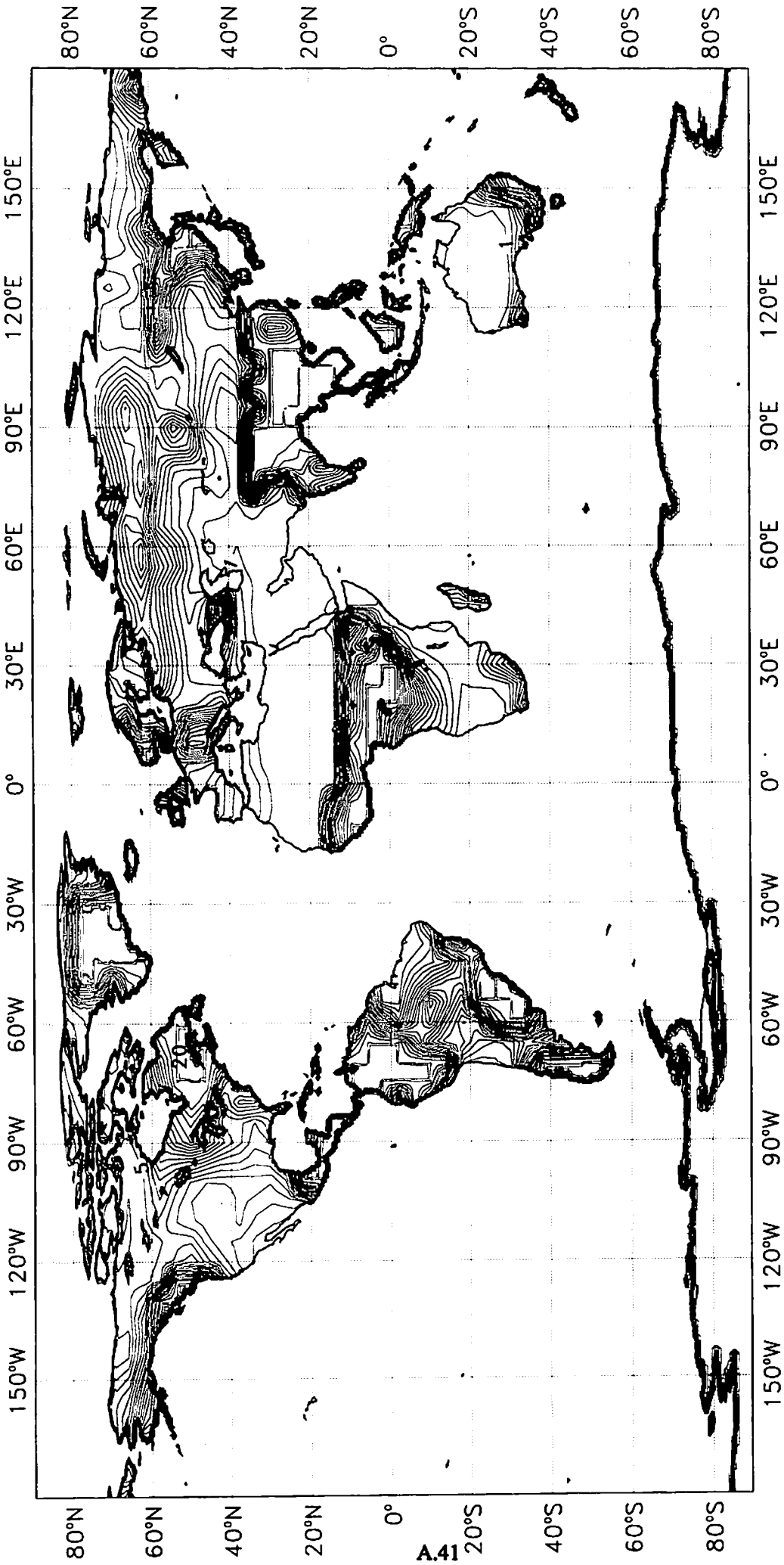


Fig. A.32 Climate deep soil wetness - November 1990. Contour interval 1 mm.

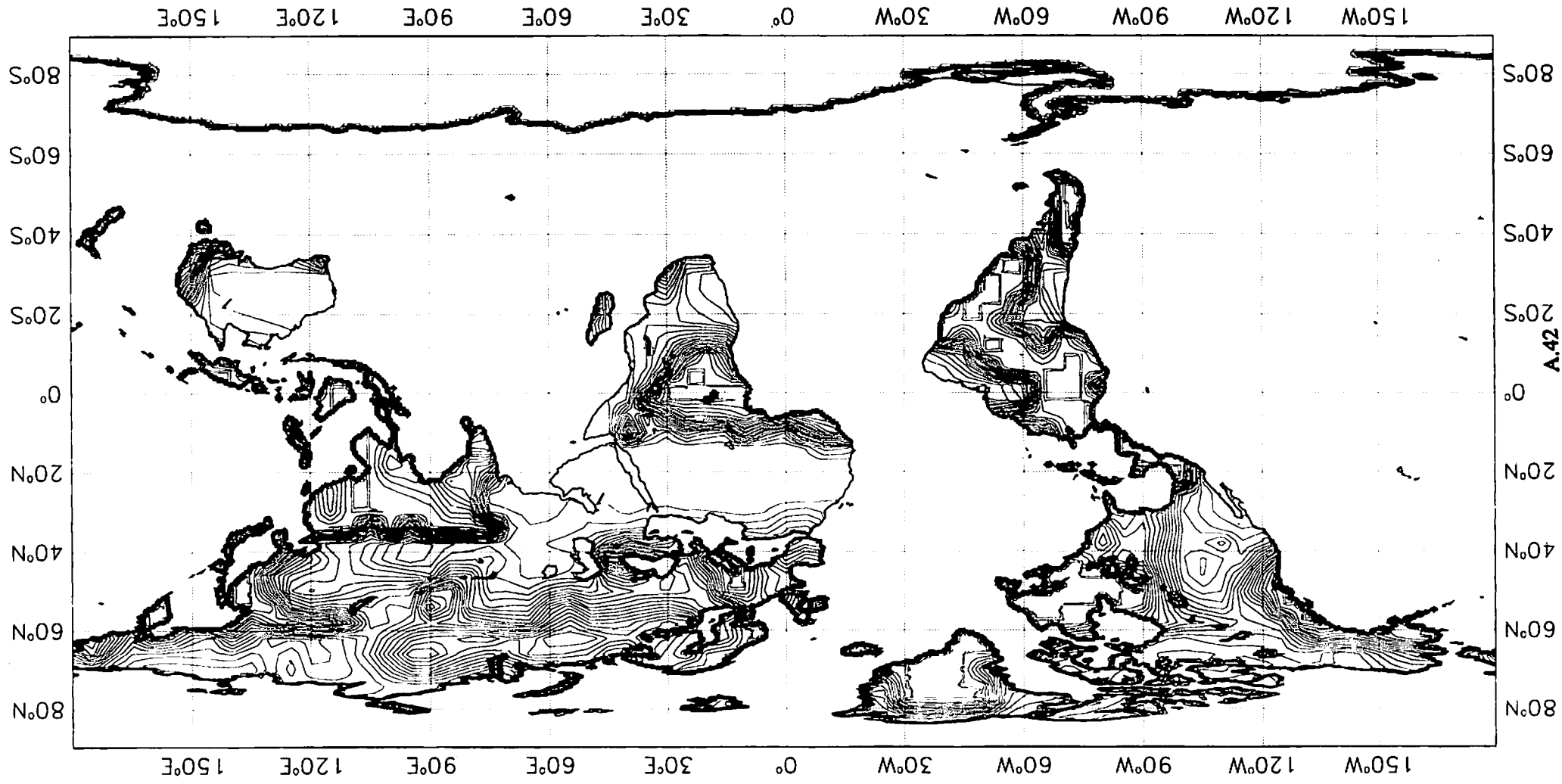


Fig. A.33 Climate deep soil wetness - December 1990. Contour interval 1 mm.

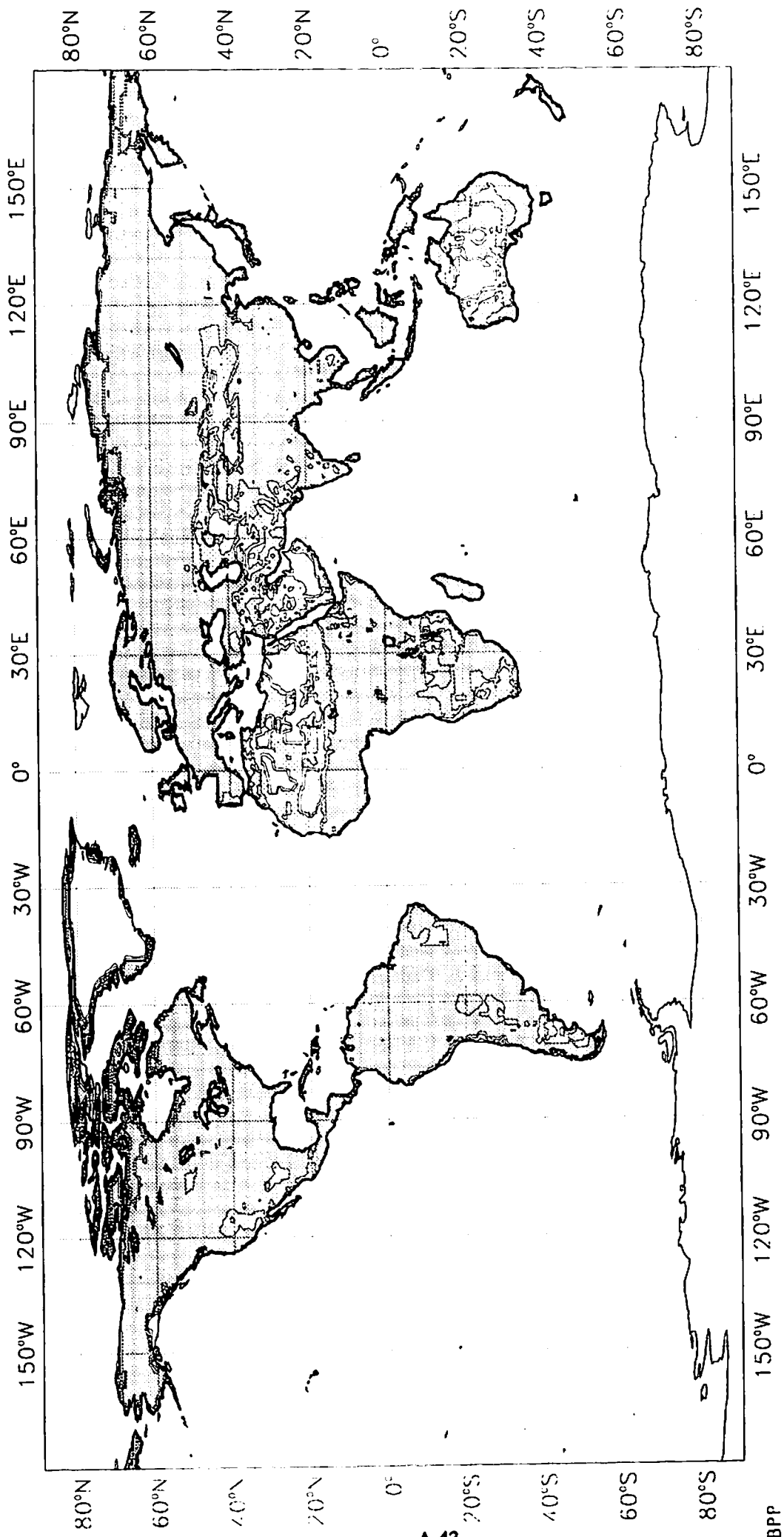


Fig. A. 34 Vegetation ratio. Contour interval 20%.

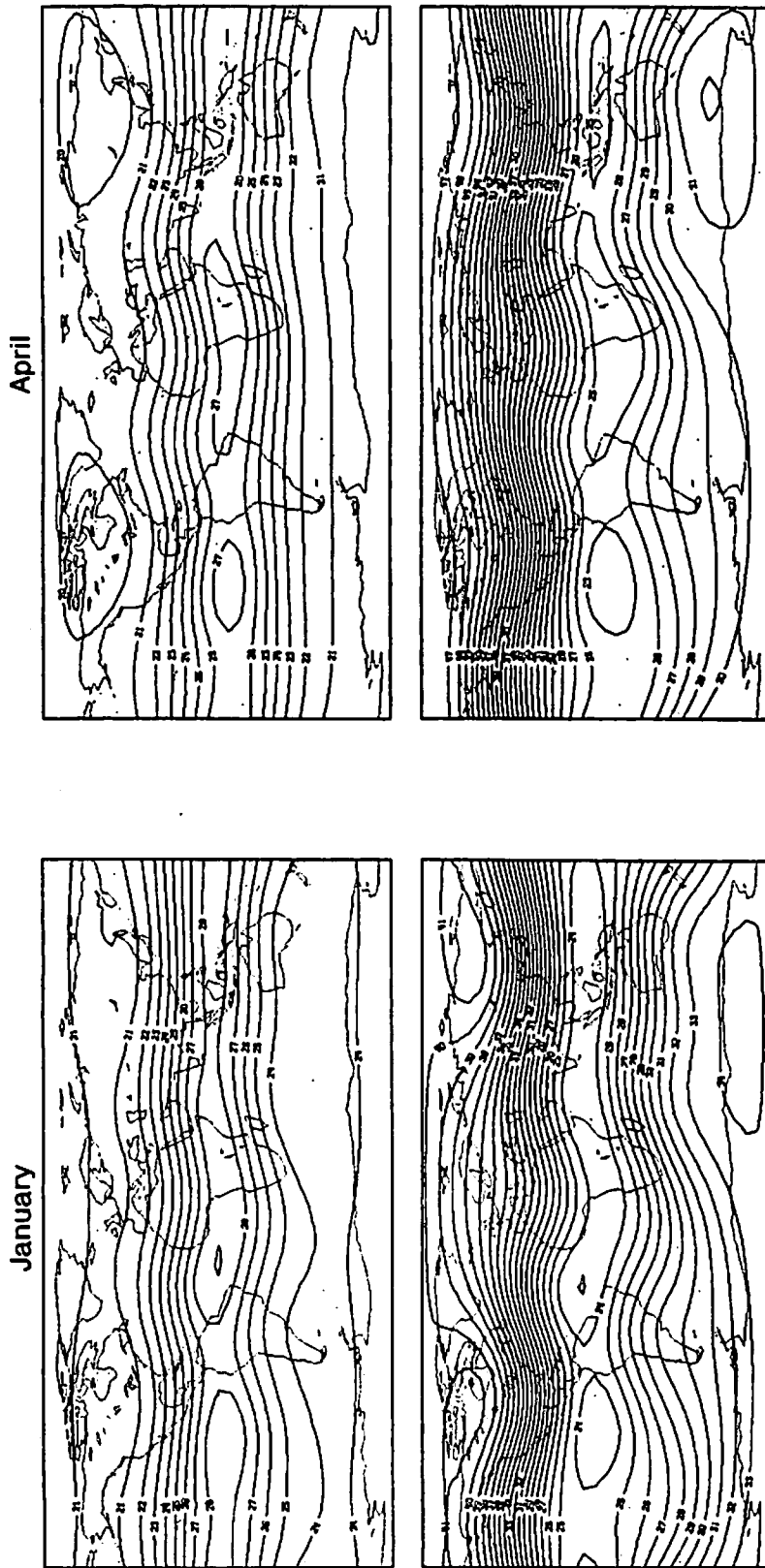


Fig. A. 35 Top: height of the maximum ozone concentration (km). Bottom: total amount of ozone (10⁴ m NTP)

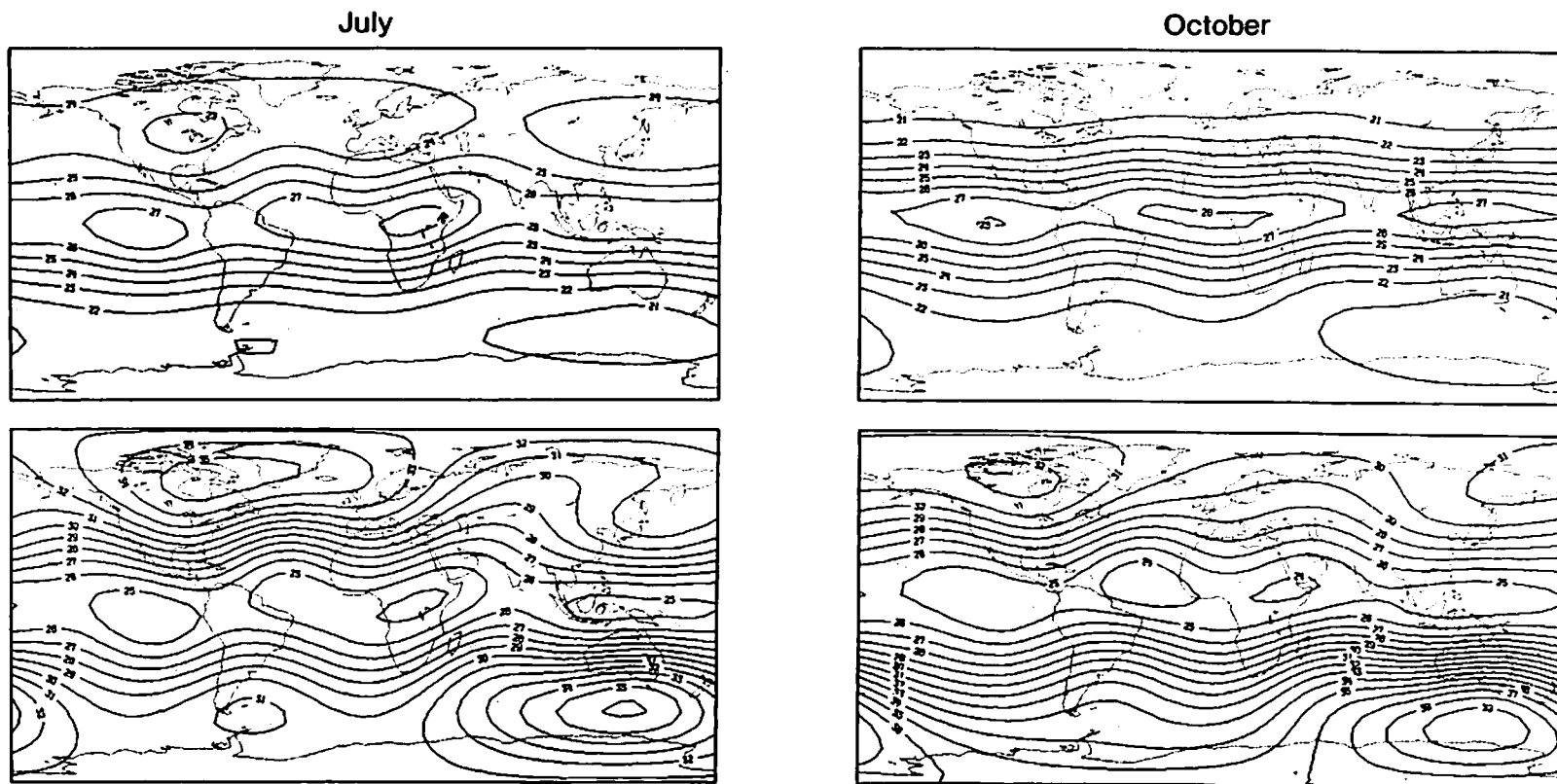


Fig. A.36. Top: height of the maximum ozone concentration (km). Bottom: total amount of ozone (10^{-4} m NTP)